2002

Numerical reservoir characterization using dimensionless scale numbers with application in upscaling

Djuro Novakovic
Louisiana State University and Agricultural and Mechanical College

NUMERICAL RESERVOIR CHARACTERIZATION USING DIMENSIONLESS SCALE NUMBERS WITH APPLICATION IN UPSCALING

A Dissertation

Submitted to the Graduate Faculty of the
Louisiana State University and
Agricultural and Mechanical College
in partial fulfillment of the
requirements for the degree of
Doctor of Philosophy

in

The Department of Petroleum Engineering

by
Djuro Novakovic
B.S. University of Zagreb, Croatia, 1996
Master of Science in Petroleum Engineering, Louisiana State University, 1999
August, 2002

ACKNOWLEDGEMENTS

The author extends his deepest gratitude and sincere appreciation to Dr. Christopher White - his major professor - for genuine interest, guidance and endless amount of patience and support during this endeavor. Exposure to mathematical intricacies of numerical methods, state-of-the-art designed reservoir simulations and modeling automation is what made this work possible.

Dr. Zaki Bassiouni and Dr. John McMullan are thankfully acknowledged for being valuable guides with both an advice and a kind word of support. If not for their encouragement to become involved in the research in this area a valuable and rewarding educational opportunity would be missed.

Dr. Julius Langlinais and Dr. Clinton Willson are thankfully acknowledged for being members of examining committee. The author would like to thank Dr. Andrew Wojtanowicz for both being a committee member and for a chance to – through extracurricular work – expand my horizons in other aspects of Petroleum Engineering.

Financial support during the research from the Department of Petroleum engineering is also acknowledged.

A special thanks is due to colleagues and friends at LSU and in Croatia to whom the author dedicates this work.

TABLE OF CONTENTS

LIST OF TABLES

LIST OF FIGURES

ABSTRACT

Dimensionless space provides a tool for analyzing the behavior of complex systems described by mathematical relationships. The limited application of dimensionless variables in numerical reservoir simulation and experimental design motivated the development of a complete set of dimensionless scaling groups. Inspectional analysis yielded 8 dimensionless groups completely describing the flow system. Further analysis of fluid interaction reduced the number of dimensionless groups to 7.

The newly developed dimensionless equations and groups were used for analytical and numerical reservoir characterization, quantifying the behavior of differential and difference equations employed in fluid flow in three-dimensional porous media.

The behavior of the dimensionless scaling is demonstrated for breakthrough time in an immiscible displacement in three dimensions. Numerical simulations were designed in dimensionless space and converted to dimensional space using several approaches. The resulting estimates of stability limits, numerical dispersion, and regime boundaries were in excellent agreement.

The application of the dimensionless groups to upscaling was investigated using designed reservoir simulations to estimate dimensionless regions corresponding to different flow regimes. Analytical development, simulation runs and literature data were in good agreement. This application demonstrates the potential benefits of the proposed dimensionless groups for upscaling, sensitivity analysis, stability analysis, and reservoir characterization.

CHAPTER 1
INTRODUCTION

Advances in computing and its low cost led to the introduction of numerical methods in all fields of engineering. Petroleum engineers have always relied heavily on numerical models, especially when reservoir management has to consider complex geologic settings and recovery processes. Analytical methods, although easy to use, cannot account for the reservoir complexity and time-varying boundary conditions. As a result numerical methods are now the *de facto* standard, providing reservoir models for management decision-making.

Sensitivity studies, history matching with production forecast and reservoir development optimization are common applications of reservoir simulations. They usually involve large numbers of runs. Two factors contribute to quality of a reservoir study - geology and physics. A good sensitivity study should

- Estimate contribution of geological uncertainty (spatial property distribution)
- Estimate physical parameters and determine optimum drive mechanism
- Minimize the effect of numerical dispersion on results

Evolution of a numerical reservoir model begins with a geological model – a description of bounding surfaces and spatially distributed flow properties outlined using a discrete grid. The geologic model is static. In creating the geological model, the modeling team focuses on flow-related geologic features of the reservoir, capturing those essential for accurate estimation of flow behavior. Because subsurface data are typically sparse, tools such as geostatistics are often used to create plausible models of geologic property distributions within the geological framework.

Because numerical simulations are dynamic, they demand much greater computing resources compared with the static geologic models. Geologic models have finer resolution and higher block counts compared with simulation models; therefore geomodels can seldom be used in numerical simulations. They are upscaled to obtain a simulation model. If the geomodel is upscaled correctly, the simulation model is an adequate representation

of reservoir geology and computationally efficient enough to enable multiple runs to optimize reservoir development.

Computational resources and modeling techniques are constantly improving. Available CPU speed doubles approximately every 18 months. This means that larger and larger simulation models can be considered. Given this, is it necessary to upscale at all?

Historically, geological models have always been larger than flow models. Geologists do not have to worry about the computational demands of dynamic models, and they are therefore free to build large static models. Furthermore, geologists often include all the features they expect to affect the flow behavior of the model, regardless of the scale of the feature. Hence, reservoir engineers will continue to need efficient and accurate methods for upscaling and numerical reservoir characterization.

Recent research (Li and Beckner, 1999; Cao and Aziz 2001; Col and Muggeridge, 2001) suggests that upscaling is most accurate if coarsening of the grid follows physical behavior observed on the fine resolution model. Rather than considering only porosity and permeability, upscaling should be based on physical driving force in each fine-scale section of the reservoir. Identification of drive mechanisms and resulting recovery traditionally utilized some form of dimensionless numbers making the results comparable between different scales.

Identification of drive mechanisms on the reservoir scale and gridblock scale for simulation optimization purpose requires numerical reservoir characterization methods independent of scale; these methods should consider the differential and difference equations that govern flow in porous media. This form should be able to provide the following:

- Flow characterization independent of scale
- Reduction of number of runs needed to quantify the reservoir behavior
- Ability to estimate numerical behavior independent of scale

Engineers commonly form dimensionless scale groups based on experience. However, for groups to be true scaling parameters, the differential equations governing the flow should be considered. Parameters in dimensionless differential equations called dimensionless scaling numbers meet the three requirements outlined above.

Some developments already exist (*X*-direction by Dake, 1977 and Lake 1989; Z-direction by Hagoort, 1980; *X*-*Z* system, Shook, 1992). No consistent development in three dimensions has been presented. This work provides mathematically succinct form of differential equation developed through Inspectional Analysis (IA). A total of 8 scaling groups are developed. Only 7 of them are shown to completely describe the flow.

The contribution of this work is that we can now use 7 dimensionless rather than more than 30 dimensional variables to analyze local and global reservoir flow and gridding effects. This improves simulation design and sensitivity studies by reducing the number of simulation runs needed to characterize any given reservoir. Observations on response behavior of dimensionless differential equations can be used to construct reservoir flow regime maps. Flow regime maps and analytical observations can now be used to optimize upscaling either through the use of pseudo-functions or uplayering.

CHAPTER 2

LITERATURE SURVEY

2.1. Important concepts for dimensionless numerical reservoir description

To properly characterize and scale a numerical model, one must consider several aspects contained within either the physics or the spatial/temporal differentiation. These are:

1. **Scalability of physical effects**. Scaling laws have to be developed on the reservoir/fluid system that recognizes general flow behavior including balance of viscous, capillary and gravity forces. It should also account for flow effects (flow regimes) that those forces introduce at the initial scale and the effect of extrapolation to the scale of interest.
2. **Scalability of boundary conditions.** Scaling laws have to introduce dimensionless scaling for initial conditions and enable scaling of production response to enable comparison and extrapolation between different scales.
3. **Scalability of reservoir shape.** Scaling laws have to enable comparison between same-shape reservoirs at different scale and account for error if the shape changes between the scales.
4. **Compatibility with existing simulation tools** to make the analytical scaling laws applicable on the numerical model. Factors such as grid geometry and temporally distributed output should be used in a development and boundary condition setting.
5. **Numerical and physical dispersion** must be taken into an account at any particular scale, together with additional dispersion introduced by the change of scale.

To compare the flow effects at different scales, scaling intervals presented in table 2.1 will be accepted and used throughout the work.

Table 2.1. Accepted scale intervals

Scale	Geometry	Size
Small	Core size	10^{-1} - 10^{0} m
Mid	Inter-well	10^{2}-10^{3} m
Large	Reservoir	10^{4}-10^{5} m

2.2. Grids

Numerical reservoir description starts with the definition of the grid. Mattax and Dalton (1990) provide an in-depth overview of the grid types in general. Even though the possibilities for gridding are vast, two types of non-radial grid geometries are accepted as industry standards – rectangular Cartesian geometry (RCG) and non-rectangular corner point geometry (CPG).

Rectangular Cartesian grid is the oldest and the simplest one, still commonly used in simulation practice today (Narayanan et al, 1999, White et al., 2000). Nonrectangular grid systems have been introduced in early seventies (e.g. Hirasaki and O'Dell, 1970, Sonier and Chaumet, 1974) in an orthogonal or near orthogonal curvilinear form to reduce the spatial truncation error. Orthogonal non-rectangular grid remains the standard for industry accepted mapping and geocellular-geological modeling tools such as ZMap™, StrataMap™, Stratamodel™. Further development in mitigating the impact of intricate sedimentary features and faults lead to the introduction of full CPG where a gridblock is represented by geometrically completely independent 8 corner-points cube

. Goldthorpe and Chow (1985), and Kydland et al (1988) who in a way introduced CPG used vectorial approach to determine the inter-block transmissibility. Peaceman (1996) presented the alternate solution by using harmonic integration. Harmonic integration is a simpler and more accurate method of determining the transmissibility, and according to Peaceman it could incorporate the sub-grid permeability anisotropy.

The effect of fine scale anisotropy after upscaling can be observed if the coarse scale flux is compared to a streamline trend in a fine scale grid. Fine scale distribution of permeability distorts the streamlines, so the resulting flux might be offset from the one suggested by local pressure field between large block centroids. White and Horne (1987) suggested the use of full permeability tensor to account for the offset in streamlines due to local sub-grid heterogeneity. Numerical simulation tools offered by vendors are not equipped to handle tensor permeability input, hence the upscaled grid geometry has to accommodate for the anisotropy offset by proper choice of corner points or proper grouping of gridblocks (similar to zonation work of Li et al, 1999) in order to align the flux with the centroid-to-centroid vector.

2.3. Scaling

Scaling is a procedure of extrapolation of results obtained at one scale to another, usually from a small-scale laboratory observation to a large-scale process. Historical developments in the field of fluid mechanics and dynamics point to dimensionless numbers as a mean of comparison. Two succinct and apparently different methods for obtaining dimensionless numbers can be found in the general fluid flow literature. General fluid dynamics literature such as Johnson (1998) and Fox and McDonald (1998) suggests Dimensional Analysis (DA), whereas petroleum related authors such as Shook et al, 1992, rely more on the Inspectional Analysis (IA).

Buckingham (1914) published the breakthrough work on dimensional analysis as a reply to Tolman's publication earlier that year. His Pi Theorem is stated to be the basis (Johnson, 1998) for later solution of Navier-Stokes equation and development of dimensionless numbers such as Reynolds' number, Freud's number etc. Ruark (1935) has published an improved method called Inspectional analysis, based on the brief description in Bridgman's book on Dimensional Analysis.

Dimensional analysis is based on the assumption that physical events and processes must be independent of the measurement scale units. It handles the mathematical portion of the development of the physical relation between the physical variables once the equation satisfies the following form:

$$e_1 = f(e_2, e_3, ...e_n) \tag{2.1}$$

where e_1 is the dependent parameter and e_2, e_3,…e_n are $n-1$ independent parameters. Each of the dependent parameters is a product of primary dimensions or

$$e = \prod_i P_i^{a_i} \tag{2.2}$$

Where P_i denotes primary dimension and a_i denotes the exponent. Functional relationship between dependent parameters can mathematically be expressed in the equivalent form as

$$g(e_1, e_2, e_3, ...e_n) = 0 \tag{2.3}$$

where g is an unspecified function making the conversion to dimensionless form easier. Two steps have to be performed to determine the needed number of dimensionless groups. The first step is determining the total number of primary dimensions designated as r. The

second step involves determining the number of repeating parameters designated as *m*. To determine *m* we need to determine the rank of the following dimensional matrix:

$$m = \therefore \begin{vmatrix} a_{11} & a_{21} & a_{31} & \cdots & a_{n1} \\ a_{12} & & & & \\ \vdots & & & & \vdots \\ a_{1r} & & & \cdots & a_{nr} \end{vmatrix} \tag{2.4}$$

According to Buckingham, the dimensionless form of the equation has to satisfy the following functional form

$$G(\pi_1, \pi_2, \pi_3, ...\pi_{n-m}) = 0 \tag{2.5}$$

where *n-m* denotes the minimum number of independent dimensionless groups (p) needed to specify the dimensions of all the parameters $e_1, e_2, e_3, \ldots e_n$. The algorithm of the dimensional analysis is presented in Figure 2.1.

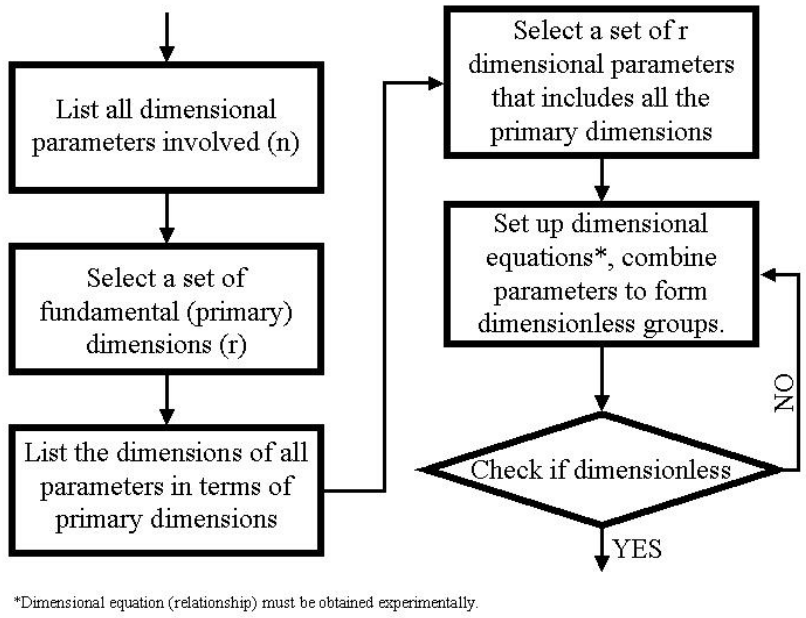

Figure 2.1. Principle algorithm for Dimensional analysis

Inspectional analysis is the extension of dimensional analysis, where a final dimensionless formulation is tested against the variables from which it has been developed. Since in the dimensional analysis we obtain only dimensionless groups without the governing equation (has to be obtained experimentally) and inspectional analysis is based on the existing differential equation with acting boundary it is a simpler and preferred

method in petroleum related literature. Since inspectional analysis is a parameter rather then dimensions procedure it can produce dependent dimensionless scaling groups. To remediate, Shook et al (1992) proposed writing the dimensional matrix for dimensionless groups in a form

$$\begin{vmatrix} \log \pi_1 \\ \log \pi_2 \\ \vdots \\ \log \pi_n \end{vmatrix} = \begin{vmatrix} a_{11}\ a_{21}\ a_{31} \cdots\ a_{n1} \\ a_{12} \\ \vdots \qquad\qquad\qquad \vdots \\ a_{1l} \qquad\qquad \cdots\ a_{nl} \end{vmatrix} \begin{vmatrix} \log e_1 \\ \log e_2 \\ \vdots \\ \log e_l \end{vmatrix} \tag{2.6}$$

Where a_{ij} is the exponent of any primary dimension e_i included in the group π_i. They suggested that reduction in number of dimensionless groups and the final succinct form can be achieved by minimizing the rank of the matrix.

Rapoport and Leas (1953) first published a work on scaling a linear waterflood. Rapoport (1955) continued the work on scaling conditions, this time including both capillary and gravity effects to aid design and interpretation of small-scale multi-phase flow in porous media. His work does not include dimensionless groups *per se* but rather an overview of accepted comparison procedure to enable scalability. Geertsma et al. (1956) introduced the DA and IA into the linear 2-D scaling. His work resulted in 3 independent variables, 6 dependent variables and 12 similarity groups needed to compare flow between scales.

Craig et al (1957) focused on gravity segregation in frontal drives. They neglected the diffusion in the DA/IA and reduced the number of scaling groups to 4. Perkins and Collins (1960) presented a full 3-D development with 5 dimensionless groups describing the flow. Inconsistencies in boundary conditions while formulating dimensionless groups and lack of appropriate full-length inspectional analysis lead to the later development published by van Daalen and van Domselaar (1972) to return to curvilinear flow with crossflow and repeat the scaling procedure. The result was 6 scaling groups in a quasi 2-D system, similar to the latest development by Shook et al. (1992).

Most of the work in the area of scaling that included DA/IA considered a homogeneous isotropic system to simplify the development. Carpenter et al., (1962) experimentally validated the Rapoport's (1955) scaling procedure on a heterogeneous

multi-layer system. Craig et al. (1957) included the heterogeneity in their study on gravity segregation and scaling. Study by van Daalen and van Domselaar (1972) relied also on simplified heterogeneity description, however heterogeneity itself was not represented as a similarity group.

Several attempts were made to characterize the reservoir heterogeneity in dimensionless form. Li and Lake (1996) were the first to include true dimensionless heterogeneity in the scaling process. Flow was characterized using Shook's dimensionless scaling numbers and development extended for scaling the anisotropic environment by defining heterogeneity numbers. Heterogeneity was, however characterized only in two dimensions.

2.4. Two-phase dimensionless numbers in literature

There is a variety of dimensionless numbers published in petroleum literature and based on the flow system they can be divided in two groups – single-phase and two-phase systems. Single-phase systems are used in pressure-test analysis; where *inspectional analysis* enables transformation to dimensionless space for any given set of given boundary conditions. Once dimensionless, the adequate solution for a diffusivity equation can be found. Several textbook authors have tackled non-dimensionality; Lee (1989), Earlougher (1977) and Sabet (1991) to name the few. The later in his book presents an excellent overview of the single-phase systems and solutions.

Unlike single-phase systems where the primary concern is a pressure distribution and the pressure response, two-phase systems are primarily focused on two-phase flow effects such as breakthrough time, breakthrough recovery, dispersion etc. Balance of four forces is controlling the two-phase flow in porous media – viscous, gravity, capillary force and dispersion.

Two-phase flow in porous media has historically looked at several dimensionless variables in order to scale the flow behavior – each capturing a portion of behavior. Overview of basic dimensionless scaling numbers used for a two-phase flow is presented in Table 2.1. General description of the numbers in Table 2.1 can be substantiated by the variety of ways some of the dimensionless numbers are determined in surveyed literature.

Further insight is needed to determine the most appropriate way of formulating the scaling groups so that the resulting numbers will be applicable at any scale.

The first and the finest scale to consider is a pore-scale modeling (Moore and Slobod, 1956, Chatzis and Morrow, 1986 etc.). Basic issue at this scale is the entrapment of wetting and non-wetting phase and determination of residual saturations and scaling groups that control them. The second scale is a medium resolution scale at which the flood front and resulting production behavior is observed (Dietz, 1953, Craig et al., 1957, Hagoort, 1980). Medium scale and large-scale (numerical models) will deal with flow property/barrier distribution (Peters et al., 1998, Pickup et al., 1999, Willis and White, 2000), geometry and effect of these factors on the observed production.

Table 2.2. Overview of basic two-phase scaling dimensionless numbers

	Variable	**Formulation**	**Comment**
Boundary conditions/ response scaling	Dimensionless time	$t_D = \frac{V_{injected}}{V_{pore}}$	Imposed injection boundary condition
	Displacement efficiency (factor)	$E_D = \frac{V_{produced}}{V_{reference}}$	Dimensionless production response
Physical effects scaling	Mobility ratio	$M = \frac{\lambda_{displaced\ fluid}}{\lambda_{displacing\ fluid}}$	Fluid-fluid-rock interaction effect on the flow behavior
	Capillary Number	$N_C = \frac{F_{capillary}}{F_{viscous}}$	Fluid-rock interaction, depicts entrapment at the small scale
	Gravity Number	$N_G = \frac{F_{gravity}}{F_{viscous}}$	Fluid-reservoir shape dependent, captures the effect of buoyant force
Reservoir geometry scaling	Dip	$N_\alpha = \tan\alpha$	Dip angle scaling
	Aspect ratio	$N_A = \frac{Length}{Height}$	Reservoir shape description

Residual or remaining saturations for any given rock are determined through small-scale laboratory-determined Capillary De-saturation Curves (CDC). CDC represents residual saturation of a phase as a function of dimensionless capillary number. Capillary

number varies through the literature and can be based either on statistics (Lake, 1989) or on the empirical Representative Elementary Volume (REV). Since the process of scaling has to incorporate underlying physics, it is prudent to focus the literature survey on empirical models.

Moore and Slobod (1956) proposed the pore doublet model. Based on the assumption of the well-developed Poiseuille flow in different-radii same-length capillaries it overestimates the amount of residual non-wetting phase. Melrose and Brandner (1974) discussed the pore snap-off model as the tool to model entrapment. They included contact angle hysteresis in their calculations. Oh and Slattery (1976) introduced sinusoidal geometry of the porous media. Chatzis et al (1983) used sinusoidal pore snap-off for their experimental work. Geometry of the model and implemented physics do not largely affect capillary number. Overview of small-scale capillary numbers is given in Table 2.3.

Table 2.3. Small-scale capillary numbers

Small scale capillary number		
Capillary number	**Comment**	**Reference**
$N_c = \frac{v \cdot \mu_1}{\sigma \cos\theta}$	Outcrop sandstone, brine-crude system	Moore and Slobod, 1956
$N_c = \frac{v \cdot \mu_1}{\sigma \cos\theta}$	Berea sandstone, brine-soltrol system	Taber, 1969
$N_c = \frac{u \cdot \mu_1}{\sigma}$	Berea sandstone, brine-oil system	Foster, 1973
$N_c = \frac{k \cdot \lvert\vec{\nabla}\Phi\rvert}{\sigma \cos\theta}$	Synthetic media, distilled water-pure organics system	Dombrowski and Brownell, 1954
$N_c = \frac{u \cdot \mu_1}{\sigma}$	Synthetic media, water-pure hydrocarbons system	Du Prey, 1973
$N_c = \frac{u \cdot \mu_1}{\sigma}$	Outcrop sandstone, brine-crude system	Erlich et al., 1974
$N_c = \frac{v \cdot \mu_1}{\sigma \cdot \Delta S} \cdot \cos\theta \cdot \left(\frac{\mu_1}{\mu_2}\right)^{0.4}$	Outcrop sandstone, brine-crude system	Abrams, 1975
$N_c = \frac{u \cdot \mu_1}{\sigma}$	Berea sandstone, brine-decane system	Gupta, 1980
$N_c = \frac{k \cdot \Delta p}{\sigma \cdot L}$	Outcrop sandstone, brine-soltrol system	Chatzis and Morrow, 1981

At the larger scale, Rapaport and Lea (1953) developed the regime indicator for scaling the capillary effects during a large-scale waterflood. Geertsma et al (1956) provided the large-scale capillary number development for both waterflood and thermal flood similar to the small-scale one. Craig et al., (1957) in their study on gravitational segregation developed a capillary number, similar to the dimensionless similarity group developed by Perkins and Collins (1960). The first complete analytical development published by van Daalen and van Doomselaar (1972) omitted the conventional capillary number, however included the similar scaling group. Shook (1992) repeated the procedure without the assumption on negligible effect of small transition zone and recorded a scaling group similar to van Daalen and Domselaar. List of numbers and corresponding author is provided in Table 2.4.

Table 2.4. Medium/large scale capillary numbers

Medium/large scale capillary number		
Capillary number	**Comment**	**Reference**
$N_{RL} = \left(\frac{\phi}{k}\right)^{\frac{1}{2}} \frac{\mu_1 \cdot u \cdot L}{k_{r1}^{o} \cdot \phi \cdot \cdot \sigma_{12} \cdot \cos\theta}$	Capillary dominated regime indicator	Rapaport and Lea, 1953
$N_c = \frac{\sigma_{12} \cdot \cos\theta \cdot \sqrt{k \cdot \phi}}{\cdot \cdot u \cdot \mu_1 \cdot L}$	Similar to small-scale N_c	Geertsma et al., 1956
$R_c = \frac{\mu_1 \cdot q_i \cdot L}{\cdot \sigma_{12} \cdot \cos\theta \cdot \sqrt{k_x}}$	Scaling dimensional number	Craig et al., 1957
$S_c = \frac{k_{r1}^{o} \cdot \sigma}{u \cdot \mu_1 \cdot L_1} \left(\frac{\phi}{k}\right)^{\frac{1}{2}}$	N_c equivalent similarity group	Perkins and Collins, 1960
$N_{Pc} = \frac{\lambda_{r2}^{o} \cdot \sigma}{L \cdot u_T} \cdot \sqrt{\phi \cdot k_x}$	Capillary scaling number	Van Daalen and van Domselaar, 1972
$N_{Pc} = \frac{\lambda_{r2}^{o} \cdot \sigma}{L \cdot u_T} \cdot \sqrt{\phi \cdot k_x}$	Scaling dimensionless number , oil-water system	Shook et al., 1992

Gravity number in surveyed literature has also varied from source to source. Even though the most logical choice would be the use in the case of large density difference (Craig et al, 1955, Hagoort, 1980), and complete abandonment in two-liquid system,

several authors (Pozzi and Blackwell, 1963, Peters et al., 1998) have considered the gravity number in two-liquid system development. Justification can be found in the aspect ratio and permeability dependence in some of the gravity numbers found in the surveyed literature. Shook et al. (1992) have directly shown the effect of dip and aspect ratio greatly amplify the gravity effect, as depicted in Figures 2.2.and 2.3.

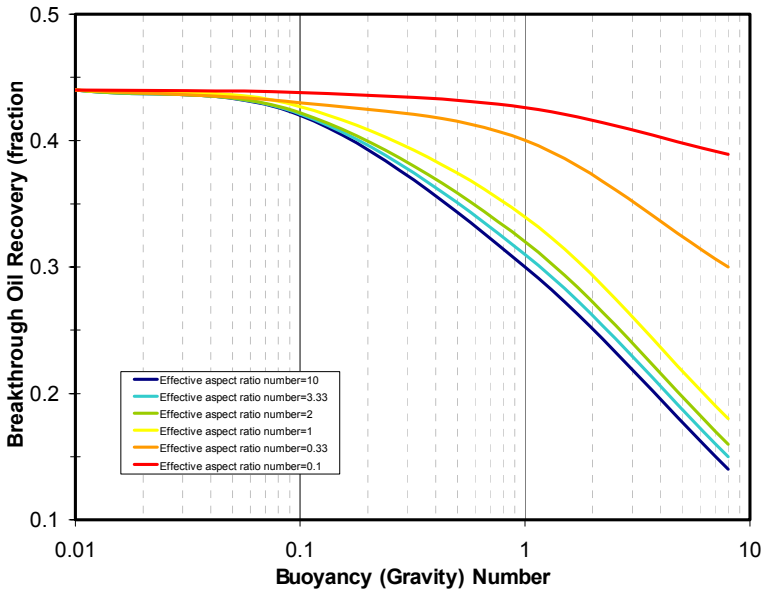

Figure 2.2. Breakthrough recovery as a function of gravity number and aspect ratio

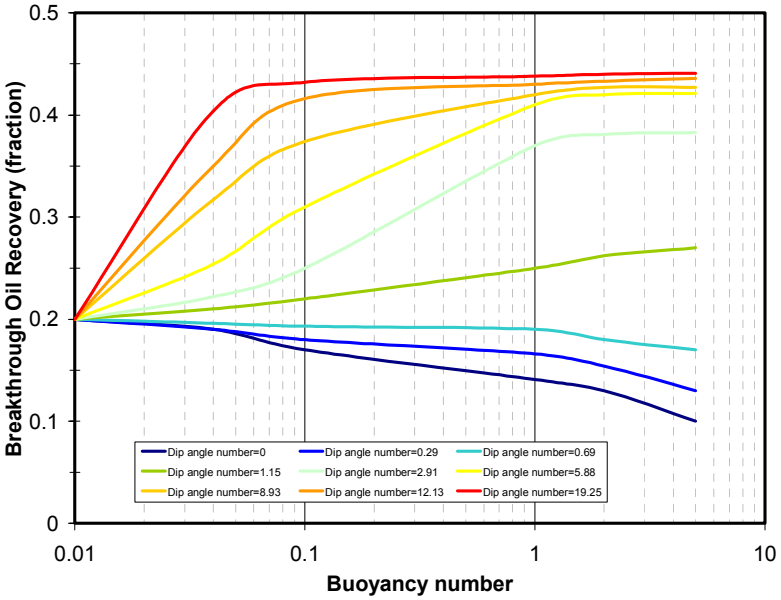

Figure 2.3. Breakthrough recovery as a function of gravity number and dip

Table 2.5. Gravity number in Petroleum engineering

Gravity Number	Comment	Reference
$N_g = \frac{\Delta\rho \cdot k_x \cdot \lambda_{T1}}{u_T}$	Not dimensionless	Rapoport, 1955
$N_g = \frac{\Delta\rho \cdot g \cdot k_x \cdot \lambda_{T1}}{u_T}$		Engleberts and Klinkenberg, 1951, Crocs and Schwartz, 1955
$N_{g1} = \frac{\rho_1 \cdot g \cdot k_x \cdot \lambda_{T1}}{u_T}, N_{g2} = \frac{\rho_1}{\rho_2}$		Geertsma et al., 1956
$N_g = \frac{u_T}{\Delta\rho \cdot g \cdot \sqrt{k_x \cdot k_z} \cdot \lambda_{T2}}$	Zero dip	Craig et al., 1957, Spivak, 1974
$N_g = \frac{\Delta\rho \cdot g \cdot k_x \cdot \lambda^o_{T1}}{u_T} \cdot \frac{H}{L}$		Perkins and Collins, 1960
$N_g = \frac{q}{\Delta\rho \cdot k_x \cdot \lambda_{T1} \cdot L^2}$	Not dimensionless	Carpenter et al., 1962
$N_g = \frac{u_T}{\Delta\rho \cdot k_x \cdot \lambda_{T2}} \cdot \frac{L}{H}$		Pozzi and Blackwell, 1963
$N_{g1} = \frac{\rho_2 \cdot g \cdot k_x \cdot \lambda_{T2}}{u_T}, N_{g2} = \frac{\rho_2}{\rho_s}$	Zero dip, solvent flood (index s)	Greenkorn, 1964
$N_g = \frac{u_T}{\Delta\rho \cdot g \cdot k_z \cdot (\lambda_1 + \lambda_3)}$	WAG process (injected gas is phase 3)	Stone, 1982
$N_g = \frac{\Delta\rho \cdot g \cdot k_z \cdot \lambda^0_{T1}}{u_T} \cdot \frac{L}{H}$		Wellington and Vinegar, 1985
$N_g = \frac{u_T}{\Delta\rho \cdot g \cdot k_x \cdot \lambda_{Ts}} \cdot \sqrt{\frac{L}{H}}$	Zero dip, solvent flood (index s)	Newley, 1987
$N_g = \frac{\Delta\rho \cdot g \cdot k_x \cdot \lambda^0_{f2}}{u_T}$	Derived using 1D fractional flow theory	Lake, 1989
$N_g = \frac{\mu \cdot u_T}{\Delta\rho \cdot g \cdot k_x} \cdot \frac{L}{H}$		Sorbie et al., 1990
$N_g = \frac{\Delta\rho \cdot g \cdot k_x}{\mu_2 \cdot u_T} \cdot \frac{H}{L}$		Yortsos, 1991
$N_g = \frac{\Delta\rho \cdot g \cdot k_x \cdot \lambda^0_{f2} \cdot \cos\alpha}{u_T} \cdot \frac{H}{L}$	Buoyancy number	Shook et al., 1992

2.5. Dispersion

When the idea of miscible displacement as a possible Enhanced Oil Recovery (EOR) method made its debut, several authors recognized the dispersion in the displacement as an important parameter in scaling the experimental data. Pozzi and Blackwell (1963) developed the basic scaling criteria adding the dispersion-scaling groups to those developed by Geertsma et al (1956) and Craig et al (1957. Warren and Skiba (1964) appraised the macroscopic dispersion effect on the flood performance. Perkins and Johnston (1965) presented a review of dispersion in different artificial porous media, with special attention given to scaling longitudinal and transverse dispersion. Lake and Hirasaki (1979) revisited the problem from the aspect of heterogeneity, analyzed dispersion and offered analytical solution for multi-layer system. Peters et al (1998) approached the problem experimentally and used dimensionless scaling numbers published by Shook et al (1992) to describe the scaling of dispersion in a two-layer system.

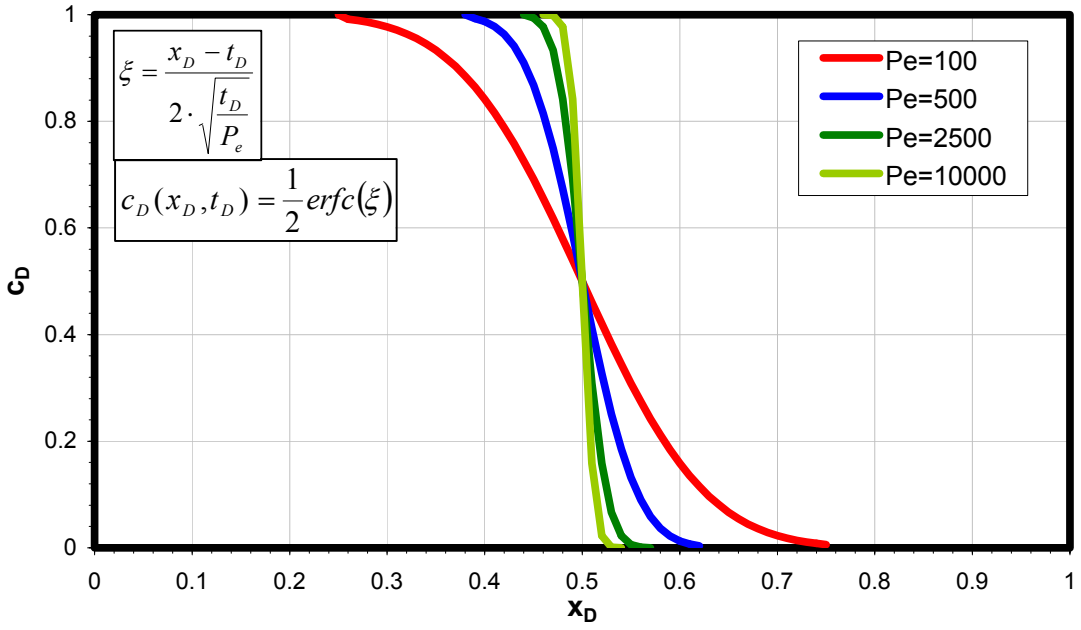

Figure 2.4. Concentration front as a function of Pecklet's number

Rather than the change in concentration, immiscible displacement deals with the dispersion introduced by a local heterogeneity at a large scale and capillary/viscous forces at the small scale. Lake's (1989) solution to advection-diffusion equation shown in Figure

2.6 can be compared to a fractional flow response curve at the production boundary as a function of time. Similarity in shape introduces the possibility of estimation of a dispersion based solely on mathematical analysis. Instead of comparison to Lake's solution through spatial saturation distribution re-creation (e.g. using method by Johnston et al., 1952), we can look at similitude through comparison between a large-scale capillary number and Pecklet's number. Assuming stationary boundary conditions (constant velocity) Pecklet's number – ratio of convective to dispersive transport - can be calculated as

$$N_{Pe} = \frac{u \cdot L}{\phi \cdot D} \tag{2.7}$$

Taking the most succinct definition from table 2.3 (Shook et al, 1992), capillary number – ratio of capillary to viscous transport - can be defined using the following equation

$$N_{Pc} = \frac{\lambda_{r2}^{o} \cdot \sigma}{L \cdot u_T} \cdot \sqrt{\phi \cdot k_x} \tag{2.8}$$

Assuming that capillary-to-viscous force ratio dominates the dispersion in the immiscible displacement, the comparison between two numbers yields

$$N_{Pc} \propto N_{Pe}^{-1} \tag{2.9}$$

Substituting 2.8 into 2.7, dispersion can be estimated as

$$D_{Pc} \propto \sqrt{\frac{\phi}{k_x}} \cdot \frac{1}{\lambda_{r2}^{o} \cdot \sigma} \tag{2.10}$$

Once the differential is substituted by a difference, the procedure introduces another form of dispersion – numerical dispersion. Lantz (1971) in his work discusses the numerical dispersion (truncation error) introduced by finite-difference approximation of differential equation. Lantz has divided the total dispersion in two additive terms, physical dispersion D' and numerical dispersion (truncation error). Hence, the total dispersion can be represented as

$$D = D' + D^{*} \tag{2.14}$$

Note that Lantz's diffusivity (dispersion) is a dimensionless number originating from equation 2.15 and represents the inverse of Pecklet's number.

$$D\frac{\partial^2 c_D}{\partial x_D{}^2} - \frac{\partial c_D}{\partial x_D} = \frac{\partial c_D}{\partial t_D} \tag{2.15}$$

We can observe that Lantz's diffusivity is actually inverse of Pecklet number. Therefore, assuming that inverses of Pecklet number are additive, we can define Pecklet error number as

$$N_{Pe}^{*} = \frac{1}{D^{*}} \tag{2.16}$$

Where numerical truncation error D* for different spatial and temporal finite difference forms for miscible and immiscible cases can be found in Table 2.5.

Table 2.6. Numerical dispersion estimate

Difference Form		**Error Forms (D*)**	
Spatial	**Time**	**Miscible**	**Immiscible**
Backward difference	Explicit	$\left(\frac{\Delta x - \Delta t}{2}\right)$	$\frac{df_w}{dS_w}\left(\frac{\Delta x}{2} - \frac{df_w}{dS_w}\frac{\Delta t}{2}\right)$
Central difference	Explicit	$-\frac{\Delta t}{2}$	$-\left(\frac{df_w}{dS_w}\right)^2\frac{\Delta t}{2}$
Backward difference	Implicit	$\left(\frac{\Delta x + \Delta t}{2}\right)$	$\frac{df_w}{dS_w}\left(\frac{\Delta x}{2} + \frac{df_w}{dS_w}\frac{\Delta t}{2}\right)$
Central difference	Implicit	$\frac{\Delta t}{2}$	$\left(\frac{df_w}{dS_w}\right)^2\frac{\Delta t}{2}$

2.6. Flow Regimes

Underground hydraulics and flow regime description is not limited to petroleum engineering only. Johnson (1998) presents the work of Ng when discussing flow regimes in porous media flow. Unlike petroleum related literature that looks at the flow regime at the large scale, Ng focuses on small-scale gas-liquid system. As depicted in Figure 2.5 Ng identified four flow regimes based on visual observations from flows on different sand-packs rather than from production behavior.

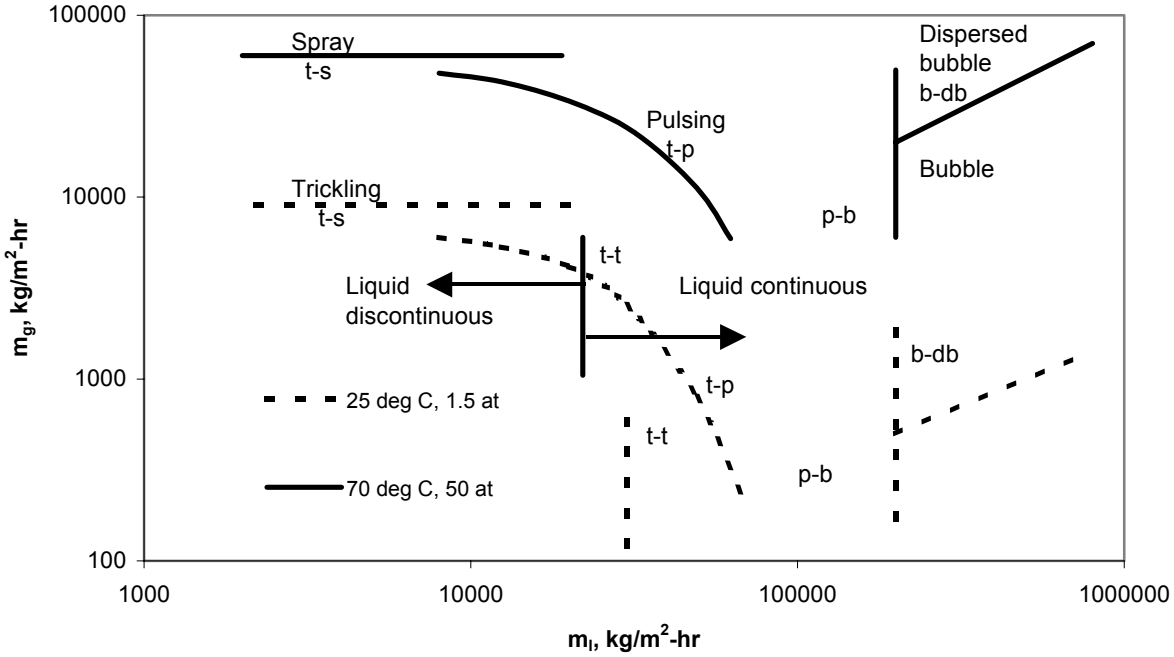

Figure 2.5. Liquid-gas flow regimes at small scale as a function of a fluid mass-flux (from: Johnson, 1998)

Trickling flow regime (t) occurs when the liquid flows over the particles and gas flows in the remaining pore space. *Pulsing flow regime* (p) occurs when the gas and liquid slugs traverse the column alternatively. The flow channels become plugged by the liquid slugs which are blown off by the gas plugs. In the *Spray flow regime* (s) the liquid travels down the column in the form of droplets entrained by the continuous gas phase. The gas flow is turbulent. *Bubble/dispersed-bubble* (b/db) regimes have the gas phase flowing as slightly elongated bubbles. As the gas flow rate increases, the bubbles become highly irregular in shape.

Ng's representation using liquid and gas mass-flux is a snapshot for a particular rock type since they do not offer a way of scaling the capillarity. Also, a global effect on the recovery is neglected. Lenormand et al. introduced the concept of ``phase-diagram'' in 1988 for small-scale drainage displacements where various experiments and simulation were plotted in a plane with the capillary number along the x-axis and the viscosity ratio along the y-axis. The plot, reproduced in Figure 2.6 clearly shows that the different

structures they obtained divide into the major flow regimes whose region of validity in capillary number and viscosity ratio space is given by the plot.

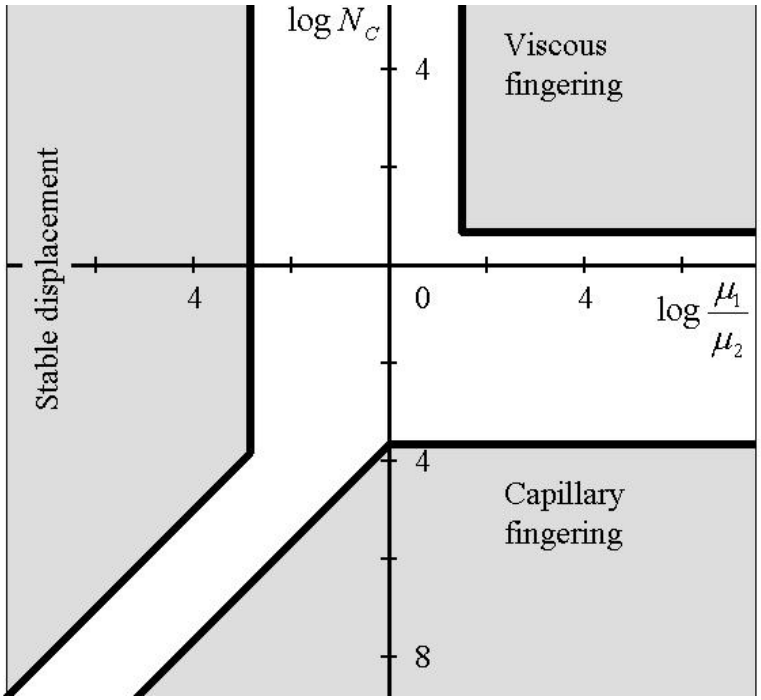

Figure 2.6. Flow regime map as a function of capillary number and viscosity ratio (from: Lenormand et al., 1988)

The boundaries of the regions were qualitatively discussed and they concluded that the drainage displacements where fully characterized by capillary number and viscosity ratio. However, it was mentioned that changing the pore size distribution of the simulation and the experiments resulted in translations of the boundaries but that the general shape should remain unchanged. The capillary number Lenormand and others used does not take into account the pore size distribution and a careful analysis is required to understand better this effect before any complete "phase-diagram" can be drawn.

Stable displacement has earlier been investigated by Dietz (1953). Based on the analysis of the flow under segregated conditions, he was able to establish the general dimensionless range for segregated flow in dipping reservoir. Stable range can be determined by

$$G > M - 1,\ M > 1,\ \beta < \theta \tag{2.17a}$$

$$G > M - 1,\ M < 1,\ \beta > \theta \tag{2.17b}$$

Where G is dimensionless gravity number, M is mobility ratio, b is displacement front angle and θ is dip angle.

Unlike Lenormand and Ng, Li *et al* (1993) used an approach based on dimensional analysis of heterogeneity on a statistically generated numerical reservoir. Instead of flow-regime description founded on the balance of local viscous-capillary-gravity-dispersive forces, they acknowledged the effect of heterogeneity only.

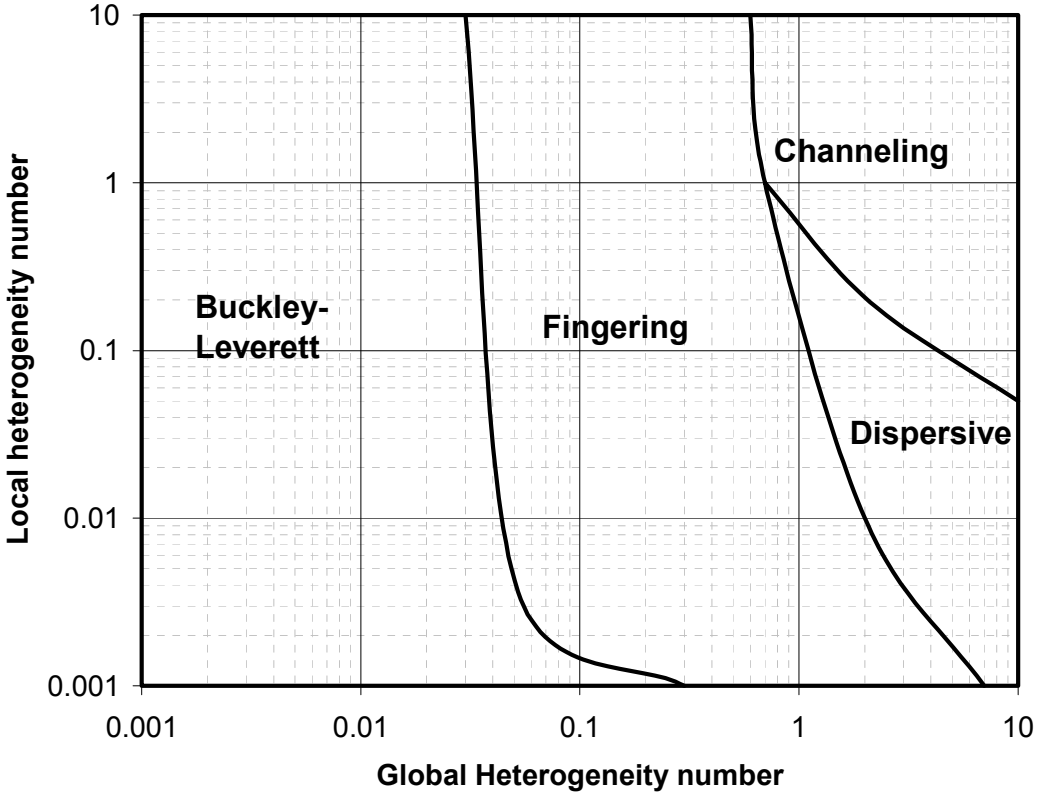

Figure 2.7. Flow regimes as a function of local and global heterogeneity (from Li et al., 1993)

Even though they captured the effect of heterogeneity on a recovery, they neglected the force balance captured in the adopted dimensionless formulation of the flow equation. Coll *et al* (2000) approached this problem using the fractional flow equation and the dimensionless scaling numbers adopted from Shook et al. (1992). Their work has been in regional upscaling, however it can be used in determination of flow regimes. They defined the flow regime based on the dominant force governing the flow. The overview of ranges is presented in Table 2.7.

Table 2.7. Gravity and Capillary dominated flow regime (from: Coll *et al.*, 2000)

Flow	Boundaries	Condition	Regime
Longitudinal	$N_{gcutoff} = \frac{\varepsilon_1}{L \cdot \sin\alpha} \cdot \lambda_{ro}^{o} \cdot \left(\frac{\lambda_{ro} + \lambda_{rw}}{\lambda_{ro} \cdot \lambda_{rw}} \right) \cdot H \cdot \cos\alpha$	$N_g > N_{gcutoff}$ $f_w << 1$ $N_{Pc} < N_{Pccutoff}$	Gravity dominated
	$N_{Pccutoff} = \frac{\eta_1 \cdot \lambda_{rw}^{o}}{\frac{\partial S_w}{\partial x}} \cdot \left(\frac{\lambda_{ro} + \lambda_{rw}}{\lambda_{ro} \cdot \lambda_{rw}} \right)$	$N_g < N_{gcutoff}$ $f_w << 1$ $N_{Pc} > N_{Pccutoff}$	Capillary dominated
Transverse	$N_{gcutoff} = \frac{\varepsilon_2 \cdot \left(\frac{v_t}{u_t} \right)}{\frac{L}{H} \cdot \left(\frac{k_z}{k_x} \right)} \cdot \lambda_{ro}^{o} \cdot \left(\frac{\lambda_{ro} + \lambda_{rw}}{\lambda_{ro} \cdot \lambda_{rw}} \right)$	$N_g < N_{gcutoff}$ $f_w << 1$ $N_{Pc} > N_{Pccutoff}$	Gravity dominated
	$N_{Pccutoff} = \frac{\eta_2 \cdot \left(\frac{v_t}{u_t} \right)}{\left(\frac{k_z}{k_x} \right)^{\frac{1}{2}} \cdot \frac{\partial S_w}{\partial z}} \cdot \lambda_{rw}^{o} \cdot \left(\frac{\lambda_{ro} + \lambda_{rw}}{\lambda_{ro} \cdot \lambda_{rw}} \right)$	$N_g < N_{gcutoff}$ $f_w << 1$ $N_{Pc} > N_{Pccutoff}$	Capillary dominated

Compared to the work of Lenormand, Coll and others introduced the gravity number as another important dimensionless parameter in flow regime determination. The use of dimensionless numbers in Coll's method enables general scalability of flow-regime cutoff values, however the approach has two case-dependent variables - ε and η. They have to be determined by running series of simulations in both homogeneous and simple layered models for a case of interest.

2.7. Upscaling

Upscaling is a reverse scaling process. Usually, scaling process involves extrapolation from a limited amount of data to cover the global behavior. Upscaling deals with abundant data within a frame being upscaled and averages all the values within the frame to a set of representative flow parameters. This way the number of gridblocks in a model is reduced by fore mentioned reduction in horizontal and/or vertical resolution. Goal of upscaling is to achieve the balance between the number of cells needed for the accurate representation of the reservoir and CPU time needed for calculation.

2.7.1. Single phase upscaling

Single phase upscaling scales only the absolute permeability. The simplest form of single-phase upscaling is pressure solver method. This method sets up a single-phase flow system with specified boundary conditions and then determines the value of effective permeability yielding the same flow rate as a fine-grid system. Results we obtain will depend on boundary conditions. In this case, vertical no-flow boundary condition is most commonly used. Christie (1996) mentions the following procedure:

-Set up a matrix to solve

$$\nabla \cdot k(\vec{x}) \nabla p = 0 \tag{2.18}$$

Boundaries are no-flow at the side with p=1 and p=0 at the inlet and outlet respectively.

-The effective permeability is then given by

$$k_e^x = -\frac{\Delta x \mu q}{A} \tag{2.19}$$

To evaluate all three directional permeabilities the setup is repeated for the remaining two directions. This approach is simple, and as reported by some authors (Begg et al, 1989, Christie, 1996) it results in values close to those obtained by history matching.

Alternatively some authors (Durlofsky, 1994, Pickup, 1992) prefer the use of periodic boundary conditions and full-tensor permeability. The approach is significantly more accurate, however most vendor simulators do not support direct input of a permeability tensor; hence the method is used more in academic environment.

Renormalization technique pioneered by King (1989) is similar to a procedure used in resistor network reduction. It is a stepwise procedure where very fine grid is slightly coarsened, then the resulting coarsened one is re-coarsened and the procedure is repeated until the desired resolution is reached. The method is faster, however it is less accurate.

Streamline method is based on the use of streamtubes derived from a single-phase fine grid simulation. It basically indicates the direction of fluid movement throughout the reservoir. Some authors, such as King (1997) use streamlines to include the effects of gridding in the upscaling effort. Others like Hewett and Yamada (1996) use streamlines bounded to grid to determine pseudo functions. Streamlines can also indicate the density of flow and hence point to regions in the model that need to be of finer resolution.

Method of zonation has been visually performed by many and preferred by some engineers for a long time. The approach was to visually group the layers before the actual model was build and it was used to reduce the vertical resolution of the model. Testerman (1962) published a statistical technique to identify and describe naturally occurring zones in a reservoir and to correlate these between wells. This method has two steps and reportedly can handle crossflow. During zonation (the first step), the set of permeability data from the wells is divided into zones. Zones are selected in such manner that variation between the layers in the zone is minimized, while the variation between zones is maximized. The following equations are recommended:

$$B = \frac{1}{L-1} \cdot \left[\sum_{i=1}^{L} m_i \cdot \left(\overline{k_i} - \overline{k} \right)^2 \right] \tag{2.20}$$

$$W = \frac{1}{L-1} \cdot \left[\sum_{i=1}^{L} \sum_{j=1}^{m_i} \left(k_{ij} - \overline{k_i} \right)^2 \right] \tag{2.21}$$

$$R = \frac{B-W}{W} \tag{2.22}$$

Variable B denotes variance between the zones, L number of zones, indices i and j are summation indices for number of zones and number of layers within each zone respectively. R is the zonation index, indicating homogeneity when it is closer to 1.0, m_i number of data within the zone, W is a pooled variance within zones, N total number of data and k_I and k are averages for the zone and the whole well, respectively.

Once the zones have been chosen, Testerman suggests the second step - correlation across the reservoir. The correlation of zones between adjacent wells is based on comparison of the difference of the means. Zones are correlated if the difference of the means is less than or equal to one expected from the individual data variation or if

$$\left(\overline{k_h} - \overline{k_i} \right) \geq \sqrt{\frac{1}{2} \cdot \left(\frac{1}{n_h} + \frac{1}{n_i} \right)} \cdot \sigma \cdot z(v, p) \tag{2.23}$$

Where k_h and k_i are the average of h zone of one well and i zone of another, n is a number of layers within the zone, σ is standard deviation for the whole reservoir and z(v,p) defines z values for given probability level.

2.7.2. Two-phase upscaling

Unlike the single phase upscaling that only accounts for the variation in absolute permeability, two-phase upscaling accounts for the dispersion effect of permeability variation on the two-phase flow. Li et al (1999, 2000) have extended Testerman's work. They used residuals as a measurement of accuracy of upscaling and instead of applying it only for permeability they applied it independently on two upscaling properties: displacing front conductivity (DFC) and facieses rules (FR). Authors suggest the following to estimate the parameters:

$$R = \sum_{k=1}^{n_z} \frac{\left(\overline{p_k^c} - \overline{p_k^f}\right)^2}{n_z} + w \sum_{k=1}^{n_z} \frac{\left(\sigma_k^c - \sigma_k^f\right)^2}{n_z} \tag{2.24}$$

Where R is residual function, p and σ are mean and standard deviation for the uplayering property of interest and w is weight varying between 0 and 1. Uplayering properties, as defined by Li et al. are defined as:

$$DFC = \frac{k_h}{\phi} f'\left(S_f\right) \tag{2.25}$$

$$FR = a\frac{k_h}{\phi} + r \tag{2.26}$$

Where k_h is horizontal permeability, ϕ porosity and r is discriminating rule for facies. Parameter a is defined as

$$a = \frac{b}{\left(\frac{k_h}{\phi}\right)_{\max}} \Delta r \tag{2.27}$$

Where max denotes maximum value among upscaled layers and b denotes scaling number varying between 0 and 1.

Comparison between this method and the one where variance was neglected and decision was made to average by keeping certain constant thickness is presented in Figure 2.6. Li's method will preserve the geological features such as shale streaks; however, optimization of the method includes assigning arbitrary values such as b and r without clear analytical mean of determination.

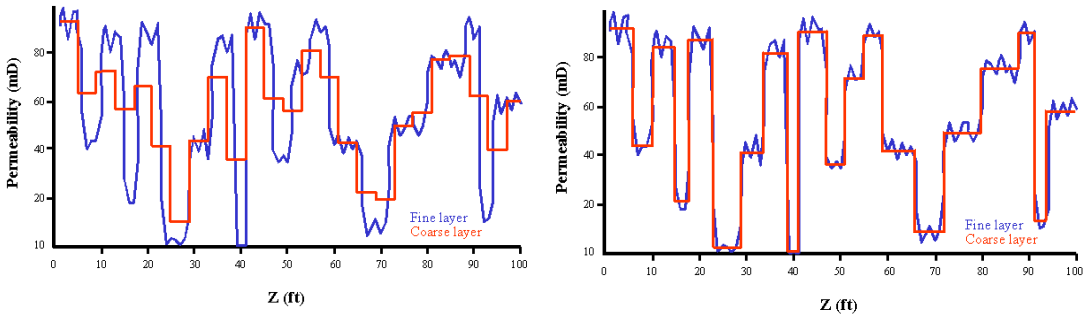

Figure 2.8. Random lumping vs. zonation (uplayering)

The last method suggested by the literature is a pseudo-function model. Pseudo functions result from observations that by replacing the distribution of permeability with an average value, reservoir behavior using intrinsic relative permeability curves yields a result that differs from initial or downscaled. In order to remediate the behavior changes are made to relative permeability curves. Using pre-set boundary conditions expected at the time of simulation and different estimation methods, we end up with set of relative permeabilities called pseudo functions. They differ from the intrinsic rock curves, however during the simulation with boundary conditions corresponding to ones used for their estimation models simulating reservoir behavior supposedly yield results similar to the original (downscaled) case. The overview of equations for some of the methods is given in Table 2.8.

The development of pseudo-function related upscaling begun with vertical equilibrium pseudo relative permeability proposed by Coats et al (1967, 1971). Authors proposed that pseudo-relative permeability is permeability weighted average of the point relative permeability, and is obtained by integration over the thickness of the reservoir. Important assumption is a vertical communication within the reservoir.

Jacks et al (1972) have introduced a method that calculates pseudo relative permeabilities based on assumption that reservoir behavior can be simulated by a 2D model. Since the pseudo functions are calculated at the certain flow potential they are called dynamic. They developed a technique that looks at the vertical saturation distribution, upscaling in vertical direction and that way reducing a number of cells. The simulation is run under conditions that are representative of those to be expected during

time periods to be covered. Needless to say, pseudo-relative permeabilities calculated that way could not be used for a prolonged simulation time period, nor could they cover a change in production setting such as changes in rates or additional wells. To generate the pseudo functions for the cross-sectional model the governing equations are applied to each vertical stack of fine grid blocks at a number of time steps.

Kyte and Berry (1975) published an improvement over Jacks' pseudo relative permeability model. Kyte and Berry attempted to overcome the assumption of equal potential in all of the vertically stacked blocks by estimating coarse grid pressures from fine grid pressures and using them to calculate coarse grid potential differences. These potential differences are then used to calculate pseudo relative permeability from Darcy's law. In addition to coarsening in vertical direction, this method simultaneously coarsens the areal grid. This is done by computing the pseudo saturations as pore volume weighted averages over the entire fine grid system lying within a coarse grid while evaluating flowrates only at the coarse grid boundary.

Stone (1991) published a critical overview of the previous work in the area of pseudo relative permeabilities. He has suggested abandoning the use of pressure potentials in the calculations and initiated the use of fractional flow. The method resembles the previous only in assumptions concerning flow through the upscaled area. To match the pressure level throughout the reservoir the coarse grid potential gradient is made a transmissibility/total mobility weighted average (accomplished by making the total pseudo mobility a transmissibility weighted average of the small ones).

There are many other methods published so far. For instance, pore volume weighted method, similar to Kyte and Berry method, uses a pore volume weighted method to calculate upscaled pressure, while Kyte and Berry use the product of effective permeability and thickness. Guzman et al (1994) proposed a flux weighted potential method. Hewett and Yamada presented a two-dimensional, semi-analytical method that does not specifically require calculation of streamlines. Even though this method considers two-phase system streamlines are designed by independent fine grid single-phase run. The single-phase transmissibility T' of each streamtube segment is first determined from the

results of a single-phase oil-flood simulation. Overview of several different pseudo functions is given in Table 2.8.

Table 2.8. General overview of pseudo functions

Pseudo function	**Corresponding saturation**	**Comment**
$(k_{ro})_{pseudo} = \frac{\sum_k (T_x k_{ro})_k}{\sum_k T_{xk}}$	$(S_w)_{pseudo} = \frac{\sum_k (V_p S_w)_k}{\sum_k V_{pk}}$	Coats (1967)
$(-T_x \frac{k_{ro}}{\mu_o} \Delta\Phi_o)_{pseudo} = -\sum_k T_{xk} \frac{K_{rok}}{\mu_o} \Delta\Phi_{ok}$ $(T_x)_{pseudo} = \sum_k T_{xk}$	$(S_w)_{pseudo} = \frac{\sum_k (V_p S_w)_k}{\sum_k V_{pk}}$	Jacks et al (1972)
$(q_o)_{pseudo} = \sum_k q_{ok} = -(\frac{T_x k_{ro}}{\mu_o} \Delta\Phi o)_{pseudo}$ $(k_{ro})_{pseudo} = -(\frac{\mu_o}{T_x \Delta\Phi_o})_{pseudo} \cdot \sum_k q_{ok}$	$(S_w)_{pseudo} = \frac{\sum_i \sum_k (V_p S_w)_{ik}}{\sum_i \sum_k (V_p)_{ik}}$	Kyte and Berry (1975)
$(\lambda_t)_{pseudo} = \frac{\sum_j \sum_k (T_x \lambda_t)_{jk}}{\sum_j \sum_k (T_x)_{jk}}$	$(S_w)_{pseudo} = \frac{\sum_i \sum_k (V_p S_w)_{ik}}{\sum_i \sum_k (V_p)_{ik}}$	Stone (1991)
$\overline{p_p} = \frac{\sum_j \left[V\phi\left(p_p + \rho_p g H\right)\right]_j}{\sum_j (V\phi)_j}$	$\overline{S_p} = \frac{\sum_i \sum_k \left[V\phi S_p\right]_{i,k}}{\sum_i \sum_k (V\phi)_{i,k}}$	Pore Volume Weighted Average, k_r and P_c similar to Kyte and Berry
$\overline{\Phi_p} = \frac{\sum_k \left[q_p \Phi_p\right]_k}{\sum_k (q)_k}$ $\overline{p}_{c,o/w} = \overline{\Phi}_o - \overline{\Phi}_w - g \cdot \Delta\overline{\rho_{ow}} \cdot \Delta\overline{D}$ $\overline{k_{rp}} = -\frac{\mu_p \sum_k \left[q_p\right]_k}{\overline{T} \cdot \Delta\overline{\Phi}_p}$	$(S_w)_{pseudo} = \frac{\sum_i \sum_k (V_p S_w)_{ik}}{\sum_i \sum_k (V_p)_{ik}}$	Guzman (1994)
$\overline{\lambda}_o = \frac{\sum_\psi (T' \lambda_o)_\psi}{\overline{T}}$, $\overline{\lambda}_w = \frac{\sum_\psi (T' \lambda_w)_\psi}{\overline{T}}$	$(S_w)_{pseudo} = \frac{\sum_i \sum_k (V_p S_w)_{ik}}{\sum_i \sum_k (V_p)_{ik}}$	Hewett and Yamada (1999)

2.8. Comment

In a multi-phase system each gridblock is conceptually defined by more than 30 variables. Upscaling methods presented earlier consider only a small fraction - effective and relative permeability. All the upscaling methods are not only a function of permeability or saturation but also initial conditions, aspect ratios, flow regime, heterogeneity etc. One of the main limitations in upscaling is that it usually gives an answer with almost no indication of whether the assumptions made in derivation process hold. Limited attempts have been made to analyze upscaling process but so far no good theory exists to show that the upscaled value the validity interval for approximation.

In general, pseudo functions are generated for given boundary conditions (well placement, rate). They depend on their assigned coarse rock properties and their placement within the reservoir. The simplest method would be to have pseudo functions generated for each coarse gridblock. Since they are dependent on boundary conditions, they can be used only for brief period of time. Several authors (Guzman et al, 1996, Barker and Thibeau 1996) have dealt with the evaluation and application of pseudo functions.

In terms of behavior Stone's method uses inconsistent set of equations when gravity and capillary terms are included, however it behaves better then Jacks' or Kyte and Berry's method. Also, it is not unusual for the last two to exert some unphysical behavior of pseudo relative permeability functions. For example, pressures in two sections, when averaged, can be the same at the coarser scale, however flow rates at fine scale are not equal to zero since there is a flow potential. That yields a pseudo permeability curve equal to infinity. There is a reported problem (Guzman, 1996) with pseudo functions being bigger than 1, less than zero or non-monotonic, things that can test how robust the simulation models are.

Some authors such as Peaceman (1996) have suggested normalization as a way to fix problems with the use of pseudo functions. The normalization is critiqued by others (Guzman et al., 1996), stating that re-normalization would introduce additional systematic error due to the artificial boundary conditions imposed on each block at each re-normalization (e.g. no flow or constant pressure). Suzuki and Hewett (2000) have also recognized boundary conditions as important parameter in determining the pseudo

functions. They have developed a method that shifts coarsening back and forth. The interval that yields negative pseudo function for given boundary conditions is neglected if it is short, or the grid is re-coarsened if the interval is long. They have also recognized the importance of flow regime on the behavior of pseudo functions. Their method behaves well under viscous-dominated flow, however under gravity dominated flow model has a problem representing the local saturation history.

Several general observations can be drawn:

1. Each coarse block might require its own set of pseudo functions since they depend on both position and heterogeneity. Having a different set of pseudo functions for every coarse grid block could be troublesome so the suggestion is to group coarse grids into several rock types, each of which has just one set of pseudo functions (or one set for each direction). Easier step in preventing the abundance of pseudo functions is the use of flow regime as a mean of grouping, similar to uplayering (Li et al, 1999).
2. Complete fine grid model cannot be run so the logical step is to run smaller regions in order to generate pseudo functions. Accuracy of prediction will depend on our ability to estimate behavior (boundary conditions) at this given moment and position. Thibeau et al (1995) introduced the concept of dual scale simulation for upscaling, which decreased error and computation time. The prediction would be more accurate if there was an *a-priori* physical mean of behavior estimate.
3. The process of constant regeneration of pseudo functions with changes in well placement or rates might make them unaffordable. We should be able to run model on pseudo functions for longer time periods. This is possible only when there are no significant changes in well rates or positions.

To make use of dimensionless numbers in the upscaling and general scaling procedures, numbers have to be developed using useful boundary conditions. Perkins and Collins (1960) applied flow boundaries at all 3 faces, however their numbers are not succinct nor applicable at all scales. Geertsma et al. (1956) development provides a useful and complete insight, however a large total number of scaling groups for only a 1-D system indicates a need for a further development in terms of determining and eliminating dependent scaling groups and hence reducing the number of dimensionless variables. The

most succinct development to date presented by Shook *et al* (1992) has already been used as a base for upscaling effort by Coll and others.

As reported in literature (Cao and Aziz, 1999, Coll *et al*, 2000) upscaling schemes are flow regime dependent. Flow regime definition in literature is dependent on reservoir heterogeneity assessment and flow effects captured in flow equations. Dimensionless scaling effort based on the analysis of flow equations could be used to define flow regimes as the balance of local forces in a homogeneous system, put in a dimensionless form. Once heterogeneity is introduced, it will contribute to the global flow behavior, however local behavior will still be controlled by a set of dimensionless variables. None of the authors except for Lantz dealt with types of effects expected once the reservoir is discretized and solved using either one of accepted solution methods (IMPES, Implicit).

Boundary conditions imposed in the dimensionless development in all of the published work are not comparable to the actual simulation boundary conditions and hence the resulting numbers are not useful in their present form as a tool of estimation and prediction of model behavior. A new 3-D development is needed, with boundary conditions similar to those expected in numerical models, enabling better estimate of performance, scaling, and error prior to actual simulation run.

CHAPTER 3

DIMENSIONLESS NUMBERS

The flow behavior to be expected in reservoir simulation models can be related to the dimensionless scaling groups of the partial differential equations for flow in porous media. This chapter presents development of the dimensionless scaling groups for application in analysis of reservoir simulation models.

Dimensionless numbers can be developed using dimensional or inspectional analysis (Johnson, 1998; Fox and McDonald, 1998; Shook et al., 1992). Dimensional analysis determines the minimum number and form of scaling groups based on the primary dimensions of any physical system (Fox & McDonald, 1998). These groups do not predict the physical behavior of the system - they simply scale it. Dimensional analysis is widely used in experimental design and analysis. Groups from dimensional analysis can be joined to form global dimensionless groups, which can be more easily interpreted physically (e.g. N_{RL} by Rapoport and Lea, 1953; G reported by Dietz, 1953). Fluid dynamics researchers (Fox and McDonald, 1998) recommend experimentation to determine the final form of physically meaningful dimensionless groups.

Inspectional analysis uses a similar premise. However, instead of being based on the primary dimensions of variables the space is transformed from dimensional to dimensionless variable-by-variable. Shook (1992) used linear (affine) transformations, which works well if the grouping and elimination of translation factors is physically meaningful. Some dimensionless scaling groups for porous media flow are available in the literature (e.g. N_{RL}, Rapoport and Leas, 1953; M and G, Dietz, 1957; R_a, R_b, R_c and R_d, Craig *et al*, 1957). The dimensionless numbers developed in this investigation will be compared with earlier work to ensure consistency and aid physical interpretation.

The model used for development of the dimensionless scaling groups is two-phase, immiscible flow of incompressible fluids through a porous, permeable medium with anisotropic permeability and density contrasts; three spatial dimensions are considered. Phase pressures and saturations are assigned at the center of the gridblock. Grid blocks are assumed to be homogeneous. Viscosity of each phase is constant, and there is no mass transfer between phases. Inlet and outlet velocities will be used as the boundary conditions.

3.1. Governing equations

There are several ways of writing the flow equations (Peaceman, 1977; Mattax and Dalton 1990). For the ease of use in stability and error analysis (Lantz, 1971; Peaceman, 1977) the system will be described using equations 3.1a through 3.2g. The displacing phase is marked using index 1, so the governing equations for a three dimensional system of two incompressible phases are (Mattax and Dalton, 1990)

$$\phi\frac{\partial S_1}{\partial t}+\frac{\partial u_{1x}}{\partial x}+\frac{\partial u_{1y}}{\partial y}+\frac{\partial u_{1z}}{\partial z}=0 \tag{3.1a}$$

$$\frac{\partial u_{1x}+\partial u_{2x}}{\partial x}+\frac{\partial u_{1y}+\partial u_{2y}}{\partial y}+\frac{\partial u_{1z}+\partial u_{2z}}{\partial z}=0 \tag{3.1b}$$

$$u_{1x}=-k_x\lambda_{r1}\left(\frac{\partial p_1}{\partial x}-\rho_1\cdot g\cdot\frac{\partial D}{\partial x}\right) \tag{3.2a}$$

$$u_{2x}=-k_x\lambda_{r2}\left(\frac{\partial p_2}{\partial x}-\rho_2\cdot g\cdot\frac{\partial D}{\partial x}\right) \tag{3.2b}$$

$$u_{1y}=-k_y\lambda_{r1}\left(\frac{\partial p_1}{\partial y}-\rho_1\cdot g\cdot\frac{\partial D}{\partial y}\right) \tag{3.2c}$$

$$u_{2y}=-k_y\lambda_{r2}\left(\frac{\partial p_2}{\partial y}-\rho_2\cdot g\cdot\frac{\partial D}{\partial y}\right) \tag{3.2d}$$

$$u_{1z}=-k_z\lambda_{r1}\left(\frac{\partial p_1}{\partial z}-\rho_1\cdot g\cdot\frac{\partial D}{\partial z}\right) \tag{3.2e}$$

$$u_{2z}=-k_z\lambda_{r2}\left(\frac{\partial p_2}{\partial z}-\rho_2\cdot g\cdot\frac{\partial D}{\partial z}\right) \tag{3.2f}$$

The general notation for velocities is

$$u_{\ell i}=-k_i\lambda_{r\ell}\left(\frac{\partial p_\ell}{\partial i}-\rho_\ell\cdot g\cdot\frac{\partial D}{\partial i}\right) \tag{3.2g}$$

where

ℓ	phase, *1* denotes displacing and *2* displaced phase
i	direction (x,y,z)
u	phase velocity
λ	phase mobility
p	phase pressure
k	directional permeability
t	time

ϕ porosity

S_1 displacing phase saturation

D elevation

Several assumptions can be made to simplify the further development. Because the phase mobility is a function of phase saturation, we can employ the Corey-Brooks' relative permeability model (Charbeneau, 2000). The phase mobility of any given phase can be defined as

$$\lambda_j = \lambda_j^o \left(\frac{S_j - S_{j\min}}{S_{j\max} - S_{j\min}} \right)^{n_j} \tag{3.3}$$

where

λ_j mobility of phase j

λ_j^o end-point mobility of phase j

$S_j, S_{j\min}, S_{j\max}$ current, minimum and maximum saturation of phase j

n_j Corey's exponent of phase j

The relative permeability model is assumed to be independent of velocity and time; wettability changes are not considered. Endpoint mobility is defined using end-point relative permeability and viscosity as

$$\lambda_j^o = \frac{k_j^o}{\mu_j} \tag{3.4}$$

where

k_j^o end-point permeability of phase j

μ_j viscosity of phase j

Phase pressures are related with capillary pressure as follows:

$$P_2 = P_1 + P_c \tag{3.5}$$

where

P_c capillary pressure

Capillary pressure is commonly scaled using dimensionless Leverett's $J(S_1)$ function. The usual equation for scaling is

$$P_C = \sigma \cdot \sqrt{\frac{\phi}{k_z}} \cdot J(S_1) \tag{3.6}$$

where

σ interfacial tension

$J(S_1)$ dimensionless Leverett's J-function

The permeability used in equation 3.6 should be the one that best scales capillary pressures to $J(S_1)$. Vertical permeability is used in this dissertation. Several inspectional analyses during the development stage have shown that the general form of dimensionless equations is not affected by choice of either k_x or k_y or k_z.

D is the elevation which may depend on *X*, *Y* and *Z*. Two approaches can be used to discretize the gridblocks and include gravity terms: coordinate system, rotation or the angles between block centers.

3.1.1. Rotation approach

Rotation approach will rotate a point with coordinates (*X*, *Y*, *Z*) around *X*-axis and *Y*-axis independently - both in a separate 2D plane. In general, rotation for an angle θ in a two-dimensional system (depicted in figure 3.1) yields the following transformation of coordinates:

$$T_1^r = T_1 \cos\theta - T_2 \sin\theta \tag{3.7a}$$

$$T_2^r = T_2 \cos\theta + T_1 \sin\theta \tag{3.7b}$$

Where

T_1, T_2 coordinates of point of interest

T_1^r, T_2^r coordinates after rotation

θ angle of rotation

Two steps perform a rotation in this three-dimensional system as presented in figure 3.2. The first step will be rotation around *Y*-axis to account for tilt in *X* direction. This

rotation will translate X and Z coordinates onto X^r and Z^r. Point with coordinates $T(X, Y, Z)$ will therefore be rotated to $T^r(X^r, Y, Z^r)$.

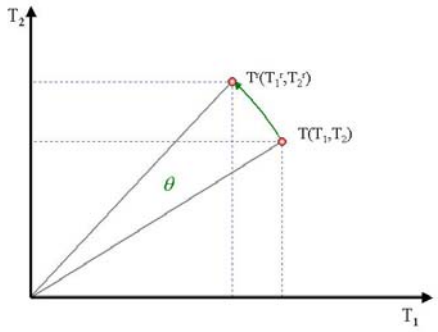

Figure 3.1. Point rotation in two-dimensional system

This point is rotated around the X-axis to account for tilt in Y direction. As a result, point $T^r(X^r, Y, Z^r)$ becomes $T^{rr}(X^r, Y^r, Z^{rr})$ or in a final notation $T^o(X^o, Y^o, Z^o)$. A general 3D rotation also includes rotation about the z-axis; no z-rotation was applied in this analysis.

Coordinates of the rotated point in the final position using the above notation is

$$X^o = X\cos\alpha_X - Z\sin\alpha_X \tag{3.8a}$$

$$Y^o = Y\cos\alpha_Y - X\sin\alpha_X\sin\alpha_Y - Z\cos\alpha_X\sin\alpha_Y \tag{3.8b}$$

$$Z^o = X\sin\alpha_X\cos\alpha_Y + Y\sin\alpha_Y + Z\cos\alpha_X\cos\alpha_Y \tag{3.8c}$$

where

X^o, Y^o, Z^o, X, Y, Z rotated and original X,Y,Z coordinates

α_X, α_Y X and Y direction tilt angle

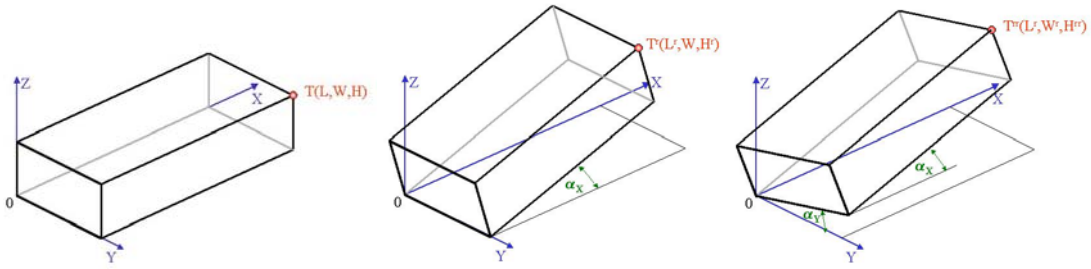

Figure 3.2. Rotation of the reservoir cell to accommodate for X and Y tilt

The vertical component of the gravity vector in the point $T^o(X^o, Y^o, Z^o)$ is therefore

$$\vec{D}\cdot\vec{R} = Z^o = X\left(\sin\alpha_X\cos\alpha_Y\right) + Y\left(\sin\alpha_Y\right) + Z\left(\cos\alpha_X\cos\alpha_Y\right) \tag{3.9}$$

Rotation is order dependent. If the order is reversed – i.e., rotation for α_X succeeds the rotation for α_Y – the vertical component of the gravity vector can be estimated as

$$\vec{D}\cdot\vec{R} = Z^o = X\left(\sin\alpha_X\right) + Y\left(\sin\alpha_Y\cos\alpha_X\right) + Z\left(\cos\alpha_X\cos\alpha_Y\right) \tag{3.10}$$

The displacing phase velocity in the *X* direction with rotation in α_X-α_Y order is then

$$u_{1x} = -k_x\lambda_{r1}\left(\frac{\partial p_1}{\partial x} - \rho_1\cdot g\cdot\sin\alpha_X\cos\alpha_Y\right) \tag{3.11}$$

If order is reversed

$$u_{1x} = -k_x\lambda_{r1}\left(\frac{\partial p_1}{\partial x} - \rho_1\cdot g\cdot\sin\alpha_X\right) \tag{3.12}$$

Similar can be done for *Y* direction velocity. The rotation approach is order independent in the *Z* direction. The *Z* direction displaced phase velocity is

$$u_{1z} = -k_z\lambda_{r1}\left(\frac{\partial p_1}{\partial z} - \rho_1\cdot g\cdot\left(\cos\alpha_X\cos\alpha_Y\right)\right) \tag{3.13}$$

Equations 3.11 through 3.13 can be written for the displaced density, phase pressure, mobility and velocity.

To eliminate the order-approach dependency we can separately rotate points (0, 1, 0) around *X*-axis to account for *X*-direction tilt and point (1, 0, 0) around *Y*-axis to account for *Y*-direction tilt. If rotated points are used to determine the rotation vectors, gravitational vector can be defined using the ex-product of two rotation vectors. Therefore, the *X*-direction tilt vector becomes

$$\vec{x}_t = \vec{i}\cos\alpha_X + \vec{k}\sin\alpha_X \tag{3.14a}$$

The *Y*-direction tilt vector can be defined as

$$\vec{y}_t = \vec{j}\cos\alpha_Y + \vec{k}\sin\alpha_Y \tag{3.14b}$$

The cross product of corresponding vectors is the determinant of the following matrix

$$\vec{D} = \vec{d}\times\vec{s} = \begin{vmatrix} \vec{i} & \vec{j} & \vec{k} \\ \cos\alpha_X & 0 & \sin\alpha_X \\ 0 & \cos\alpha_Y & \sin\alpha_Y \end{vmatrix} \tag{3.15}$$

Therefore the desired gravity vector is

$$\vec{D} = -\vec{i}\sin\alpha_d \cos\alpha_s + \vec{j}\sin\alpha_s \cos\alpha_d + \vec{k}\cos\alpha_d \cos\alpha_s \quad (3.16)$$

Investigating the signs in equation 3.16 shows that the $\vec{i}$ component is negative, so if the X increases Z would decrease. This is a result from the coordinate system notation.

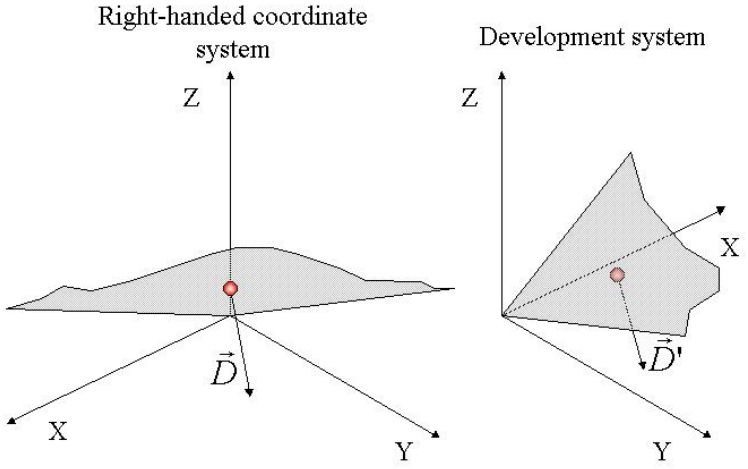

Figure 3.3. Right-handed coordinate system and the system of interest

The development is mathematically correct for a right-handed coordinate system. Note that negative side of X-axis of right-handed coordinate system corresponds to the positive side X-axis of the system on which all the previous development is made. Instead of changing the system, we can simply correct the difference by writing the gravity vector as

$$\vec{D} = \vec{i}\sin\alpha_X \cos\alpha_Y + \vec{j}\sin\alpha_Y \cos\alpha_X + \vec{k}\cos\alpha_X \cos\alpha_Y \quad (3.16)$$

The velocities in equations 3.2a though 3.2f can be defined as

$$u_{1x} = -k_x\lambda_{r1}\left(\frac{\partial p_1}{\partial x} - \rho_1 \cdot g \cdot \sin\alpha_X \cos\alpha_Y\right) \quad (3.17a)$$

$$u_{2x} = -k_x\lambda_{r2}\left(\frac{\partial p_2}{\partial x} - \rho_2 \cdot g \cdot \sin\alpha_X \cos\alpha_Y\right) \quad (3.17b)$$

$$u_{1y} = -k_y\lambda_{r1}\left(\frac{\partial p_1}{\partial y} - \rho_1 \cdot g \cdot \sin\alpha_Y \cos\alpha_X\right) \quad (3.17c)$$

$$u_{2y} = -k_y\lambda_{r2}\left(\frac{\partial p_2}{\partial y} - \rho_2 \cdot g \cdot \sin\alpha_Y \cos\alpha_X\right) \quad (3.17d)$$

$$u_{1z} = -k_z\lambda_{r1}\left(\frac{\partial p_1}{\partial z} - \rho_1 \cdot g \cdot \cos\alpha_X \cos\alpha_Y\right) \quad (3.17e)$$

$$u_{2z} = -k_z \lambda_{r2} \left(\frac{\partial p_2}{\partial z} - \rho_2 \cdot g \cdot \cos\alpha_X \cos\alpha_Y \right) \tag{3.17f}$$

3.1.2. Block-center approach

A common gridding approach in numerical models should be investigated to corroborate or discard the rotation approach. Each gridblock can be assumed as horizontal with block centers vertically aligned as shown in figure 3.4.

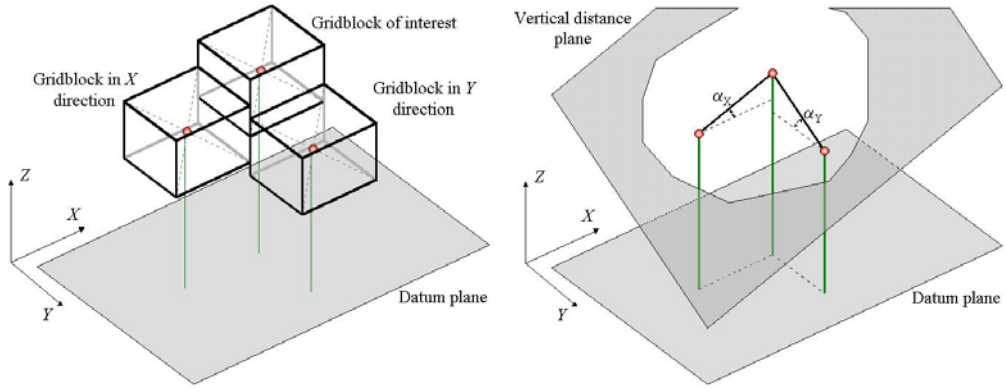

Figure 3.4. Tilt representation in numerical model

Elevation change in numerical simulations is the vertical distance between two centers in the direction of interest. To make the development more general, the vertical distance change from gridblock to gridblock can be assumed constant in X and constant in Y direction throughout the system. A vertical distance plane can be introduced such that all the block-centers fall onto the plane (figure 3.4). Rather than rotating the coordinate system, the elevation is computed by projecting a point onto the vertical distance plane. Vertical distance plane can be determined using several approaches (e.g., a plane through 3 points). To make the rotation and block-center approach methods comparable the elevation needs to be increasing in X and Y direction. Assuming the plane has a zero elevation at the origin with angles α_X and α_Y introduced as in Figure 3.3 we can determine the elevation as a function of X and Y as

$$Z = X \tan\alpha_X + Y \tan\alpha_Y \tag{3.18}$$

Rearranging the elevation and accounting for the fact that gravity vectors is pointing vertically downward provides the final form for the plane equation as

$$X \sin\alpha_X \cos\alpha_Y + Y \sin\alpha_Y \cos\alpha_X + Z \cos\alpha_X \cos\alpha_Y = 0 = \vec{D} \cdot \vec{R} \tag{3.19}$$

Therefore the velocities in equations 3.2a through 3.2f can be defined as

$$u_{1x} = -k_x \lambda_{r1} \left(\frac{\partial p_1}{\partial x} - \rho_1 \cdot g \cdot \sin \alpha_X \cdot \cos \alpha_Y \right) \tag{3.20a}$$

$$u_{2x} = -k_x \lambda_{r2} \left(\frac{\partial p_2}{\partial x} - \rho_2 \cdot g \cdot \sin \alpha_X \cdot \cos \alpha_Y \right) \tag{3.20b}$$

$$u_{1y} = -k_y \lambda_{r1} \left(\frac{\partial p_1}{\partial y} - \rho_1 \cdot g \cdot \sin \alpha_Y \cos \alpha_X \right) \tag{3.20c}$$

$$u_{2y} = -k_y \lambda_{r2} \left(\frac{\partial p_2}{\partial y} - \rho_2 \cdot g \cdot \sin \alpha_Y \cos \alpha_X \right) \tag{3.20d}$$

$$u_{1z} = -k_z \lambda_{r1} \left(\frac{\partial p_1}{\partial z} - \rho_1 \cdot g \cdot \cos \alpha_X \cos \alpha_Y \right) \tag{3.20e}$$

$$u_{2z} = -k_z \lambda_{r2} \left(\frac{\partial p_2}{\partial z} - \rho_2 \cdot g \cdot \cos \alpha_X \cos \alpha_Y \right) \tag{3.20f}$$

Both approaches yield same form of the equation, once the rotation-order dependence was removed in rotation approach. Equations 3.1a, 3.1b and 3.20a through 3.20f are the base equations used for the transformation to dimensionless space.

3.2. Transformation to dimensionless space

The previous equations describe the system of interest. In general, the rectangular system presented previously has a total of 20 parameters (L, W, H, σ, S_{1r}, S_{2r}, ϕ, u_T, k_x, k_y, k_z, ρ_1, ρ_2, λ_{r1}^o, λ_{r2}^o, P_1^o, α_s, α_d, n_1, n_2) affecting 9 variables (S_1, P_1, P_2, u_{1x}, u_{2x}, u_{1y}, u_{2y}, u_{1z} and u_{2z}). These parameters and variables comprise the system for dimensional and inspectional analysis.

3.2.1. Dimensional analysis

Dimensional analysis considers the total number of dimensional parameters. Because dimensional analysis determines the minimum number of groups based on primary dimensions, all relevant parameters must be included in the analysis. Equations include the parameters L, W, H, ϕ, $(S_1)^{n1}$, $(S_2)^{n2}$, u_T, u_{1x}, u_{2x}, u_{1y}, u_{2y}, u_{1z}, u_{2z}, p_1, p_2, p_C, μ_1, μ_2, $\Delta\rho$, ρ_1, ρ_2, σ, $\sin\alpha_X$, $\sin\alpha_Y$, $\cos\alpha_X$, $\cos\alpha_Y$, g, k_x, k_y, k_z, k_{r1}^o and k_{r2}^o – 32 in total. This differs from the number obtained before: the difference is then number of elementary dimensionless

functions on parameters (viz., different trigonometric for angles or exponential functions of saturation) that have been included. If only dimensional parameters were included the analysis would – based on dimensionality – group dimensionless variables together. For example one of the groups might become S_1/α_X or ϕ/n_1. This would make physical interpretation of the groups more difficult.

There are 3 primary dimensions defining the parameters – length [L], mass [M] and time [T]. If we were to exclude trigonometric functions, saturation, porosity and relative permeability (which are intrinsically dimensionless) the dimensional analysis will not provide us with succinct groups. Therefore we consider the nondimensional groups have a fourth dimension with unit [N.D.]. Some of the parameters are repeating (e.g., k_x, k_y and k_z or ρ_1, ρ_2 and $\Delta\rho$) so the general notation can be used for discussion on primary dimensions. Primary dimensions (e.g. length over time for velocity) for *dimensionally* different parameters are known and can be represented as shown in table 3.1.

Table 3.1. Primary dimensions

S	**X**	**T**	**K**	**u**	**G**	**σ**	**μ**	**P**	**ρ**
N.D.	L	T	$\frac{1}{L^2}$	$\frac{L}{T}$	$\frac{L}{T^2}$	$\frac{M}{T^2}$	$\frac{ML}{T}$	$\frac{ML}{T^2}$	$\frac{M}{L^3}$

Some of the variables are not dimensionally independent and hence can be presented as a combination of others–. For example, pressure can be expressed as a combination of interfacial tension and velocity. To proceed with dimensional analysis it is crucial to determine the minimum number of independent groups. We can create a matrix representing parameters and their units (table 3.2).

Table 3.2. Parameter dimension matrix

	X	**t**	**K**	**σ**	**u**	**G**	**S**	**μ**	**P**	**ρ**
N.D.	0	0	0	0	0	0	1	0	0	0
L	1	0	-2	0	1	1	0	1	1	-3
M	0	0	0	1	0	0	0	1	1	1
T	0	1	0	-2	-1	-2	0	-1	-2	0

All the parameters (table 3.2) can be expressed using four basic dimensions. For example, permeability has a dimension of $[L^2]$ so it can be written as $[ND^0L^2M^0T^0]$. To determine the fewest independent parameters we need to determine the rank of the parameter matrix. Parameters that have identical dimensions were again replaced with general notation (table 3.2) because the rank of the matrix and the number of primary dimensions is not affected. This method is different from the one proposed by Buckingham (1914). The approach was adopted from Fox and McDonald (1998) who presented dimensional analysis on general flow in horizontal pipe.

The rank of the parameter matrix is 4 (shaded area in the matrix in the table 3.2). The number of independent dimensionless groups can is the difference between the number of variables and the number of independent parameters, or in this case 28. The rank of parameter matrix indicates the number of parameters that will be used as a basis throughout the dimensional analysis.

The following can be written for each variable

$$e_1^A \cdot e_2^B \cdot e_3^C \cdot e_4^D \cdot e_i = 1 \tag{3.21}$$

Where

e_1, e_2, e_3, e_4	four repeating variables
A, B, C, D	exponents on repeating parameters
e_i	investigated non-repeating variable

Because all the variables are a product of (at most) four primary dimensions we can write the following for each repeating variable in the equation 3.14

$$e_j = \left(M^{m_{jM}}\right)^A \left(L^{m_{jL}}\right)^B \left(T^{m_{jT}}\right)^C \left(N.D.^{m_{jN.D.}}\right)^D \tag{3.22}$$

where

e_j	repeating variable
$m_{jM}, m_{JL}, m_{JT}, m_{jN.D.}$	exponents on primary dimensions M, L, T and N.D., respectively

A similar equation can be written for non-repeating variable, except that A, B, C and D are set to 1. Rearrangement of equations and taking the logarithm results in the following matrix

$$\begin{bmatrix} m_{1M}A & m_{2M}B & m_{3M}C & m_{4M}D \\ m_{1L}A & m_{2L}B & m_{3L}C & m_{4L}D \\ m_{1T}A & m_{2T}B & m_{3T}C & m_{4T}D \\ m_{1N.D.}A & m_{2N.D.}B & m_{3N.D.}C & m_{4N.D.}D \end{bmatrix} = \begin{bmatrix} -m_{iM} \\ -m_{iL} \\ -m_{iT} \\ -m_{iN.D.} \end{bmatrix} \tag{3.23}$$

where

$m_{iM}, m_{iL}, m_{iT}, m_{iN.D.}$ exponents as in eqn. 3.15, set for non-repeating investigated variable

The exponents A, B, C and D for all 28 investigated variables are obtained by solving equation 3.16; this can be done in a spreadsheet (figure 3.5). Assignment of repeating parameters is arbitrary – as can be observed from figure 3.5 - the choice was made to repeat t, P_1, Δp and k_x. Theoretically, any 4 of the 32 parameters could have been chosen. However, the parameters chosen to be repeating have to be independent; otherwise the matrix system (eqn 3.16) cannot be solved.

The primary dimensions for each variable are in upper part of the matrix. For example, porosity is nondimensional hence the exponent for N.D. is set to 1 and exponents for mass, length and time to 0. Density is a combination of mass and length (M/L^3) hence the exponent for mass is set to 1, exponent for length to –3 and remaining time [T] and non-dimensional [N.D.] exponent to 0.

	B	C	D	E	F	G	H	I	J	K	L	M	N	O	P	Q	R	S	T	U	V	W	X	Y	Z	AA	AB	AC	AD	AE	AF	AG	AH	AI	AJ	AK	AL
1																																				
2	N.D.	1	0	1	1	0	0	0	0	0	0	0	0	0	0	0	0	0	0	0	0	0	0	1	1	1	1	0	0	0	0	1	1				
3	T	0	1	0	0	0	0	0	-1	-1	-1	-1	-1	-1	-1	-2	-2	-2	−1	−1	0	0	0	0	0	0	0	-2	0	0	0	0	0				
4	L	0	0	0	0	1	1	1	1	1	1	1	1	1	1	-1	-1	0	1	1	−3	−3	−3	0	0	0	0	1	-2	-2	-2	0	0				
5	M	0	0	0	0	0	0	0	0	0	0	0	0	0	0	1	1	1	1	1	1	1	1	0	0	0	0	0	0	0	0	0	0				
6		ϕ	t	$(S_1)^{nl}$	$(S_1)^{n}$	x	y	z	u_T	u_{1x}	u_{1y}	u_{1z}	u_{2x}	u_{2y}	u_{2z}	P_1	P_2	σ	μ_1	μ_2	Δρ	ρ_1	ρ_1	$\sin\alpha_X$	$\sin\alpha_Y$	$\cos\alpha_X$	$\cos\alpha$	g	K_x	K_y	K_z	K_{r1}	K_{r2}	A	B	C	D
7	Π_1	A	1													B					C								D					0	0.5	-0.5	0.5
8	Π_2	A		1												B					C								D					-1	0	0	0
9	Π_3	A			1											B					C								D					-1	0	0	0
10	Π_4	A				1										B					C								D					0	0	0	0.5
11	Π_5	A					1									B					C								D					0	0	0	0.5
12	Π_6	A						1								B					C								D					0	0	0	0.5
13	Π_7	A							1							B					C								D					0	-0.5	0.5	0
14	Π_8	A								1						B					C								D					0	-0.5	0.5	0
15	Π_9	A									1					B					C								D					0	-0.5	0.5	0
16	Π_{10}	A										1				B					C								D					0	-0.5	0.5	0
17	Π_{11}	A											1			B					C								D					0	-0.5	0.5	0
18	Π_{12}	A												1		B					C								D					0	-0.5	0.5	0
19	Π_{13}	A													1	B					C								D					0	-0.5	0.5	0
20	Π_{14}	A														B	1				C								D					0	-1	0	0
21	Π_{15}	A														B		1			C								D					0	-1	0	0.5
22	Π_{16}	A														B			1		C								D					0	-0.5	-0.5	1.5
23	Π_{17}	A														B				1	C								D					0	-0.5	-0.5	1.5
24	Π_{18}	A														B					C	1							D					0	0	-1	0
25	Π_{19}	A														B					C		1						D					0	0	-1	0
26	Π_{20}	A														B					C			1					D					-1	0	0	0
27	Π_{21}	A														B					C				1				D					-1	0	0	0
28	Π_{22}	A														B					C					1			D					-1	0	0	0
29	Π_{23}	A														B					C						1		D					-1	0	0	0
30	Π_{24}	A														B					C							1	D					0	-1	1	-0.5
31	Π_{25}	A														B					C								D	1				0	0	0	-1
32	Π_{26}	A														B					C								D		1			0	0	0	-1
33	Π_{27}	A														B					C								D			1		1	0	0	0
34	Π_{28}	A														B					C								D				1	1	0	0	0

Figure 3.5. Example solution spreadsheet for dimensional analysis

Exponents A, B, C and D for each dimensionless group Π and all remaining non-repeating variables (marked with 1 in the matrix) are then computed using matrix algebra to obtain 28 dimensionless variables (table 3.3).

Table 3.3. Dimensionless groups definition using dimensional analysis

$\Pi_1 = \frac{t}{\sqrt{P_1 \Delta\rho k_x}}$	$\Pi_8 = u_{1x}\sqrt{\frac{P_1}{\Delta\rho k_x}}$	$\Pi_{15} = \frac{\sigma}{P_1}\sqrt{k_x}$	$\Pi_{22} = \frac{\cos\alpha_X}{\phi}$
$\Pi_2 = \phi(S_1)^{n_1}$	$\Pi_9 = u_{2x}\sqrt{\frac{P_1}{\Delta\rho k_x}}$	$\Pi_{16} = \mu_1 k_x\sqrt{\frac{k_x}{P_1\Delta\rho}}$	$\Pi_{23} = \frac{\cos\alpha_Y}{\phi}$
$\Pi_3 = \phi(S_2)^{n_2}$	$\Pi_{10} = u_{1y}\sqrt{\frac{P_1}{\Delta\rho k_x}}$	$\Pi_{17} = \mu_2 k_x\sqrt{\frac{k_x}{P_1\Delta\rho}}$	$\Pi_{24} = \frac{\Delta\rho}{P_1\sqrt{k_x}}$
$\Pi_4 = \frac{x}{\sqrt{k_x}}$	$\Pi_{11} = u_{2y}\sqrt{\frac{P_1}{\Delta\rho k_x}}$	$\Pi_{18} = \frac{\rho_1}{\Delta\rho}$	$\Pi_{25} = \frac{k_y}{k_x}$
$\Pi_5 = \frac{y}{\sqrt{k_x}}$	$\Pi_{12} = u_{1z}\sqrt{\frac{P_1}{\Delta\rho k_x}}$	$\Pi_{19} = \frac{\rho_2}{\Delta\rho}$	$\Pi_{26} = \frac{k_z}{k_x}$
$\Pi_6 = \frac{z}{\sqrt{k_x}}$	$\Pi_{13} = u_{2z}\sqrt{\frac{P_1}{\Delta\rho k_x}}$	$\Pi_{20} = \frac{\sin\alpha_X}{\phi}$	$\Pi_{27} = \phi K_{r1}{}^{o}$
$\Pi_7 = u_T\sqrt{\frac{P_1}{\Delta\rho k_x}}$	$\Pi_{14} = \frac{P_2}{P_1}$	$\Pi_{21} = \frac{\sin\alpha_Y}{\phi}$	$\Pi_{28} = \phi K_{r2}{}^{o}$

The development complies with Buckingham's (1914) rules for dimensionality. Even though the number of variables is reduced from 32 to 28 with dimensional variables being replaced with dimensionless, the lack of physical explanation of the meaning of variables and sheer number makes them less practical.

Discussion on applicability can be taken further by stating that already dimensionless groups do not have to be included in the analysis. They could simply be added later by multiplying them with the group of choice since this would not change the dimensionless formulation. Arbitrarity in a method of choice of repeating parameters and the way of treating already dimensionless ones makes this method useful for experimental work but deeper insight and analysis of flow equations is needed to reduce the arbitrariness introduced by choice of repeating parameters.

3.2.2. Inspectional analysis

Dimensionless numbers obtained through inspectional analysis are generally considered to be more useful (Craig et al., 1957, Shook et al., 1992). The flow equations are included in the analysis to improve the description of reservoir behavior. Because the flow equations neither alter the number of primary dimensions nor introduce new parameters to the system, the dimensional analysis still holds. The primary goal of the inspectional analysis on the expanded set of equations is to introduce the necessary boundary conditions. Boundary conditions can be introduced through the process of transformation from dimensional to dimensionless space or through later rearrangement of already developed dimensionless equations. To minimize possible error in development the chosen approach is to introduce boundary conditions before the transformation takes place.

Boundary conditions are defined as follows

- Phase pressures are assigned at the center of the system
- Phase saturations are assigned at the center of the system
- Inlet and outlet boundary conditions are defined using phase velocity

Pressure in the displacing phase at any point is a function of a known pressure P_1^o, viscous gradient, and gravity pressure gradient:

$$P_1 = P_1^o - \Delta P_{viscous} - \Delta P_{gravity} \tag{3.24}$$

Viscous pressure drop in any direction *i* can be estimated integrating viscous pressure drop over the length:

$$\Delta p_{viscous}(I) = \int_0^I \frac{u_i}{k_i \lambda_{rj}} di \tag{3.25a}$$

Directional velocity u_i is a function of space. Mathematically succinct way of writing the integral in a three-dimensional space would be

$$\Delta p_{viscous}(I) = \int_0^I \frac{u_i\left(i, j = j_o, k = k_o\right)}{k_i \lambda_{rj}} di \tag{3.25b}$$

where

j_o, k_o constant *j* and *k* coordinates along which the *i*-direction viscous pressure drop is estimated

Notation in equation 3.25b is dropped in further and equation 3.25a is used for simplicity.

Assuming that pressure P_1^o is given at the center of the gridblock, pressure at any other point with coordinates (*x, y, z*) for a block-centered discretization leads to

$$P_1(x,y,z) = P_1^o - \int_{\frac{L}{2}}^{x} \frac{u_{1x}}{k_x \lambda_{r1}} dx - \int_{\frac{W}{2}}^{y} \frac{u_{1y}}{k_y \lambda_{r1}} dy - \int_{\frac{H}{2}}^{z} \frac{u_{1z}}{k_z \lambda_{r1}} dz -$$
$$\rho_1 \cdot g \cdot \left(\left(x - \frac{L}{2} \right) \cdot \sin\alpha_X \cos\alpha_Y + \left(y - \frac{W}{2} \right) \cdot \sin\alpha_Y \cos\alpha_X + \left(z - \frac{H}{2} \right) \cdot \cos\alpha_X \cos\alpha_Y \right)$$
$$\forall x \in [0, L], y \in [0, W], z \in [0, H], t \qquad (3.26)$$

The corresponding equation for displaced phase is

$$P_2(x,y,z) = P_2^o - \int_{\frac{L}{2}}^{x} \frac{u_{2x}}{k_x \lambda_{r2}} dx - \int_{\frac{W}{2}}^{y} \frac{u_{2y}}{k_y \lambda_{r2}} dy - \int_{\frac{H}{2}}^{z} \frac{u_{2z}}{k_z \lambda_{r2}} dz -$$
$$\rho_2 \cdot g \cdot \left(\left(x - \frac{L}{2} \right) \cdot \sin\alpha_X \cos\alpha_Y + \left(y - \frac{W}{2} \right) \cdot \sin\alpha_Y \cos\alpha_X + \left(z - \frac{H}{2} \right) \cdot \cos\alpha_X \cos\alpha_Y \right)$$
$$\forall x \in [0, L], y \in [0, W], z \in [0, H], t \qquad (3.27)$$

Phase pressures change from P_1^o and P_2^o at the center to P_1 and P_2 at any point. The gravity-capillary transition zone is a vertical effect, with the transition height related to the upscaled capillary pressure by

$$P_c^*(S_w) = P_2 - P_1 = h_T(S_w) \Delta\rho \cdot g \cdot \cos\alpha_X \cos\alpha_Y \qquad (3.28)$$

The transition zone is used in conventional reservoir engineering (Dake, 1978) to determine the type of flow (i.e. diffuse or segregated) and estimate the production response. Flow in numerical models is generally diffuse and transition zone was considered only to assist in inspectional analysis. It can be shown, however, that these dimensionless numbers can be used for flow analysis on a reservoir scale. Additional equations help by providing a way of testing the validity of transformation.

Because pressures at the center are known the height of transition zone at the center is also known. Therefore substituting equations 3.26 and 3.27 into equation 3.28 leads to following formulation for the height of transition zone in any other point in the reservoir:

$$H_T\Delta\rho\cdot g\cdot\cos\alpha_d\cos\alpha_s = H_T^o\Delta\rho\cdot g\cdot\cos\alpha_d\cos\alpha_s -$$
$$\left(\int_{\frac{L}{2}}^{x}\frac{u_{2x}}{k_x\lambda_{r2}}dx+\int_{\frac{W}{2}}^{y}\frac{u_{2y}}{k_y\lambda_{r2}}dy+\int_{\frac{H}{2}}^{z}\frac{u_{2z}}{k_z\lambda_{r2}}dz-\int_{\frac{L}{2}}^{x}\frac{u_{1x}}{k_x\lambda_{r1}}dx-\int_{\frac{W}{2}}^{y}\frac{u_{1y}}{k_y\lambda_{r1}}dy-\int_{\frac{H}{2}}^{z}\frac{u_{1z}}{k_z\lambda_{r1}}dz\right)-$$
$$\left\{\rho_1\cdot g\cdot\left(\left(x-\frac{L}{2}\right)\cdot\sin\alpha_X\cos\alpha_Y+\left(y-\frac{W}{2}\right)\cdot\sin\alpha_Y\cos\alpha_X\left(z-\frac{H}{2}\right)\cdot\cos\alpha_X\cos\alpha_Y\right)-\right.$$
$$\left.\rho_2\cdot g\cdot\left(\left(x-\frac{L}{2}\right)\cdot\sin\alpha_X\cos\alpha_Y+\left(y-\frac{W}{2}\right)\cdot\sin\alpha_Y\cos\alpha_X+\left(z-\frac{H}{2}\right)\cdot\cos\alpha_X\cos\alpha_Y\right)\right\}$$
$$\forall x\in[0,L],y\in[0,W],z\in[0,H],t \qquad (3.29)$$

where

H_T^o height of transition zone imposed by p_1^o and p_2^o

Rearranging to account for density difference $\Delta\rho=(\rho_1-\rho_2)$ we get the final form as

$$\left(H_T-H_T^o\right)\Delta\rho\cdot g\cdot\cos\alpha_X\cos\alpha_Y=\int_{\frac{L}{2}}^{x}\frac{u_{2x}}{k_x\lambda_{r2}}-\frac{u_{1x}}{k_x\lambda_{r1}}dx+\int_{\frac{W}{2}}^{y}\frac{u_{2y}}{k_y\lambda_{r2}}-\frac{u_{1y}}{k_y\lambda_{r1}}dy+\int_{\frac{H}{2}}^{z}\frac{u_{2z}}{k_z\lambda_{r2}}-\frac{u_{1z}}{k_z\lambda_{r1}}dz+$$
$$\Delta\rho\cdot g\cdot\left(\left(x-\frac{L}{2}\right)\cdot\sin\alpha_X\cos\alpha_Y+\left(y-\frac{W}{2}\right)\cdot\sin\alpha_Y\cos\alpha_X+\left(z-\frac{H}{2}\right)\cdot\cos\alpha_X\cos\alpha_Y\right)$$
$$\forall x\in[0,L],y\in[0,W],z\in[0,H],t \qquad (3.30)$$

Equations 3.26, 3.27, 3.28 and 3.30 complete the set needed for analysis. Inspectional analysis of these equations is detailed in Appendix A.

Inspectional analysis yields 8 numbers formulating equations 3.1a, 3.1b and 3.2a through 3.2f in a following way

$$\frac{\partial S_{1D}}{\partial t_D}+\frac{\partial u_{1xD}}{\partial x_D}+\frac{\partial u_{1yD}}{\partial y_D}+\frac{\partial u_{1zD}}{\partial z_D}=0 \qquad (3.31a)$$

$$\frac{\partial u_{1xD}+\partial u_{2xD}}{\partial x_D}+\frac{\partial u_{1yD}+\partial u_{2yD}}{\partial y_D}+\frac{\partial u_{1zD}+\partial u_{2zD}}{\partial z_D}=0 \qquad (3.31b)$$

$$u_{1xD}=-\frac{1}{N_{RX}}\left(S_{1D}\right)^{n_1}\left(\frac{\partial p_{1D}}{\partial x_D}-\frac{N_gN_{TX}}{N_\rho}\right) \qquad (3.31a)$$

$$u_{2xD}=-\frac{1}{N_{RX}M}\left(S_{2D}\right)^{n_{12}}\left(\frac{\partial p_{2D}}{\partial x_D}-\frac{N_g\left(1-N_\rho\right)N_{TX}}{N_\rho}\right) \qquad (3.31b)$$

$$u_{1yD} = -\frac{1}{N_{RY}}\left(S_{1D}\right)^{n_1}\left(\frac{\partial p_{1D}}{\partial y_D} - \frac{N_g N_{TY}}{N_\rho}\right) \tag{3.31c}$$

$$u_{2yD} = -\frac{1}{N_{RY}M}\left(S_{2D}\right)^{n_{12}}\left(\frac{\partial p_{2D}}{\partial y_D} - \frac{N_g\left(1-N_\rho\right)N_{TY}}{N_\rho}\right) \tag{3.31d}$$

$$u_{1zD} = -\left(S_{1D}\right)^{n_1}\left(\frac{\partial p_{1D}}{\partial z_D} - \frac{N_g}{N_\rho}\right) \tag{3.31e}$$

$$u_{2zD} = -\frac{1}{M}\left(S_{2D}\right)^{n_{12}}\left(\frac{\partial p_{2D}}{\partial z_D} - \frac{N_g\left(1-N_\rho\right)}{N_\rho}\right) \tag{3.31f}$$

Equation 3.26 becomes

$$P_{1D} = P_{1D}{}^{o} - N_{RX}\int_{\frac{1}{2}}^{x_D} u_{1xD}\,dx_D - N_{RY}\int_{\frac{1}{2}}^{y_D} u_{1yD}\,dy_D - \int_{\frac{1}{2}}^{z_D} u_{1zD}\,dz_D$$
$$-\frac{N_g}{N_\rho}\left(N_{TX}\left(x_D-\frac{1}{2}\right)+N_{TY}\left(y_D-\frac{1}{2}\right)+\left(z_D-\frac{1}{2}\right)\right)$$

$$\forall x_D, y_D, z_D, t_D \tag{3.32}$$

Similarly, for equation 3.27

$$P_{2D} = P_{2D}^{o} - MN_{RX}\int_{\frac{1}{2}}^{x_D} u_{2xD}\,dx_D - MN_{RY}\int_{\frac{1}{2}}^{y_D} u_{2yD}\,dy_D - M\int_{\frac{1}{2}}^{z_D} u_{2zD}\,dz_D$$
$$-\frac{N_g\left(1-N_\rho\right)}{N_\rho}\left(N_{TX}\left(x_D-\frac{1}{2}\right)+N_{TY}\left(y_D-\frac{1}{2}\right)+\left(z_D-\frac{1}{2}\right)\right)$$

$$\forall x_D, y_D, z_D, t_D \tag{3.33}$$

Finally, dimensionless transition zone height is

$$\Delta z_D N_g = N_{RX}\int_{\frac{1}{2}}^{x_D}\left(Mu_{2xD}-u_{1xD}\right)dx_D + N_{RY}\int_{\frac{1}{2}}^{y_D}\left(Mu_{2yD}-u_{1yD}\right)dy_D + \int_{\frac{1}{2}}^{z_D}\left(Mu_{2yD}-u_{1yD}\right)dz_D$$
$$+N_g\left(N_{TX}\left(x_D-\frac{1}{2}\right)+N_{TY}\left(y_D-\frac{1}{2}\right)+\left(z_D-\frac{1}{2}\right)\right)$$

$$\forall x_D, y_D, z_D, t_D \tag{3.34}$$

The dimensionless numbers used in equations 3.31 through 3.34 are defined in table 3.4.

Table 3.4. Dimensionless groups for incompressible two-phase three-dimensional flow

Group	Symbol	Formulation
X-direction aspect ratio	N_{RX}	$\frac{L^2}{H^2}\frac{k_z}{k_x}$
Y-direction aspect ratio	N_{RY}	$\frac{W^2}{H^2}\frac{k_z}{k_y}$
X-direction tilt number	N_{TX}	$\frac{L}{H}\tan\alpha_X$
Y-direction tilt number	N_{TY}	$\frac{W}{H}\tan\alpha_Y$
Density number	N_{ρ}	$\frac{\Delta\rho}{\rho_1}$
Gravity number	N_g	$\frac{k_z\lambda_{r1}^{\ o}\Delta\rho g\cdot\cos\alpha_X\cos\alpha_Y}{u_T}$
Mobility ratio	M	$\frac{\lambda_{r1}^{\ o}}{\lambda_{r2}^{\ o}}$
Capillary number	N_c	$\frac{\sigma k_z\lambda_{r1}^{\ o}}{u_T H}\sqrt{\frac{\phi}{k_z}}$

3.3. Validity of proposed numbers

The last step in the development is to outline when the previously presented dimensionless set is physically valid and provide the analytical confirmation that set can be used to describe previously known dimensionless developments.

3.3.1. Physical validity

The assumptions made in the development are as follows

- Incompressible, two-phase system
- Constant viscosity for each phase
- No mass transfer between phases

- Residual saturations are constant
- Capillary pressure is scalable through Leverett's $J(S_1)$ function
- Corey-Brooks' model for relative permeability (no capillary number dependence)

Lake's (1989) overview of studies on behavior of residual saturations as a function of capillary desaturation curves provides the physical limit where this type of dimensionless description would fail. Capillary desaturation curves reach the plateau value with constant residual saturation when small-scale capillary number is less than $\approx 10^{-5}$. Small-scale capillary number is defined as

$$N_{vc} = \frac{u_T \mu}{\sigma} \tag{3.35}$$

Because the small scale capillary number is already included in the large-scale one the limit can be set as

$$\frac{\lambda_{r1}{}^{o} \sqrt{k_z \phi}}{N_c} \leq 10^{-5} \tag{3.36}$$

Scaling through Leverett's $J(S_1)$ function and Corey-Brooks' relative permeability model are commonly used. If the system could not be scaled through the Leverett's $J(S_1)$ function, the developed dimensionless capillary number would be lost and the scaling function would have to multiplied with $\lambda_{r1}^{0} k_z / u_T H$. The generality of equation would be lost because the dimensionless capillary number would not be a constant for a given system.

The Corey-Brooks relative permeability model utilizing $(S_{1D})^{n1}$ and $(S_{2D})^{n2}$ can be replaced by any set of functions $f_1(S_{1D})$ and $f_2(S_{2D})$ providing that the function argument is dimensionless saturation defined as shown in Appendix A.

3.3.2. Development validity in 1D

To further validate the development it is tested for segregated flow. Segregated flow (Dake, 1978) occurs when displacing and displaced front have an equal flux, capillary pressure is negligible, and displacement is piston-like. Gravity forces alone govern the vertical distribution of fluids, creating an angle β of the inclination of the fluid interface with respect to reservoir boundary in Z direction. The angle β is assumed constant

throughout the displacement Dietz (1953) showed that the interface angle and dimensionless groups in a tilted, homogeneous, isotropic reservoir are related by

$$-\tan\beta = \left(\frac{M-1-G}{G}\right)\tan\alpha_d \tag{3.37}$$

Where

β	displacement front angle
α_d	reservoir tilt angle
M	mobility ratio
G	dimensionless gravity number

Mobility is defined the same way as defined in table 3.4, however gravity number defined differently (Dietz, 1953):

$$G = \frac{\lambda_{r1}{}^{o} k \Delta\rho g \sin\alpha_d}{u_T} \tag{3.38}$$

where

α_d	dip angle

The rest of the notation is the same as used throughout this chapter. The function $\tan\beta$ in equation 3.37 is a measure of stability and must be negative for a stable displacement. The transition between a stable flow and bypassing shown in figure 3.5 in a form of water tongue is observed when

$$\tan\beta = 0 \tag{3.39}$$

The injection rate for the stable displacement has to satisfy the following in a consistent unit system

$$q \le \frac{u_T A G}{M-1} \tag{3.40}$$

where

q	injection rate
A	injection area
u_T	total flux through the system

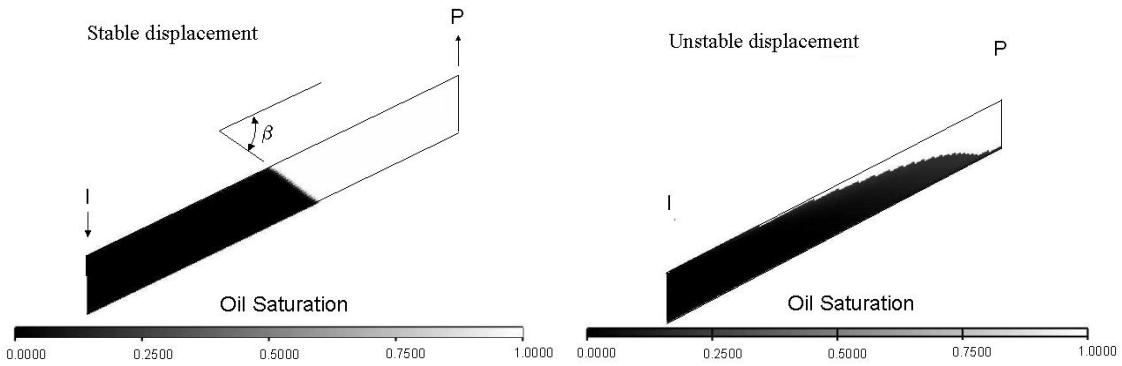

Figure 3.6 Stability as a function of front angle

To validate the development boundary conditions have to match. Therefore the system is limited to two-dimensional system with no-flow boundaries at the top and bottom of the zone of interest. The dimensionless flux in Y and Z direction is equal to 0 and dimensionless flux is equal to total flux. Equations 3.31a and 3.31b can therefore be rewritten to account for the change in pressure as

$$\frac{\partial p_{1D}}{\partial x_D} = -\frac{N_{RX}}{(S_{1D})^{n_1}} u_{1xD} + \frac{N_g N_{TX}}{N_\rho} \tag{3.41a}$$

$$\frac{\partial p_{2D}}{\partial x_D} = -\frac{N_{RX} M}{(S_{2D})^{n_2}} u_{2xD} + \frac{N_g (1 - N_\rho) N_{TX}}{N_\rho} \tag{3.41b}$$

For segregated flow is that there is no transition zone; hence we eliminate intermediate saturations and assume the mobility ratio to be equal to end-point mobility ratio. This will render equations 3.41a and 3.41b in the form

$$\frac{\partial p_{1D}}{\partial x_D} = -N_{RX} u_{1xD} + \frac{N_g N_{TX}}{N_\rho} \tag{3.42a}$$

$$\frac{\partial p_{2D}}{\partial x_D} = -M N_{RX} u_{2xD} + \frac{N_g (1 - N_\rho) N_{TX}}{N_\rho} \tag{3.42b}$$

Dimensionless flux in the X direction in dimensionless form is now equal to 1, providing the following

$$\frac{\partial p_{1D}}{\partial x_D} = -N_{RX} + \frac{N_g N_{TX}}{N_\rho} \tag{3.43a}$$

$$\frac{\partial p_{2D}}{\partial x_D} = -MN_{RX} + \frac{N_g(1-N_\rho)N_{TX}}{N_\rho} \tag{3.43b}$$

Dimensionless phase pressure difference term is

$$\frac{\partial p_{2D}}{\partial x_D} - \frac{\partial p_{1D}}{\partial x_D} = -N_{RX}\left(M + \frac{N_g(1-N_\rho)N_{TX}}{N_{RX}N_\rho} - 1 - \frac{N_g N_{TX}}{N_{RX}N_\rho} \right) \tag{3.44}$$

Rearranging the terms on the right-hand side yields

$$\frac{\partial p_{2D}}{\partial x_D} - \frac{\partial p_{1D}}{\partial x_D} = -N_{RX}\left(M - 1 - \frac{N_g N_{TX}}{N_{RX}} \right) \tag{3.45}$$

The left-hand side can be rearranged as a dimensionless pressure difference providing the following statement

$$\frac{\partial(p_{2D} - p_{1D})}{\partial x_D} = -N_{RX}\left(M - 1 - \frac{N_g N_{TX}}{N_{RX}} \right) \tag{3.46}$$

The difference in phase pressures is defined as pseudocapillary pressure or equivalent height acting perpendicular to reservoir boundary in Z direction. Using the chain rule we obtain

$$\frac{\partial(p_{2D} - p_{1D})}{\partial z_D}\frac{\partial z_D}{\partial x_D} = -N_{RX}\left(M - 1 - \frac{N_g N_{TX}}{N_{RX}} \right) \tag{3.47}$$

Dimensionless direction derivative term in equation 3.47 accounts for both the transformation to dimensionless space effect the angle between the front and upper reservoir boundary at z_D=1. It has the same form as the X-direction tilt number, except that the angle corresponds to front angle rather than tilt angle. Hence

$$\frac{\partial z_D}{\partial x_D} = N_{TX}(\alpha_X = \beta) = \frac{L}{H}\tan\beta \tag{3.48}$$

Assuming no transition zone the pressure difference partial derivative becomes

$$\frac{\partial(p_{2D} - p_{1D})}{\partial z_D} = N_g \tag{3.49}$$

If we substitute terms in equations 3.49 and 3.48 in the equation 3.47 the form of the stability criteria takes shape as presented in equation 3.50.

$$N_g \frac{L}{H} \tan\beta = -N_{RX}\left(M - 1 - \frac{N_g N_{TX}}{N_{RX}} \right) \tag{3.50}$$

Assuming that $\alpha_Y=0$ and $\alpha_X=\alpha_d$ (hence $N_{TX}=N_d$)

$$-\tan\beta = \frac{\left(M - 1 - \frac{N_g N_d}{N_{RX}} \right)}{\frac{N_g N_d}{N_{RX}}} \tan\alpha_d \tag{3.51}$$

Equation 3.51 resembles equation 3.37 proposed by Dietz. If we force the system to be isotropic

$$N_{RL} = \frac{L^2}{H^2} \tag{3.52}$$

Dietz assumed the flux in X direction to be equal to total. To compare dimensionless spaces, we need to accommodate for the difference in scaling procedures. From development presented in Appendix A

$$u_{TDietz} = u_x = u^*_{1x1} = \frac{H}{L} u_T \tag{3.53}$$

Where

u_{TDietz} total flux per Dietz (1953)

u_x flux in X direction

u^*_{1x1} dimensionless space transform

Once the following transformation is performed, assuming that $\alpha_s=0$ equation 3.51 takes the same form as equation 3.37 therefore validating the development. Due to similarity between systems, behavior of dimensionless system with flow in X direction can be accounted for the same way as described by Dietz, which validates analytically the presented development.

3.4. Discussion

Three-dimensional system is represented using 8 dimensionless variables. If the interaction of fluids is analyzed rather than behavior of individual phase, dimensionless

system is reduced to 7 variables. Density number in that case plays no role since it is used to scale the behavior of each individual phase. Remaining 7 numbers fall into three separate groups. These are

- Aspect numbers
- Tilt numbers
- Physical numbers

3.4.1. Aspect number

Reservoir aspect ratio is the most versatile number in the set. Several physical meanings can be assigned. The first meaning is the most commonly used in scaling. It is *effective* or *heterogeneity scaled* aspect ratio (L/H). The second meaning can be observed if number is rearranged in a following form

$$N_R = \frac{L^2}{H^2}\frac{k_z}{k_x} = \frac{L \cdot \dfrac{k_z \cdot \lambda \cdot \Delta p}{H}}{H \cdot \dfrac{k_x \cdot \lambda \cdot \Delta p}{L}} = \frac{L}{H} \cdot \frac{u_z}{u_x} = \frac{t_z}{t_x} \tag{3.54}$$

Where

u	corresponding directional velocity
Δp	imposed pressure difference
t	time

Equation 3.54 indicates that the aspect ratio besides the reservoir aspect scales the velocity as well. Aspect number represents the time ratio for a fluid to flow vertical distance H and horizontal distance L if the same pressure difference is applied. Hence the second meaning is the *relative flow capacity* of the medium in vertical and horizontal direction.

The third meaning used in this research can be observed if the number is rearranged using the following approach

$$N_R = \frac{L^2}{H^2}\frac{k_z}{k_x} = \frac{L \cdot \dfrac{k_z \cdot \lambda}{H \cdot u}}{H \cdot \dfrac{k_x \cdot \lambda \cdot}{L \cdot u}} = \frac{L}{H} \cdot \frac{\Delta p_x A}{\Delta p_z A} = \frac{F_{vx}}{F_{vx}} \tag{3.55}$$

Where

A	flow area

F_v viscous force in corresponding direction

Hence, the aspect number represents the *viscous force ratio* occurring in horizontal and vertical direction yielding the equal flux across the equal flow area. This explanation will later be used in analytical determining of the flow regimes.

3.4.2. Tilt number

Tilt number is a pure geometric factor and can be rearranged as

$$N_T = \frac{L}{H}\tan\alpha = \frac{L}{H}\cdot\frac{\sin\alpha}{\cos\alpha} = \frac{\frac{L}{\cos\alpha}}{\frac{H}{\sin\alpha}} = \frac{L'}{H'} \tag{3.56}$$

Where

L', H' projection of corresponding rotated dimension

As a result the tilt number represents the *measure of rotation* of the system. When multiplied with other numbers it scales their representative meaning from horizontal-vertical to longitudinal-transverse accounting that way for a tilt.

3.4.3. Gravity number

Gravity number is a ratio of *gravity* and *viscous* effects and has so far been assigned either using potential or time approach. For a non-tilted reservoir with length L and height H, pressure difference due to buoyancy is equal to

$$\Delta p_g = \Delta\rho \cdot g \cdot H \tag{3.57a}$$

The potential difference across the reservoir due to viscous forces can be written as

$$\Delta p_v = \frac{u_T \cdot L}{k_x \cdot \lambda_1} \tag{3.57b}$$

Corresponding gravity number (Shook et al, 1992) is therefore

$$N_g{}^P = \frac{\Delta p_g}{\Delta p_v} = \frac{H}{L}\frac{k_x \cdot \lambda \cdot \Delta\rho \cdot g}{u_T} \tag{3.58}$$

This gravity number indicates the expected behavior that gravity effects are larger in *thicker* reservoirs. If time is used as a reference, time necessary for the fluid to be moved across the reservoir as a result of buoyancy is

$$t_g = \frac{H}{k_z \cdot \lambda_1 \cdot \Delta\rho \cdot g} \tag{3.59a}$$

Similarly, time to move the fluid across the reservoir due to viscous forces can be defined as

$$t_v = \frac{L}{u_T} \tag{3.59b}$$

Resulting gravity number (Pozzi and Blackwell, 1963) is

$$N_g = \frac{t_v}{t_g} = \frac{L}{H}\frac{k_z \cdot \lambda \cdot \Delta\rho \cdot g}{u_T} \tag{3.60}$$

Time-defined gravity number indicates that buoyancy effect is more pronounced in *longer* and *thinner* reservoir. Peters et al (1998) experimentally studied this apparent paradox and concluded that both numbers are valid within a given endpoint mobility ratio domain.

For a favorable mobility ratio (M<1), viscous and gravity forces oppose (water under-runs oil) each other and as a result *shorter* and *thicker* medium gave better production response. Unfavorable mobility ratio experiments (M>1) had viscous and gravity forces acting in the same direction (water over-runs oil) so the longer and thinner reservoir gave better production response.

Development presented in this chapter is based under the assumption that dimensionless scale numbers should be independent - however, true independence can only be achieved thru combination of appropriate scaling numbers (equation 3.51). Hence the conclusion of contribution of gravity forces has to be tied with contribution of other numbers.

3.4.4. Capillary number

To be able to compare effects and perform the analysis in terms of flow regimes capillary and gravity number have to be comparable. Link between the buoyancy and capillary effect is achieved using

$$\Delta\rho \cdot g = \frac{P_c(S_1)}{H} = \frac{\sigma}{H}\sqrt{\frac{\phi}{k}} \cdot J(S_1) \tag{3.62}$$

If Leverett's $J(S_1)$ term in equation 3.62 is taken out and remaining terms introduced in equation 3.61 the capillary number becomes a ratio of capillary imbibition velocity and horizontal velocity or

$$N_c = \frac{k_z \cdot \lambda \cdot \sigma}{u_T H}\sqrt{\frac{\phi}{k}} = \frac{u_g}{u_v} \tag{3.63}$$

The development presented here uses the most general set of flow equations. Lack of dependence between the numbers and non-dimensionality enables the comparison between different shapes and scales. The proposed set is more general and more useful for analysis of the governing forces than the previous developments.

An analytical example shows the ease of manipulation with boundary conditions in dimensionless form. Preliminary analysis of figure 3.4 permits a stipulation that some care will have to be taken in terms of representation of gravity and tilt numbers during discretization. Finally, finite differences equation in dimensionless form can now be tested using published approaches for stability (Peaceman, 1977; Aziz and Settari, 1979) and error (Lantz, 1971) making analysis easier and results more general.

CHAPTER 4

ANALYTICAL APPLICATION

Dimensionless numbers are used for analysis and scaling of experimental results. Most studies have been in one spatial dimension, and two-dimensional are often reduced to one-dimensional using pseudofunctions (Lake, 1989). Dimensionless space simplifies analysis and representation of results. To show the ease of developments and visually verify the developed dimensionless system the Dietz stability criteria is extended to 3D.

Inspectional analysis of 3D difference equations and development of fractional flow equation for a 3D dimensionless space can be used to improve reservoir characterization for numerical simulation. These developments, in conjunction with existing work in the area of stability, provide dimensionless criteria for numerically stable displacement. Numerical dispersion is estimated using a similar approach.

The accuracy of upscaling depends on the grouping and averaging based on local flow regimes. Explicit flow-regime cutoffs do not exist so dimensionless equations are used to estimate the extent of particular flow regimes in the dimensionless space. Comparison with small number of published global flow-regime cutoffs leads to a global flow regime map. This map guides the dimensionless ranges for the simulations in chapter 5.

4.1. Segregated flow in three dimensional system

The system is now extended in three spatial dimensions. No-flow boundaries are at the top and bottom of the zone of interest. The dimensionless flux in *Z*-direction is equal to 0 and the sum of dimensionless fluxes in *X*- and *Y*-direction is equal to total flux. Equations 3.31a and 3.31b can therefore be rewritten to account for the change in pressure as

$$\frac{\partial p_{1D}}{\partial x_D} = -\frac{N_{RX}}{\left(S_{1D}\right)^{n_1}} u_{1xD} + \frac{N_g N_{TX}}{N_\rho} \tag{4.1a}$$

$$\frac{\partial p_{2D}}{\partial x_D} = -\frac{N_{RX} M}{\left(S_{2D}\right)^{n_2}} u_{2xD} + \frac{N_g \left(1 - N_\rho\right) N_{TX}}{N_\rho} \tag{4.1b}$$

Again, flow is assumed to be piston-like and the mobility ratio to be equal to end-point mobility ratio. Equations 4.18a and 4.18b become

$$\frac{\partial p_{1D}}{\partial x_D} = -N_{RX} u_{1xD} + \frac{N_g N_{TX}}{N_\rho} \tag{4.2a}$$

$$\frac{\partial p_{2D}}{\partial x_D} = -MN_{RX} u_{2xD} + \frac{N_g (1 - N_\rho) N_{TX}}{N_\rho} \tag{4.2b}$$

Dimensionless flux in the X direction in dimensionless form is now equal to u_{TxD}, providing the following

$$\frac{\partial p_{1D}}{\partial x_D} = -N_{RX} u_{TxD} + \frac{N_g N_{TX}}{N_\rho} \tag{4.3a}$$

$$\frac{\partial p_{2D}}{\partial x_D} = -MN_{RX} u_{TxD} + \frac{N_g (1 - N_\rho) N_{TX}}{N_\rho} \tag{4.3b}$$

Rearranged, dimensionless phase pressure difference term can be written as

$$\frac{\partial (p_{2D} - p_{1D})}{\partial x_D} = -N_{RX} u_{TxD} \left(M - 1 - \frac{N_g N_{TX}}{N_{RX} u_{TxD}} \right) \tag{4.4}$$

The difference in phase pressures is the pseudocapillary pressure or equivalent height acting perpendicular to reservoir boundary in Z direction. Using the chain rule we obtain

$$\frac{\partial (p_{2D} - p_{1D})}{\partial z_D} \frac{\partial z_D}{\partial x_D} = -N_{RX} u_{TxD} \left(M - 1 - \frac{N_g N_{TX}}{N_{RX} u_{TxD}} \right) \tag{4.5}$$

Accounting for the front angle and transformation to dimensionless space effect the angle the front plane closes with boundary at z_D=1 in X-direction becomes

$$\frac{\partial z_D}{\partial x_D} = N_{TX} (\alpha_X = \beta_x) = \frac{L}{H} \tan \beta_x \tag{4.6}$$

Assuming no transition zone the pressure difference partial derivative becomes

$$\frac{\partial (p_{2D} - p_{1D})}{\partial z_D} = N_g \tag{4.7}$$

If in equations 4.24 and 4.23 are substituted in the equation 4.22 the form of the stability criterion is

$$N_g \frac{L}{H} \tan \beta = -N_{RX} \left(M - 1 - \frac{N_g N_{TX}}{N_{RX} u_{TxD}} \right) \tag{4.8}$$

Rearranging the equation 4.10 explicitly for the front angle provides

$$-\tan\beta_x = \frac{\left(M-1-\dfrac{N_g N_{TX}}{N_{RX}u_{TxD}}\right)}{\dfrac{N_g N_{TX}}{N_{RX}u_{TxD}}}\tan\alpha_{TX} \tag{4.9a}$$

Similarly, for the Y-direction,

$$-\tan\beta_y = \frac{\left(M-1-\dfrac{N_g N_{TY}}{N_{RY}u_{TyD}}\right)}{\dfrac{N_g N_{TY}}{N_{RY}u_{TyD}}}\tan\alpha_{TY} \tag{4.9b}$$

Applying Dietz's reasoning we obtain the following

$$1 < \frac{\dfrac{N_g N_{TX}}{N_{RX}u_{TxD}}}{M-1} \tag{4.10a}$$

$$1 < \frac{\dfrac{N_g N_{TY}}{N_{RY}u_{TyD}}}{M-1} \tag{4.10b}$$

Both equations can now be multiplied by q_T and corresponding dimensionless velocity component.

$$u_{TxD}\cdot q_T < \frac{q_T\dfrac{N_g N_{TX}}{N_{RX}}}{M-1} \tag{4.11a}$$

$$u_{TyD}\cdot q_T < \frac{q_T\dfrac{N_g N_{TY}}{N_{RY}}}{M-1} \tag{4.11b}$$

Left-hand side in equations 4.11a and 4.11b is q_X and q_Y respectively. Total rate on the right-hand side can be expressed using the following

$$q_T = u_T HW \tag{4.12}$$

Height H multiplied by width W is flow area in Z direction. For flow in X- and Y-direction $q_T - u_T$ relationship should be transformed using appropriate flow area. To keep the left-hand side in equations 4.9a and 4.9b negative and maintain segregated flow (the Dietz (1953) criterion based on geometric arguments), the limit on flow rate becomes

$$q_X \le \frac{u_T \frac{L}{H} A_x \frac{N_g N_{TX}}{N_{RX} u_{TxD}}}{M-1} \tag{4.13a}$$

$$q_Y \le \frac{u_T \frac{W}{H} A_y \frac{N_g N_{TY}}{N_{RY} u_{TyD}}}{M-1} \tag{4.13b}$$

Returning to dimensional space yields the critical injection rates for *X*- and *Y*-direction as

$$q_{Xcrit} = 4.9\times10^{-4} \frac{A_x k_x \lambda_{r1}{}^o \Delta\gamma g \cdot \sin\alpha_X \cos\alpha_Y}{(M-1)} \tag{4.14a}$$

$$q_{Ycrit} \le 4.9\times10^{-4} \frac{A_y k_y \lambda_{r1}{}^o \Delta\gamma g \cdot \sin\alpha_Y \cos\alpha_X}{(M-1)} \tag{4.14b}$$

The difference between standard Dietz and presented equations is the tilt in two directions accounted for in 3D, rather than dip used in the original 2D Dietz's system. If the system is re-aligned to account for maximum angle, cosine terms will disappear. Remaining trigonometric term would include dip in original form $sin(\alpha_D)$ same as in chapter 3. This term would be contained only in the dipping direction. Horizontal direction would have the sine function equal to zero hence the Dietz type of analysis could not be applied.

Aligning the system with the dip is not always possible so a novelty - two tilts in the gravity component governing the flow in a 3D dimensionless system and additional aspect ratio and tilt number – can now be visually tested. If the dimensionless numbers are developed correctly, canceling out the variables contained in dimensionless numbers should show that the behavior is scaled properly using proposed dimensionless numbers (equations 4.12a and 4.12b).

Two directional stability criteria (equations 4.14a and 4.14b) provide four separate stability cases. Conceptual schematics of displacing fluid front for these cases are shown in figures 4.1 through 4.4.

- $q_x \leq q_{x_{crit}}$, $q_y \leq q_{y_{crit}}$

Flow is stable in both directions. Displacement front becomes a plane with X- and Y- direction differentials equal to $tan\beta_X$ and $tan\beta_Y$ respectively.

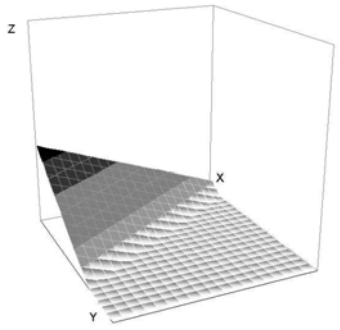

Figure 4.1. *X* stable, *Y* stable

- $q_x > q_{x_{crit}}$, $q_y \leq q_{y_{crit}}$

Flow is stable in Y- direction. X-direction flow exhibits unstable behavior. Front in X-direction forms a water tongue. Stability in Y-direction dictates a constant Y-direction derivative along the front ($tan\beta_Y$).

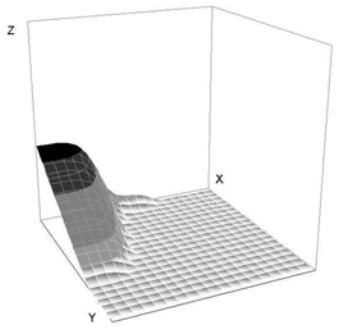

Figure 4.2. *X* unstable, *Y* stable

- $q_x \leq q_{x_{crit}}$, $q_y > q_{y_{crit}}$

Flow is stable in X- direction. Similar as in previous partially stable system, Y-direction front forms a water tongue. X-direction derivative is constant along the front and equal to $tan\beta_X$.

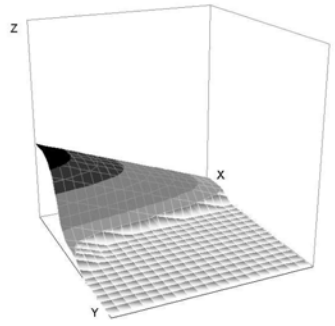

Figure 4.3. *X* stable, *Y* unstable

- $q_x > q_{x_{crit}}$, $q_y > q_{y_{crit}}$

  Flow is unstable in both directions. As a result, directional derivatives are not constant in either direction. They become a function of position along the front. Water tongue will form in both directions.

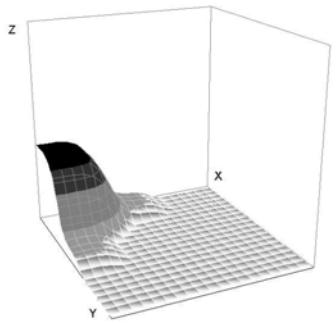

Figure 4.4. *X* unstable, *Y* unstable

These observations together with equations 4.14a and 4.14b can be used for visual verification of the validity of 3D dimensionless system. Three assumptions have to be made for simulation purposes:

- Injection from point source - well is connected to a most bottom gridblock
- Production from surfaces away from a source – production wells are connected to a face of interest instead of usual linear sink
- Steady-state incompressible flow, vertical equilibrium

These assumptions make the flow from the injection point to production face linear. The system streamlines become linear fairly close to the source point and observed front stabilizes at rates suggested by equations 4.14a and 4.14b.

Model used for verification needed rotated 3D Cartesian system. To allow for rotation in ECLIPSE, system used cornerpoint geometry to accommodate for tilt angles while maintaining the gridblock faces perpendicular. Length, height and width of the gridblock are the same.

Gravity stable displacement in figure 4.5 is indicated by a straight-line front at the edge of the model. To accent the stable and unstable direction, the shape of front is marked with additional line. Displacement was stable in both directions if the rates were at or below critical rate. A slight increase in rate in one direction leads to instability in the form of

water-tongue. Displacing fluid saturation snapshots for different stability cases are presented in figure 4.5.

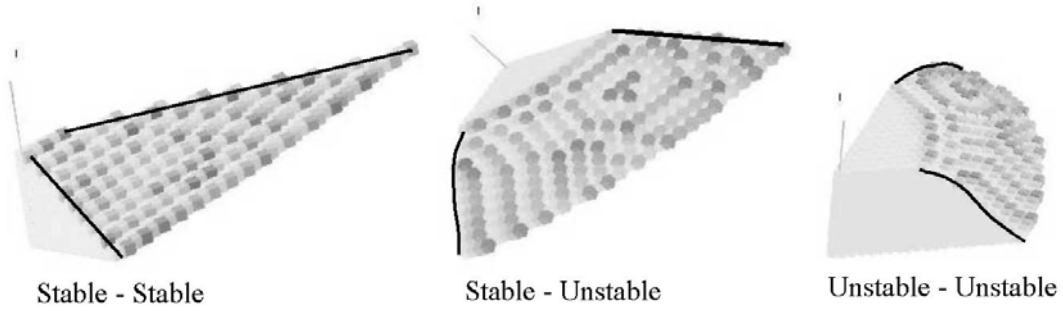

Figure 4.5. Water front from numerical simulation cases (M=0.5)

Visual inspection of saturation distribution aided in validating the critical rates and also provided the proof that in a 3D system each of the directions can be dominated by different flow regime – i.e. one direction can exhibit gravity stable flow while another can be unstable.

4.2. Fractional flow equation in dimensionless space

Several authors presented the fractional flow equations in one-dimensional space (Dake, 1978; Lake 1989). Boundary conditions for analysis in three dimensions are different. Flow occurs in all three directions and flowing fractions may differ by direction. Directional total fluxes are defined as

$$u_{TxD} = u_{1xD} + u_{2xD} \tag{4.15a}$$

$$u_{TyD} = u_{1yD} + u_{2yD} \tag{4.15b}$$

$$u_{TzD} = u_{1zD} + u_{2zD} \tag{4.15c}$$

where

$u_{TxD}, u_{TyD}, u_{TzD}$ total dimensionless velocity in X, Y and Z direction, respectively

From boundary conditions imposed during the development sum of directional dimensionless velocities is a total flux or in dimensionless form

$$u_{TxD} + u_{TyD} + u_{TzD} = 1 \tag{4.16}$$

Phase velocities in *X*-direction from chapter 3 in dimensionless form are

$$u_{1xD} = -\frac{1}{N_{RX}}(S_{1D})^{n_1}\left(\frac{\partial p_{1D}}{\partial x_D} - \frac{N_g N_{TX}}{N_\rho}\right) \tag{4.17a}$$

$$u_{2xD} = -\frac{1}{N_{RX}M}(S_{2D})^{n_2}\left(\frac{\partial p_{2D}}{\partial x_D} - \frac{N_g(1-N_\rho)N_{TX}}{N_\rho}\right) \tag{4.17b}$$

Total velocity term from equation 4.1a can be rearranged in a form of

$$u_{2xD} = u_{TxD} - u_{1xD} \tag{4.18}$$

Material balance for two-phase system dictates

$$S_{2D} = 1 - S_{1D} \tag{4.19}$$

Substituting equation 4.18 in 4.17b and rearranging yields

$$\frac{N_{RX}M}{(1-S_{1D})^{n_2}}u_{TxD} - \frac{N_{RX}M}{(1-S_{1D})^{n_2}}u_{1xD} = -\left(\frac{\partial p_{2D}}{\partial x_D} - \frac{N_g(1-N_\rho)N_{TX}}{N_\rho}\right) \tag{4.20}$$

Equation 4.3a can also be rearranged to take the following form

$$\frac{N_{RX}}{(S_{1D})^{n_1}}u_{1xD} = -\left(\frac{\partial p_{1D}}{\partial x_D} - \frac{N_g N_{TX}}{N_\rho}\right) \tag{4.21}$$

If equations 4.7 and 4.6 are subtracted fractional flow equation becomes

$$\frac{N_{RX}}{(S_{1D})^{n_1}}u_{1xD} - \frac{N_{RX}M}{(1-S_{1D})^{n_2}}u_{TxD} + \frac{N_{RX}M}{(1-S_{1D})^{n_2}}u_{1xD} = \frac{\partial p_{2D}}{\partial x_D} - \frac{\partial p_{1D}}{\partial x_D} - N_g N_{TX} \tag{4.22}$$

Knowing that dimensionless pressure differentials can be related as

$$\frac{\partial p_{2D}}{\partial x_D} - \frac{\partial p_{1D}}{\partial x_D} = N_c\frac{\partial J(S_{1D})}{\partial x_D} \tag{4.23}$$

After rearranging, the equation 4.22 is

$$u_{1xD}\left(\frac{N_{RX}}{(S_{1D})^{n_1}} + \frac{N_{RX}M}{(1-S_{1D})^{n_2}}\right) - \frac{N_{RX}M}{(1-S_{1D})^{n_2}}u_{TxD} = N_c\frac{\partial J(S_{1D})}{\partial x_D} - N_g N_{TX} \tag{4.24}$$

Fractional flow in the reservoir in the *X*-direction of the dimensionless space at any point x_D, y_D, z_D is

$$f_{1xD} = \frac{u_{1xD}}{u_{TxD}} \tag{4.25}$$

Where f_{1xD} is the fractional flow in *X*-direction in dimensionless space. Substituting equation 4.25 in equation 4.24 yields

$$f_{1xD}u_{TxD}\left(\frac{N_{RX}}{(S_{1D})^{n_1}}+\frac{N_{RX}M}{(1-S_{1D})^{n_2}}\right)-\frac{N_{RX}M}{(1-S_{1D})^{n_2}}u_{TxD}=N_c\frac{\partial J(S_{1D})}{\partial x_D}-N_gN_{TX} \tag{4.26}$$

Rearranging for fractional flow and generalizing the notation provides the final equation in the following form

$$f_{1xD}=A_D+A_D\frac{(1-S_{1D})^{n_2}}{M}\left(\frac{N_c}{N_{RX}u_{TxD}}\frac{\partial J(S_{1D})}{\partial x_D}-\frac{N_gN_{TX}}{N_{RX}u_{TxD}}\right) \tag{4.27a}$$

Development can be repeated for remaining two directions. Resulting fractional flow equations in *Y*- and *Z*-direction are

$$f_{1yD}=A_D+A_D\frac{(1-S_{1D})^{n_2}}{M}\left(\frac{N_c}{N_{RY}u_{TyD}}\frac{\partial J(S_{1D})}{\partial y_D}-\frac{N_gN_{TY}}{N_{RY}u_{TyD}}\right) \tag{4.27b}$$

$$f_{1zD}=A_D+A_D\frac{(1-S_{1D})^{n_2}}{M}\left(\frac{N_c}{u_{TxD}}\frac{\partial J(S_{1D})}{\partial z_D}-\frac{N_g}{u_{TxD}}\right) \tag{4.27c}$$

The constant component A_D is estimated as

$$A_D=\frac{M(S_{1D})^{n_1}}{M(S_{1D})^{n_1}+(1-S_{1D})^{n_2}} \tag{4.28}$$

To verify the development the system can be reduced to one dimension. Assuming the total flow is only in X direction u_{TxD} becomes equal to 1. Equation 4.27a reduces to

$$f_{1xD}=\frac{M(S_{1D})^{n_1}}{M(S_{1D})^{n_1}+(1-S_{1D})^{n_2}}+\frac{(S_{1D})^{n_1}(1-S_{1D})^{n_2}}{M(S_{1D})^{n_1}+(1-S_{1D})^{n_2}}\left(\frac{N_c}{N_{RX}}\frac{\partial J(S_{1D})}{\partial x_D}-\frac{N_gN_{TX}}{N_{RX}}\right)$$

$$\forall x_D\in[0,1],y_D=0,z_D\in[0,1] \tag{4.29}$$

To compare the developed equation with already existing equation 4.29 is transformed form dimensionless space to dimensional. *X*-direction velocity is scaled using

$$u_x=u^*_{1x1}=\frac{H}{L}u_T \tag{4.30}$$

Neglecting the *Y*-direction tilt and applying the transform from equation 4.30, equation 4.29 becomes

$$f_{1xD} = \frac{M\left(S_{1D}\right)^{n_1}}{M\left(S_{1D}\right)^{n_1} + \left(1 - S_{1D}\right)^{n_2}} + \frac{\left(S_{1D}\right)^{n_1}\left(1 - S_{1D}\right)^{n_2}}{M\left(S_{1D}\right)^{n_1} + \left(1 - S_{1D}\right)^{n_2}} \left(\begin{array}{l} \dfrac{\sigma k_x \lambda_{r1}{}^{o}}{u_x} \sqrt{\dfrac{\phi}{k_z}} \dfrac{\partial J\left(S_{1D}\right)}{\partial x} - \\ \dfrac{k_x \lambda_{r1}{}^{o} \Delta\rho g \cdot \sin\alpha_X}{u_x} \end{array} \right)$$

$$\forall x \in [0, L], y \in [0, W], z \in [0, H] \tag{4.31}$$

Equation 4.47 is the same as presented in literature (Dake, 1978; Lake 1989) validating the development. To make the equation similar to those in the 1D space we made the assumption of only one angle mapping the contribution of *Z*-direction effects on the flow in *X*-direction. This might be true for simple conceptual studies. Petroleum reservoirs are geologically complex so – similar to reasoning made for 3D segregated flow- flow is not always aligned with the direction of largest angle (dip). The system presented here accounts for all the effects.

The dimensionless approach presented enables more general behavior analysis. Total number of variables is reduced from more than 30 to 7 hence simulation design can be improved by reduction in number of necessary runs. Since the system is dimensionless, any reservoir having the same value of dimensionless variables will exhibit the same behavior.

Several references exist for a 1D fractional flow development utilizing dimensionless numbers - Lake (1989) for *X*-direction only and Hagoort (1980) for *Z*-direction only. Both one-dimensional developments assumed pseudo-vertical equilibrium hence the only resulting dimensionless numbers are gravity and capillary number. Derivation approach was not identical so referenced numbers do not match. As a result the system in 2D scaled by directly accepting individual equations would not be consistent. The system presented here is unique since it is applicable in 3D and the most succinct since the reduction in any dimension is achieved simply by dropping the dimension of interest.

Fractional flow equation in 3D space can also be used for stability and error analysis in reservoir simulations. Using the transforms presented in previous sections equation 3.31a from Chapter 3 can now be rearranged in a form of

$$\frac{\partial S_{1D}}{\partial t_D} + \frac{\partial f_{1xD}}{\partial x_D} + \frac{\partial f_{1yD}}{\partial y_D} + \frac{\partial f_{1zD}}{\partial z_D} = 0 \tag{4.32}$$

This is the three-dimensional convection equation in dimensionless space written in terms of fractional flow.

4.3. Numerical reservoir characterization

Dimensionless numbers have so far been used to scale the behavior from laboratory measurements to a particular reservoir of interest (Rapoport, 1954; Craig *et al*, 1957; van Daalen and van Domselaar, 1972). Inspectional analysis presented in Appendix A shows that the general form of equations is preserved during the transformation from dimensional to dimensionless space. Similitude between equations and lack of dimensionality makes *analytical* dimensionless groups an ideal tool for general observations on flow behavior.

Numerical simulations are based on spatial and temporal discretization of differential flow equations. Flow equations in dimensionless and dimensional form are of similar order and shape. Therefore if both are written in the same discrete manner a comparison between dimensional and dimensionless difference equations can provide an accurate way to determine *numerical* dimensionless groups.

The number of parameters in dimensional difference equation is much larger than for the dimensionless case. Therefore, if the difference equation in dimensionless form is used, any estimate in terms of stability, error and regimes governing the flow can be related through numerical dimensionless groups. This approach would provide a screening test for the discretization scheme and enable the *a priori* estimate of the behavior of the model.

Inspectional analysis on general difference equations is discussed in Appendix B. Comparison with Appendix A shows that inspectional analysis kept the form of the difference equations and that related dimensionless groups are obtained. Unlike analytical groups used to quantify global behavior, numerical groups can be calculated to enable estimate for each gridblock on local, regional and global scale by applying the appropriate L, W and H (see Appendix B).

4.3.1. Numerical stability analysis and time step length

Numerical simulation solves differential equations through substitution of differential by difference equations. Three independent cases could be considered for each of the

independent variables. Spatial differences can be downstream, center-in-distance or upstream approximation, whereas differentiation in time can be explicit, center-in-time and implicit. Peaceman (1977) presents simplified general analysis for all nine resulting cases.

Implicit and center-in-time schemes are considered stable (Peaceman, 1977, Aziz and Settari, 1979). Further investigation focuses on the explicit differentiation approach. The case of interest is fully explicit sequential scheme (e.g., UTCHEM, Saad, 1989).

Any computation scheme is considered stable if the effect of an error made in one stage of computation does not propagate into larger error in later stage of computation. Peaceman (1977) suggests the use of von Neumann criteria for stability analysis. The method in three dimensions consists of writing the error in a Fourier series with a form

$$\varepsilon_{I,J,K}^{m} = \gamma^{(m-1)} e^{ip\Delta x} e^{iq\Delta y} e^{ir\Delta y} \quad \text{(4.33)}$$

Where

$\varepsilon_{I,J,K}^{m}$	error introduced at time step *m* and gridblock *I*, *J*, *K*
γ	amplification factor
p, q, r	number of gridblocks in *X*, *Y*, *Z* direction (upstream positive and downstream negative)
i	imaginary component $\left(\sqrt{-1}\right)$

The output error in a linear equation can be obtained by solving the linear equation using the error as the unknown. Amplification factor γ between two time steps is obtained by introducing the error term from equation 4.1 in the linear difference. Stable system is inferred if γ satisfies the following

$$-1 \le \gamma \le 1 \quad \text{(4.34)}$$

Appendix B presents the inspectional analysis of finite difference equation. Because the dimensional and dimensionless equations must have the same form, analysis of stability and error can be performed in dimensionless space.

Fractional flow is a function of displacing phase saturation and a set of dimensionless numbers (equations 4.27a through 4.27c). If the chain rule is applied equation 4.32 becomes

$$\frac{\partial S_{1D}}{\partial t_D}+\frac{\partial f_{xD}}{\partial S_{1D}}\frac{\partial S_{1D}}{\partial x_D}+\frac{\partial f_{yD}}{\partial S_{1D}}\frac{\partial S_{1D}}{\partial y_D}+\frac{\partial f_{zD}}{\partial S_{1D}}\frac{\partial S_{1D}}{\partial z_D}=0 \tag{4.35}$$

If differentials in equation 4.35 are substituted with differences,

$$\frac{{S_{1D,i,j,k}}^{m+1}-{S_{1D,i,j,k}}^{m}}{\Delta t_D}+\left[\begin{array}{l}\left(\frac{\partial f_{xD}}{\partial S_{1D}}\right)^{z}\left(\frac{{S_{1D,i,j,k}}^{z}-{S_{1D,i-1,j,k}}^{z}}{\Delta x_D}\right)+\\ \left(\frac{\partial f_{yD}}{\partial S_{1D}}\right)^{z}\left(\frac{{S_{1D,i,j,k}}^{z}-{S_{1D,i,j-1,k}}^{z}}{\Delta y_D}\right)+\\ \left(\frac{\partial f_{zD}}{\partial S_{1D}}\right)^{z}\left(\frac{{S_{1D,i,j,k}}^{z}-{S_{1D,i,j,k-1}}^{z}}{\Delta z_D}\right)\end{array}\right]=0 \tag{4.36}$$

Coefficient z marks the time step at which the non-linear fractional flow term is being estimated. If z is set to m the mobility will be estimated at the current time step so the method tested for stability corresponds to explicit procedure. If z is set to $m+1$, we can test the stability requirements for the fully implicit sequential procedure.

To test the stability of explicit procedure equation 4.32 is written in a difference form as

$$\frac{{S_{1D,i,j,k}}^{m+1}-{S_{1D,i,j,k}}^{m}}{\Delta t_D}+\left[\begin{array}{l}\left(\frac{\partial f_{xD}}{\partial S_{1D}}\right)^{m}\left(\frac{{S_{1D,i,j,k}}^{m}-{S_{1D,i-1,j,k}}^{m}}{\Delta x_D}\right)+\\ \left(\frac{\partial f_{yD}}{\partial S_{1D}}\right)^{m}\left(\frac{{S_{1D,i,j,k}}^{m}-{S_{1D,i,j-1,k}}^{m}}{\Delta y_D}\right)+\\ \left(\frac{\partial f_{zD}}{\partial S_{1D}}\right)^{m}\left(\frac{{S_{1D,i,j,k}}^{m}-{S_{1D,i,j,k-1}}^{m}}{\Delta z_D}\right)\end{array}\right]=0 \tag{4.37}$$

Where

$\left(\frac{\partial f_{xD}}{\partial S_{1D}}\right)^{m}$ dimensionless fractional flow chord estimated in *X*-direction

$\left(\frac{\partial f_{xD}}{\partial S_{1D}}\right)^{m}$ dimensionless fractional flow chord estimated in *Y*-direction

$\left(\frac{\partial f_{xD}}{\partial S_{1D}}\right)^{m}$ dimensionless fractional flow chord estimated in *Z*-direction

Introducing the error term equation 4.12 becomes

$$\frac{\gamma-1}{\Delta t_D}+\left[\left(\frac{\partial f_{xD}}{\partial S_{1D}}\right)^m\left(\frac{1-e^{-ip\Delta x_D}}{\Delta x_D}\right)+\left(\frac{\partial f_{yD}}{\partial S_{1D}}\right)^m\left(\frac{1-e^{-iq\Delta y_D}}{\Delta y_D}\right)+\left(\frac{\partial f_{zD}}{\partial S_{1D}}\right)^m\left(\frac{1-e^{-ir\Delta z_D}}{\Delta z_D}\right)\right]=0 \qquad (4.38)$$

If non-linear term is estimated correctly the amplification term becomes

$$\gamma=1+\Delta t_D\left[\left(\frac{\partial f_{xD}}{\partial S_{1D}}\right)^m\frac{\left(1-e^{-ip}\right)}{\Delta x_D}+\left(\frac{\partial f_{yD}}{\partial S_{1D}}\right)^m\frac{\left(1-e^{-iq}\right)}{\Delta y_D}+\left(\frac{\partial f_{zD}}{\partial S_{1D}}\right)^m\frac{\left(1-e^{-ir}\right)}{\Delta z_D}\right] \qquad (4.39)$$

Using the criteria from equation 4.34 the stability interval is determined from

$$-1\le 1+\Delta t_D\left[\left(\frac{\partial f_{xD}}{\partial S_{1D}}\right)^m\frac{\left(1-e^{-ip}\right)}{\Delta x_D}+\left(\frac{\partial f_{yD}}{\partial S_{1D}}\right)^m\frac{\left(1-e^{-iq}\right)}{\Delta y_D}+\left(\frac{\partial f_{zD}}{\partial S_{1D}}\right)^m\frac{\left(1-e^{-ir}\right)}{\Delta z_D}\right]\le 1 \qquad (4.40)$$

Right-hand side of the term or minimum time-step is easy to accommodate for - t_D has to be greater than zero. The left-hand side or the maximum time-step can be expressed as

$$\Delta t_D\le\frac{2}{\left[\frac{1}{\Delta x_D}\left(\frac{\partial f_{xD}}{\partial S_{1D}}\right)^m\left(1-e^{-ip\Delta x_D}\right)+\frac{1}{\Delta y_D}\left(\frac{\partial f_y}{\partial S_{1D}}\right)^m\left(1-e^{-iq\Delta y_D}\right)+\frac{1}{\Delta z_D}\left(\frac{\partial f_z}{\partial S_{1D}}\right)^m\left(1-e^{-ir\Delta z_D}\right)\right]}$$

$$\forall i,j,k \qquad (4.41a)$$

Analysis of equation 4.41a shows that the minimum value of timestep occurs when exponential terms become equal to 2. By bounding the arguments equation 4.41a takes the following form

$$\Delta t_D\le\frac{1}{\left[\frac{1}{\Delta x_D}\left(\frac{\partial f_{xD}}{\partial S_{1D}}\right)^m+\frac{1}{\Delta y_D}\left(\frac{\partial f_y}{\partial S_{1D}}\right)^m+\frac{1}{\Delta z_D}\left(\frac{\partial f_z}{\partial S_{1D}}\right)^m\right]} \qquad (4.41b)$$

The maximum time step size for stable run at any point in time *m* is equal to minimum value of Δt_D estimated from equation 4.14a for all the gridblocks in the system. If the time step is larger than minimum, gridblocks (*i, j, k*) with $(\Delta t_D)_{i,j,k}$ larger than chosen Δt_D become a possible source of instability.

If dimensionless numbers in equation 4.41 are estimated locally Δx_D, Δy_D and Δz_D become equal to one. As a result, dimensionless time difference becomes equal to gridblock pore volume per unit time.

Similar dimensionless solution could be obtained by using existing stability analysis and inspectional analysis procedure provided in Appendix B. However, surveyed literature usually excludes gravity and capillary effects to simplify the development.

Purpose of this study is to provide the tool that scales all the variables affecting the flow and resulting effects on the numerical model. Therefore, rather than combining observations and repeating inspectional analysis, the stability analysis is repeated including all the effects in the dimensionless space.

4.3.2. Numerical dispersion

Whenever a differential equation is replaced by a difference equation replacement introduces a truncation error. Truncation error mathematically originates from neglecting the high order terms. Lantz (1971) gave the truncation error a physical meaning. To illustrate the method of quantifying numerical dispersion, he considered the convection-diffusion equation in the following form

$$\frac{\partial C_D}{\partial t_D} = D\frac{\partial^2 C_D}{\partial x_D{}^2} - \frac{\partial C_D}{\partial x_D} \tag{4.42}$$

Where

C_D	dimensionless concentration
D	dispersion coefficient
t_D, x_D	dimensionless time and distance, respectively
$D\frac{\partial^2 C_D}{\partial x_D{}^2}$	diffusion term
$\frac{\partial C_D}{\partial x_D}$	convection term

To compare the convection-diffusion equation to the two-phase flow equation, Lantz used the frontal advance equation. Frontal advance equation can be written as

$$\frac{\partial S_{1D}}{\partial t_D} = -\frac{df_1}{dS_{1D}}\frac{\partial S_{1D}}{\partial x_D} \tag{4.43}$$

If the source is assumed at the origin of coordinate system and upstream mobility is used, frontal advance equation can be written in a form of Taylor's series as

$$\frac{\partial S_{1D}}{\partial t_D} = -\frac{df_1}{dS_{1D}}\frac{\partial S_{1D}}{\partial x_D} + \frac{df_1}{dS_{1D}}\left(\frac{\Delta x_D - \frac{df_1}{dS_{1D}}\Delta t_D}{2}\right)\frac{\partial^2 S_{1D}}{\partial x_D^{\,2}} + \theta(x_D, t_D) \tag{4.44}$$

Where

$\theta(x_D, t_D)$ high-order error term

High order error term in equation 4.22 is usually neglected therefore equation 4.22 is similar to equation 4.20. As a result, truncation error can therefore be estimated as a numerical equivalent to dispersion as

$$D_n = \frac{df_1}{dS_{1D}}\left(\frac{\Delta x_D - \frac{df_1}{dS_{1D}}\Delta t_D}{2}\right) \tag{4.45}$$

Lantz verified this solution to the convection-dispersion equation using well-known solution to the equivalent convection-diffusion equation (Koonce *et al*, 1965; Lake, 1989; Charbeneau, 2000). Lantz's estimation of the truncation error for different differentiation scheme is presented in table 2.6 in Chapter 2.

Dispersion in porous media is a directional property so modified approach has to be taken in a three-dimensional space. Equivalent general solute transport equation for this problem (Charbeneau, 2000) can be written as

$$\frac{\partial C}{\partial t} = -v_x\frac{\partial C}{\partial x} - v_y\frac{\partial C}{\partial y} - v_z\frac{\partial C}{\partial z} + D_{xx}\frac{\partial^2 C}{\partial x^2} + D_{yy}\frac{\partial^2 C}{\partial y^2} + D_{zz}\frac{\partial^2 C}{\partial z^2} \tag{4.46}$$

Where

C concentration

D_{xx}, D_{yy}, D_{zz} X, Y and Z direction dispersion coefficients

v_x, v_y, v_z X, Y, Z direction advection velocity

To estimate the numerical dispersion by analogy to the solute transport equation, the fractional flow equation for a three-dimensional system can be written as

$$\frac{\partial S_{1D}}{\partial t_D} = -\frac{df_x}{dS_{1D}}\frac{\partial S_{1D}}{\partial x_D} - \frac{df_y}{dS_{1D}}\frac{\partial S_{1D}}{\partial y_D} - \frac{df_z}{dS_{1D}}\frac{\partial S_{1D}}{\partial z_D} \tag{4.47}$$

Expanding the equation 4.47 around x_D, y_D, z_D using Taylor's series and eliminating high order terms provides the following equation

$$\frac{\partial S_{1D}}{\partial t_D} = \left(\begin{array}{l} -\frac{df_x}{dS_{1D}}\frac{\partial S_{1D}}{\partial x_D} - \frac{df_y}{dS_{1D}}\frac{\partial S_{1D}}{\partial y_D} - \frac{df_z}{dS_{1D}}\frac{\partial S_{1D}}{\partial z_D} + \frac{df_x}{dS_{1D}}\left(\frac{\Delta x_D - \frac{df_x}{dS_{1D}}\Delta t_D}{2} \right)\frac{\partial^2 S_{1D}}{\partial x_D^{\,2}} \\ + \frac{df_y}{dS_{1D}}\left(\frac{\Delta y_D - \frac{df_y}{dS_{1D}}\Delta t_D}{2} \right)\frac{\partial^2 S_{1D}}{\partial y_D^{\,2}} + \frac{df_z}{dS_{1D}}\left(\frac{\Delta z_D - \frac{df_z}{dS_{1D}}\Delta t_D}{2} \right)\frac{\partial^2 S_{1D}}{\partial z_D^{\,2}} \end{array} \right) \tag{4.48}$$

The result is similar to the solution proposed by Lantz, except the directionality of the numerical dispersion indicated by the directional dimensionless fractional flow. The fractional flow derivative is a function of saturation and contains saturation derivative of $J(S_{1D})$ (see equations 4.27a through c). Literature suggests that gravity and capillary effects tend to smooth the saturation front.

Overview of the numerical dispersion for upstream weighted mobility is presented in table 4.1.

Table 4.1. Numerical dispersion in three-dimensional anisotropic media

Scheme	D_{xx}	D_{yy}	D_{zz}
Explicit	$\frac{df_x}{dS_{1D}}\left(\frac{\Delta x_D - \frac{df_x}{dS_{1D}}\Delta t_D}{2} \right)$	$\frac{df_y}{dS_{1D}}\left(\frac{\Delta y_D - \frac{df_y}{dS_{1D}}\Delta t_D}{2} \right)$	$\frac{df_z}{dS_{1D}}\left(\frac{\Delta z_D - \frac{df_z}{dS_{1D}}\Delta t_D}{2} \right)$
Implicit	$\frac{df_x}{dS_{1D}}\left(\frac{\Delta x_D + \frac{df_x}{dS_{1D}}\Delta t_D}{2} \right)$	$\frac{df_y}{dS_{1D}}\left(\frac{\Delta y_D + \frac{df_y}{dS_{1D}}\Delta t_D}{2} \right)$	$\frac{df_z}{dS_{1D}}\left(\frac{\Delta z_D + \frac{df_z}{dS_{1D}}\Delta t_D}{2} \right)$

Even though the implicit formulation is unconditionally stable, results in table 4.1 show that the error for implicit formulations is always larger than for explicit formulations. Implicit simulators obtain this stability at the expense of increased smoothing or numerical dispersion. Indeed, the stability criteria are equivalent to requiring that the numerical dispersion is nonnegative. For explicit formulations, large timesteps cause negative numeric dispersion, which results in instability. On the other hand, if the time step size is too large in implicit formulations, the dispersion increases (smoothing the front and reducing accuracy) but the model remains stable.

Similar to physical dispersion, numerical dispersion in 3D system is a tensor and depends on fractional flow derivative term.

4.4. Numerical flow characterization

Most recent work in the upscaling recognizes flow regimes as an important parameter in reduction of upscaling error. To analyze the flow behavior in dimensionless space fractional flow equation in dimensionless form (equations 4.27a through 4.27c) is expressed using the following general notation

$$f_{1Di} = \left[A_D - A_D \cdot \left(A_{Gi} - A_{Ci} \frac{\partial J(S_{1D})}{\partial S_{1D}} \frac{\partial S_{1D}}{\partial i_D} \right) \right] \tag{4.49}$$

Where

i	direction (X, Y or Z)
f_{1D}	directional fractional flow in dimensionless space
A_D, A_{Gi}, A_{Ci}	dispersive, directional gravity and capillary component, respectively

To simplify analysis equation 4.49 can be re-written as

$$f_{1Di} = A_D \left[1 - A_{Gi} + A_{Ci} \frac{\partial J(S_{1D})}{\partial S_{1D}} \frac{\partial S_{1D}}{\partial i_D} \right] \tag{4.50}$$

Dispersive component is defined as in equation 4.28.

Three general flow regimes can be considered based on the balance of forces. Balance of gravity and capillary forces depends on $J(S_{1D})$ and saturation derivative term. The

capillary function $J(S_{1D})$ function derivative is always nonpositive; hence the saturation derivative sign controls whether the capillary and gravity effects offset (negative derivative) or enhance each other (positive derivative). For maximum gravity-capillary effect equation 4.49 can be re-written as

$$f_{1Di} = \left[A_D - A_D \cdot A_{Gi} \cdot \left(1 + \frac{A_{Ci}}{A_{Gi}} \left| \frac{\partial J(S_{1D})}{\partial S_{1D}} \frac{\partial S_{1D}}{\partial i_D} \right| \right) \right] \tag{4.51}$$

Ideal viscous flow would have A_D terms cancel. However, viscous flow in this work is treated as any flow where increase in rate does not affect the recovery. Minimum requirement for *viscous dominated flow* is therefore

$$A_D \cdot A_{Gi} \cdot \left(1 + \frac{A_{Ci}}{A_{Gi}} \left| \frac{\partial J(S_{1D})}{\partial S_{1D}} \frac{\partial S_{1D}}{\partial i_D} \right| \right) << 1 \tag{4.52}$$

Gravity dominated flow is a flow with a single gravity tongue and will occur if capillary effects are negligible, hence

$$A_{Gi} >> A_{Ci} \frac{\partial J(S_{1D})}{\partial S_{1D}} \frac{\partial S_{1D}}{\partial i_D} \tag{4.53a}$$

This will reduce the equation 4.51 to

$$f_{1Di} = \left[A_D (1 - A_{Gi}) \right] \tag{4.53b}$$

To be gravity dominated requirement from equation 4.52 becomes the opposite. Maximizing gravity and minimizing viscous forces requires

$$A_D \cdot A_{Gi} >> 1 \tag{4.53c}$$

Similarly, for a *capillary dominated flow* when

$$A_{Ci} \frac{\partial J(S_{1D})}{\partial S_{1D}} \frac{\partial S_{1D}}{\partial i_D} >> A_{Gi} \tag{4.54a}$$

Requirement from equation 4.52 in this case becomes

$$A_D \cdot A_{Ci} \frac{\partial J(S_{1D})}{\partial S_{1D}} \frac{\partial S_{1D}}{\partial i_D} >> 1 \tag{4.54b}$$

Equation 4.51 is therefore reduced to

$$f_{1Di} = \left[A_D \left(1 + A_{Ci} \left| \frac{\partial J(S_{1D})}{\partial S_{1D}} \frac{\partial S_{1D}}{\partial i_D} \right| \right) \right] \tag{4.54c}$$

Beside these three regimes, an additional flow regime can be defined if capillary and gravity forces are in balance. *Capillary-gravity (CG) equilibrium* requirement is

$$A_{Gi} = A_{Ci} \frac{\partial J(S_{1D})}{\partial S_{1D}} \frac{\partial S_{1D}}{\partial i_D} \tag{4.55}$$

Overview of these requirements is provided in table 4.2.

Table 4.2. General flow regime requirements

Flow regime	**Requirement**
Viscous	$A_D \cdot A_{Gi} \cdot \left(1 + \frac{A_{Ci}}{A_{Gi}} \left| \frac{\partial J(S_{1D})}{\partial S_{1D}} \frac{\partial S_{1D}}{\partial i_D} \right| \right) << 1$
Gravity	$A_{Gi} >> A_{Ci} \frac{\partial J(S_{1D})}{\partial S_{1D}} \frac{\partial S_{1D}}{\partial i_D}, A_D \cdot A_{Gi} >> 1$
Capillary	$A_{Ci} \frac{\partial J(S_{1D})}{\partial S_{1D}} \frac{\partial S_{1D}}{\partial i_D} >> A_{Gi}, A_D \cdot A_{Ci} \frac{\partial J(S_{1D})}{\partial S_{1D}} \frac{\partial S_{1D}}{\partial i_D} >> 1$
CG Equilibrium	$A_{Gi} = A_{Ci} \frac{\partial J(S_{1D})}{\partial S_{1D}} \frac{\partial S_{1D}}{\partial i_D}$

Petroleum reservoirs have upper and lower no-flow boundary. The regime limits can take less general form if the following is assumed:

- u_{1zD} and u_{2zD} are equal to zero at the upper and lower boundary
- inlet and outlet pressures are constant with respect to time
- Dimensionless system enables analysis in two dimensions

Gravity term and capillary terms in table 4.3 become equal to gravity number and capillary number divided by the displaced phase mobility or

$$A_{Gi} = \frac{(1 - S_{1D})^{n_2} N_g}{M \cdot u_{TzD}} \tag{4.56a}$$

$$A_{Ci} = \frac{(1 - S_{1D})^{n_2} N_c}{M \cdot u_{TzD}} \tag{4.56b}$$

Two additional observations can analytically be made for a viscous dominated flow. Dimensionless pressures in viscous dominated regime become equal so equations 3.31a, 3.31b, 3.31e and 3.31f can be rearranged as

$$N_{RX} \cdot u_{TxD} = \frac{\partial p_{2D}}{\partial x_D}\left((S_{1D})^{n_1} + \frac{(1-S_{1D})^{n_2}}{M} \right) \tag{4.57a}$$

$$u_{TzD} = \frac{\partial p_{2D}}{\partial z_D}\left((S_{1D})^{n_1} + \frac{(1-S_{1D})^{n_2}}{M} \right) \tag{4.57b}$$

Dividing equations 4.57a and 4.57b yields

$$N_{RX} \cdot \frac{u_{TxD}}{u_{TzD}} = \frac{\dfrac{\partial p_{2D}}{\partial x_D}}{\dfrac{\partial p_{2D}}{\partial z_D}} \tag{4.58}$$

Assuming that pressure gradients and imposed flux are kept constant, increase in aspect ratio would result in an increase in vertical crossflow velocity. Two limits can therefore be set:

- $N_{RX} >> 1$, viscous crossflow equilibrium
- $N_{RX} << 1$, no viscous crossflow

Further simplification can be done if the mid-range saturations are neglected and mobility ratio is used to scale the behavior. In this case variables of interest become aspect ratio and simplified gravity and capillary coefficient in the final form of

$$A_{Gi} = \frac{N_g}{M+1} \tag{4.57a}$$

$$A_{Ci} = \frac{N_c}{M+1} \tag{4.57b}$$

Literature survey on these general requirements (Zhou et a., 1993) provided observations on the following global ranges

- Fayers and Muggeridge's work (1990) is used as a lower limit, suggesting the transition from viscous to gravity stable flow in the interval

$N_g/(M+1) \in [0.2, 2]$. The upper limit for transition can be set as $Ng/(M+1) > 5$ according to work by Pozzi and Blackwell (1963) and Insoy and Skjaeveland (1990).

- Analysis of Ahmed et al.'s work (1988) sets the capillary-to-viscous transition zone in the range of $N_g/(M+1) \in [0.2,6]$. Work of Yokohama and Lake (1981) lowers the upper boundary to $N_c/(M+1) > 4.1$.
- Du Prey (1978) and Schechter et al (1991) studied the interplay between gravity and capillary forces. Analysis of both works puts the transition zone within the interval $N_c/N_g \in [0.2,5]$

Viscous dominated flow observation can according to Zapata et al (1980) be quantified into following regions

- $N_{RX} < 0.01$ - no vertical crossflow
- $N_{RX} > 100$ - viscous equilibrium

Shook has shown that when N_{RX}>2 the flow becomes in vertical equilibrium Overview of flow-regime limits is presented in table 4.3.

Table 4.3. General flow-regime limits

FLOW REGIME		N_{RX}	$\frac{N_g}{M+1}$	$\frac{N_c}{M+1}$
Gravity dominated		>2	>5	$<5\frac{N_g}{M+1}$
Capillary dominated		>2	$<5\frac{N_c}{M+1}$	>5
Viscous dominated	No communication	<0.01	<0.2	<0.2
	Viscous equilibrium	>100		

Ranges from literature can be used to plot a broad flow regime map depicted in figure 4.6. Suggested limits and proposed flow-regime map are based on published sensitivity studies usually involving one pronounced effect. Surveyed systems were mostly layered with displacement ranging from immiscible to miscible. Experiments involved both laboratory

and virtual floods. No uniform designed simulation or laboratory report was available systematically capturing all the effects on the same system.

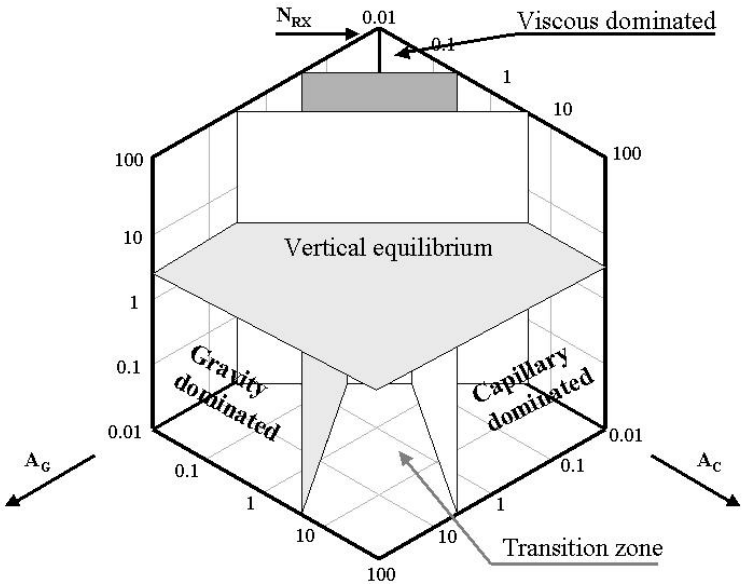

Figure 4.6. Broad-range flow regime map

Following can be conclude from existing experimental results:

- Gravity and capillary effect mirror each other at N_{RX}<2 and N_g and N_c ≥5. Transition zone between them is Capillary-Gravity equilibrium, where both gravity and capillary effects could be neglected ($\Delta\rho$=0 and P_c=0).
- If N_{RX} is larger than 2 then the change in vertical permeability doesn't change recovery hence the system is in vertical equilibrium. 2D *X*-*Z* system can be replaced by 1D *X*-direction system.
- Once N_g and N_c ≤0.2 the system is viscous dominated. The vertical crossflow is a function of vertical permeability. For extremely small N_{RX} (<0.01) vertical permeability and hence crossflow is negligible. Inversely, for large N_{RX} (<0.01) vertical permeability is large hence the system is in viscous equilibrium.

4.5. Discussion

Dimensionless development in this and chapter 3 for Dietz stability criteria – has shown that proposed numbers predict the behavior well. Comparison to original Dietz's

work proves that Buckingham's π theorem also applies once the system is already dimensionless. The only difference is that a combination of dimensionless groups forms a new scaling group. Hence, instead of using one single group such as tilt number or gravity number a joint scaling group should be used for proper scaling. This answers the gravity number paradox imposed by Peters et al (1993). Gravity number scales viscous and capillary forces however the aspect ratio scales the spatial interplay. If used jointly (i.e. in equations 4.10a and 4.10b) with the mobility ratio then the system behavior is scaled properly.

Fractional flow equation developed in dimensionless space can be re-scaled back to dimensional. Lack of dimensionality makes it ideal tool for analysis of numerical stability, reliability and error. Inspectional analysis shows that the dimensional difference equation can be transformed the same way as the differential – hence further work in the area can be done in dimensionless space.

Analytical solution for solute transport equation in 3D space with comparable boundary condition could not be found. A possible way to study effects of independent groups is numerical sensitivity study where the results are compared to fine-grid small-time step reference run.

Difference equation analysis revealed the fourth meaning of aspect ratio scaling group - dimensionless transmissibility. Observation on trigonometric function contained in gravity number made during the development of base equations was justified in the differentiation scheme. If gridblocks are aligned vertically, trigonometric term in numerical gravity number is lost. The only remaining term is contained within the numerical tilt number.

Using the similarity between dimensionless differential and difference equation, analytical boundaries for flow regimes are set. Flow regime map is constructed based on observations from the literature on global trends. Assumptions made for constructing the map helped generalizing, however for practical application on the gridblock scale heterogeneity effect should be taken out. Gridblocks do not have sub-grid heterogeneity; by definition, this heterogeneity is contained in effective properties. Similar uncertainty exists with the use of mobility ratio rather than the mobility at intermediate saturation. To

verify validity and create a more accurate map on the gridblock scale further numerical experimental work must be done.

CHAPTER 5

EXPERIMENTAL APPPLICATION

Dimensionless numbers scale flow behavior and identify flow regimes. Boundary conditions are often difficult to generalize in 3D. In 2D, Shook (1992) treats edges of the upscaling reservoir as wells and imposes desired pressure and saturation gradients. In 3D, a reasonable approach is to model the well as a linear source/sink

The case study presented in this chapter examines upscaling by considering flow regimes. Dimensionless breakthrough time was used as the diagnostic response. Dimensionless breakthrough time defined as the fraction of the mobile, displaced phase that has been recovered when the fractional flow of the displacing phase is one percent. The initial saturation of displacing phase was equal to connate saturation. The model was 3D. Response curves of the case study were visually inspected to determine flow regimes. Flow regimes are defined as follows:

- *Viscous dominated flow regime* occurs at high viscous pressure drops $u\mu / k$ when further increases in rate do not change the breakthrough recovery.
- *Gravity dominated regime* is regime where displacing phase flows as a stable tongue.
- *Capillary dominated regime* occurs when the flow is faster in lower than higher permeability area.

The models analyzed in this chapter were for homogeneous isotropic media. Flow regimes were determined by interpreting inflection points in breakthrough time plotted as a function of dimensionless scaling groups. Effects of the shape of relative permeability curves and Leverett's J(S_1) function were not studied.

5.1. Verification of 3D scale numbers

Fractional flow equations in *X*- and *Y*- direction of dimensionless space are

$$f_{1xD} = A_D\left[1+\frac{(1-S_{1D})^{n_2}}{M}\left(\frac{N_c}{N_{RX}u_{TxD}}\frac{\partial J(S_{1D})}{\partial x_D}-\frac{N_g N_{TX}}{N_{RX}u_{TxD}}\right)\right] \tag{5.2a}$$

$$f_{1yD} = A_D\left[1+\frac{(1-S_{1D})^{n_2}}{M}\left(\frac{N_c}{N_{RY}u_{TyD}}\frac{\partial J(S_{1D})}{\partial y_D}-\frac{N_g N_{TY}}{N_{RY}u_{TyD}}\right)\right] \tag{5.2b}$$

$$f_{1zD} = A_D\left[1+\frac{(1-S_{1D})^{n_2}}{M}\left(\frac{N_c}{u_{TzD}}\frac{\partial J(S_{1D})}{\partial y_D}-\frac{N_g}{u_{TzD}}\right)\right] \tag{5.2c}$$

The coefficients are defined as in chapter 4. If all dimensionless groups are identical, the fractional flow is necessary the same. This behavior can be used to scale a set of simulations in a general way. Rather than looking at the possible interval of all variables, a set of dimensionless simulations can examine system scaling and flow regimes.

5.2. Dimensionless simulation design

Dimensionless groups can simplify design of reservoir simulation studies. Rather than varying more than 30 variables, we can describe the behavior by using only 7 dimensionless. Varying these seven groups will assess the full range of system variability; it is far easier to do a sensitivity study in 7 dimensions than in 30. To illustrate, a 2-level full factorial with 7 factors is perfectly feasible (128 simulations), whereas one would not consider a full factorial study with 30 factors $\left(2^{30} > 10^9\right)$.

The range for gravity number was determined from analysis of gravity-stabilized displacements in dipping systems (chapter 4). Ranges for directional groups (N_R and N_T) were within the range needed to determine the vertical equilibrium. Mobility ratio was determined in a similar manner, aiming to encompass effects of both favorable and unfavorable mobility ratio. Along with capillary number, this completes the specification of the flow system (table 5.1). Five levels are used to aid in detection of flow regimes; a two-level factorial would not be adequate for regime mapping. For 7 dimensionless variables and 5 levels, the total number of simulations required is $5^7 = 78{,}125$.

Table 5.1. Dimensionless design in 3D

Dimensionless variable ranges						
N_g	**N_{RX}**	**N_{RY}**	**N_{TX}**	**N_{TY}**	**M**	**N_c**
0.1	0.1	0.1	0.1	0.1	0.1	0.1
0.5	0.5	0.5	0.5	0.5	0.5	0.5
1	1	1	1	1	1	1
5	5	5	5	5	5	5
10	10	10	10	10	10	10

Dimensionless design takes each separate dimensionless component and decomposes it to primary, dimensional variables. To do the decomposition, some of the dimensional variables have to be assigned using physically reasonable values. Shook (1992) verified that dimensionless groups for 2D systems are not dependent on choice of fixed variables. That verification need not be repeated in 3D. Because of the large number of simulations to be run, the size of each numerical model was kept small, with 10 gridblocks in *X*-, *Y*- and *Z*-direction. Fixed values are presented in table 5.2.

Table 5.2. Overview of fixed dimensional design parameters

Fixed dimensional parameters						
NX	**NY**	**NZ**	**k_x (mD)**	**k_y (mD)**	**k_z (mD)**	**λ_2^o (cp^{-1})**
10	10	10	300	500	40	1
k_{r1}^o	**n_1,n_2**	**$\Delta\rho$ (kg/m^3)**	**S_{1r}**	**S_{2r}**	**ΔZ (m)**	**ϕ**
0.5	3	250	0.3	0.3	1	0.3

Because there are seven independent dimensionless groups, we can freely specify 7 dimensional variables. The remaining dimensional variables are set consistently with the value required by the dimensionless design. Some of the groups contain similar values – for example group N_{RX} and N_{TX} both contain length L. This indicates that for a fixed height H every time the N_{RX} changes, the angle in trigonometric term contained in N_{TX} will need to be recalculated (table 5.3).

Table 5.3. Estimated dimensional variables in 3D

Dimensional design					
N_g **$u_T/(\cos\alpha_X \cos\alpha_y)$**	**N_{RX}** **ΔX**	**N_{RY}** **ΔY**	**N_{TX}** **$\Delta X \tan\alpha_x$**	**N_{TY}** **$\Delta Y \tan\alpha_y$**	**M** **μ_1**
8.36	0.87	1.12	0.1	0.1	5.00
1.67	1.94	2.50	0.5	0.5	1.00
0.84	2.74	3.54	1	1	0.50
0.17	6.12	7.91	5	5	0.10
0.08	8.66	11.18	10	10	0.05

A similar observation holds for the Y-direction, so each direction requires 25 separate cases. Total of 625 different angle-length combinations is calculated resulting in 625 separate grids. Knowing all the possible combinations of angles, total velocity u_T is estimated for all 5 values of gravity number (3125). Total velocity as defined in Appendix A and Chapter 4 consists of three components. However, because the flow is directional, dimensionless flux component in *X*- and *Y*-direction (u_{TxD} and u_{TyD}) are set to 1 for *X*- and *Y*-direction injection.

All runs used relative permeability and capillary pressure data for Berea Sandstone (Oak et al., 1990). Capillary pressure was scaled to obtain the Leverett's $J(S_1)$ function. Relative permeability curves were fitted to a Corey model. Exponents for both phases were 3. Leverett's $J(S_1)$ function was fitted to the following equation

$$J(S_{1D}) = 0.9735 \cdot \left(1 - S_{1D}^{\ 0.25}\right) + 0.0265 \qquad (5.1)$$

Where S_{1D} is normalized saturation of displacing phase.

Each of the 78,125 simulation runs was performed for duration of 1 PV of injection. Breakthrough time was estimated from each simulation by linear interpolation. This provided pore volumes injected at the time the displaced phase fractional flow reached 1 percent, considered being a breakthrough point.

5.3. Analysis

Dimensionless groups were analyzed to determine points where the response curve changes shape: this may be convergence of trends for distinct physical systems, slope changes, or inflection points. Inspection of the recovery plots and physical interpretation of dimensionless groups guided flow regime identification.

A typical recovery curve is presented in figure 5.1. Dimensionless breakthrough time is plotted as a function of gravity number and aspect ratio. Two flow regimes can be identified, gravity dominated (G) and viscous dominated zone (V). The upper bound of the viscous regime occurs at lower gravity number where response curve changes shape. The transition zone presented in chapter 4 was interpreted as intermediate zone between two trends (figure 5.1.)

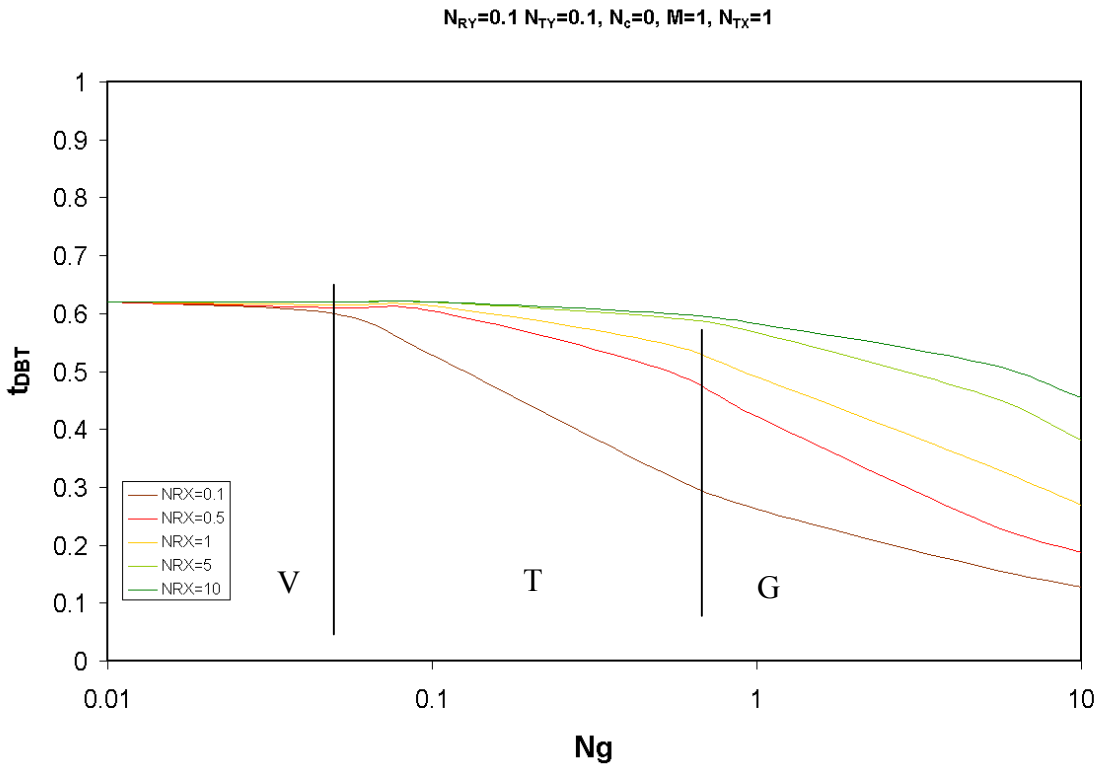

Figure 5.1. Breakthrough recovery as a function of aspect ratio for *X*-direction injection

Similarity between equations 5.2a and 5.2b is reflected in the near-identical responses if the scaling groups are kept constant for both flow directions. Dimensionless fractional flows in *X*- and *Y*-direction are in that case equal for any given dimensionless time. Identical behavior is in this case identified through single response (breakthrough time) for a range of aspect ratios and gravity and tilt numbers. To simplify comparison and examine the aspect ratio and tilt number in the Y direction, N_c was set to zero. Lack of capillary pressure does not denote miscible displacement because interfacial tension is still manifested in the relative permeability curves.

For the equal mobility ratio and $N_g N_T/N_R$ flow responses were similar (figures 5.1 and 5.2). Response curves for injection in X- and Y-direction had identical transition zone intervals and dimensionless time (breakthrough time recovery efficiency). Error in breakthrough time between all similar cases in *X*- and *Y*- direction was less than 3%. This difference is attributed to errors caused by linear interpolation between the coarse time steps used in the numerical models.

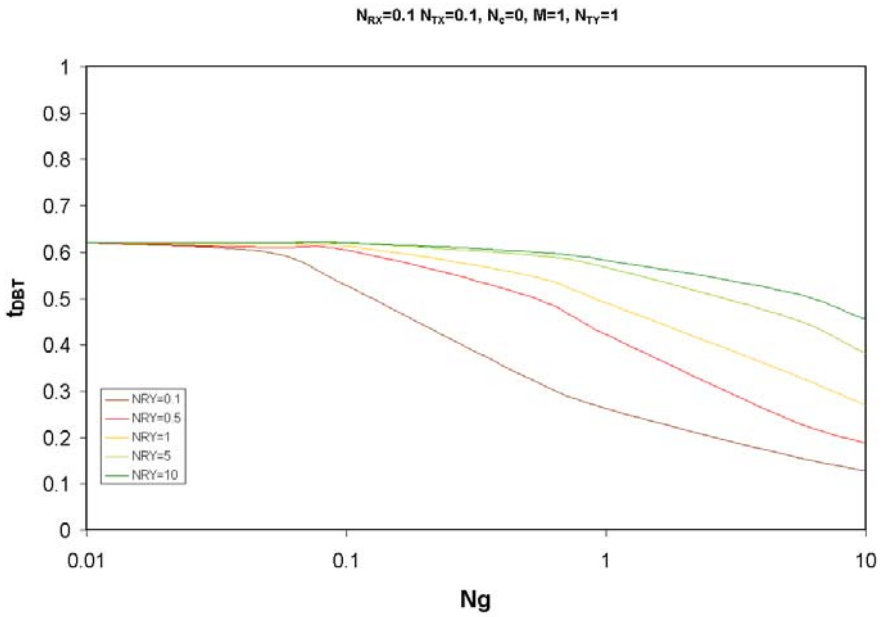

Figure 5.2. Breakthrough recovery as a function of aspect ratio in Y-direction

Mobility ratio affected the flow as expected from analytical flow regime boundaries presented in Chapter 4. To illustrate the dependence, figure 5.3, a plot of dimensionless time as a function of gravity number for different mobility ratios, has upper transition zone boundary (beginning of gravity dominated flow regime) marked with circles.

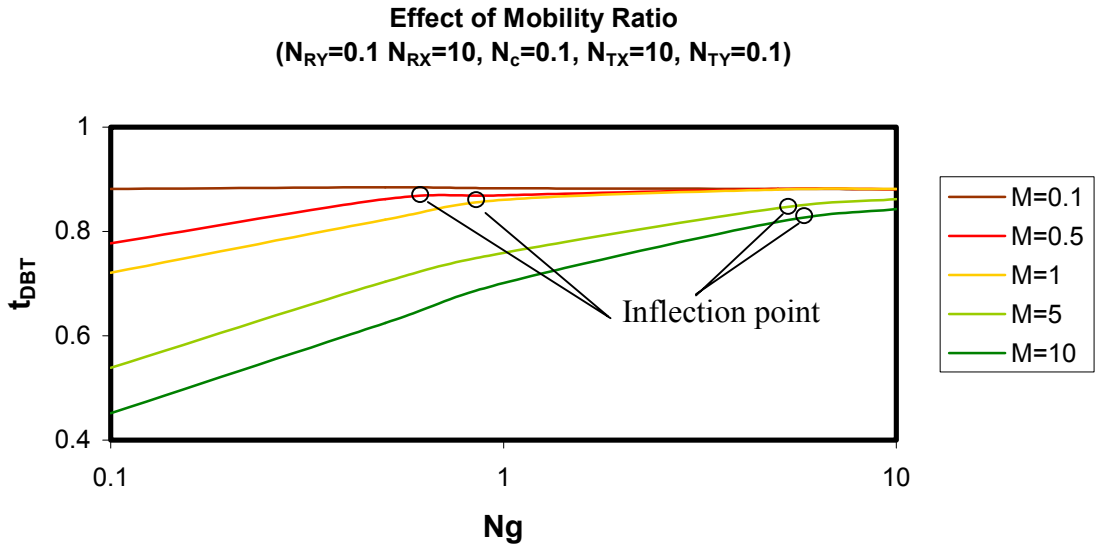

Figure 5.3. Effect of mobility ratio on the flow regime

If transition value of gravity number is determined from figure 5.3 for each mobility ratio and scaled using *1/(M+1)* approach all the values for $N_g/(M+1)$ become approximately 0.5. This differs from suggested cutoff in the literature (≈5). Figure 5.3 is plotted for high tilt angle in the direction of flow (N_{TX}=10). If the behavior is scaled using $N_{TX}N_g/(M+1)$ than the gravity effect in X-direction is scaled properly according to equation 5.2a and the upper boundary of transition zone becomes equal to 5.

Individual recovery cases for favorable and unfavorable mobility ratio are shown in figures 5.4 and 5.5. Analysis reveals the relative insensitivity of dimensionless time on change in tilt below certain value of tilt number (≈5) for unfavorable mobility ratio. If tilt number is below 0.5 the effective decrease in recovery is fairly small. A large change in gravity number is needed to observe the change in system behavior. The reason is fairly large denominator *(M+1)*.

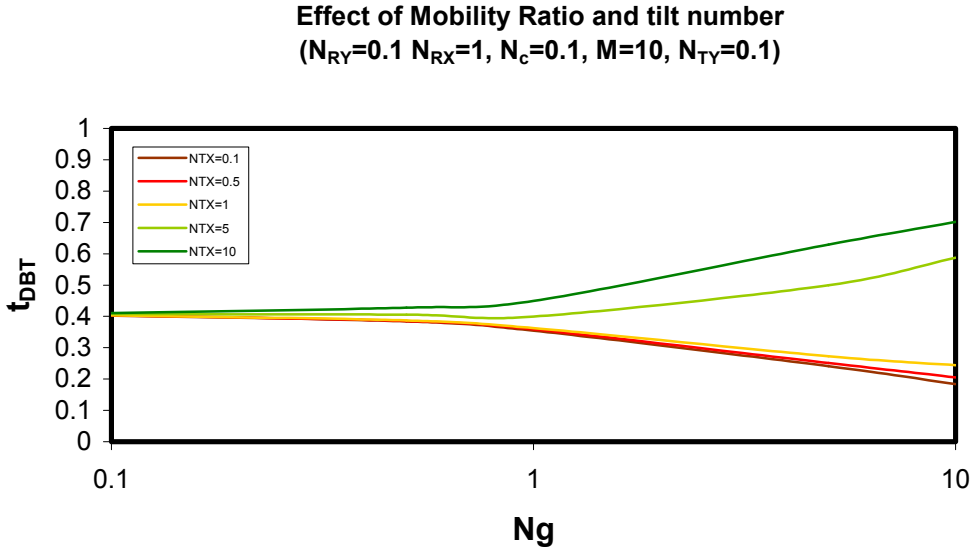

Figure 5.4. Unfavorable mobility effect on response curves

Opposite can be shown for a favorable mobility ratio. The breakthrough recovery will be more sensitive to change in gravity or tilt number for *(M+1)* is fairly small with maximum value of 2. Figure 5.5 shows that change in either tilt or gravity number always results in change of breakthrough recovery. No equilibrium range could be observed. The scaling of complete recovery curves one on top of another is not possible. To illustrate this

the dimensionless time can be read for unfavorable case and randomly selected values of N_g=1 and N_{TX}=1. Dimensionless time is approximately 0.36 for scaling group $N_{TX}N_g/(M+1)$ value of 0.091. For favorable mobility ratio an equivalent tilt for the same gravity number and $N_{TX}N_g/(M+1)$ would be ≈13.6. Dimensionless time would in this case be higher than 0.7 if extrapolated from figure 5.5. Explanation for this behavior can be found in theory presented by Dietz (1957).

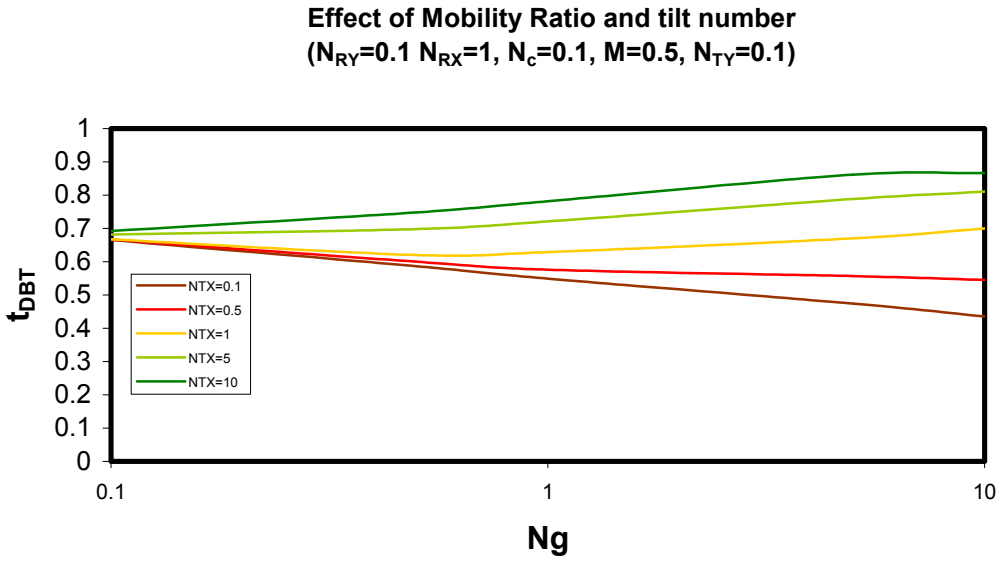

Figure 5.5. Favorable mobility effect on response curves

Several different runs in *X*-direction were plotted as slices to investigate the effect of aspect ratio. Figure 5.6 compares responses for different aspect ratio on each slice. Slices are drawn in 3D for the different tilt number. Analysis of figure 5.6 reveals that after a certain aspect ratio (≈5) a vertical equilibrium is reached. Vertical equilibrium is indicated by a small change in breakthrough recovery with increase in aspect ratio.

Tilt number effect and therefore gravity effect in *X*-direction is more pronounced at lower aspect ratios. This reflects the more limited vertical flow capacity in systems with small dimensionless aspect ratios. Response curves for tilt number are shifted in N_g direction with an increase in aspect ratio. For this set of response curves, viscous regime is indicated by point where all recovery curves for each slice converge. The regime cutoff

points depend on aspect ratio as well, as predicted in Chapter 4 so one should use the aspect ratio as well to assess the effects of gravity-driven crossflow.

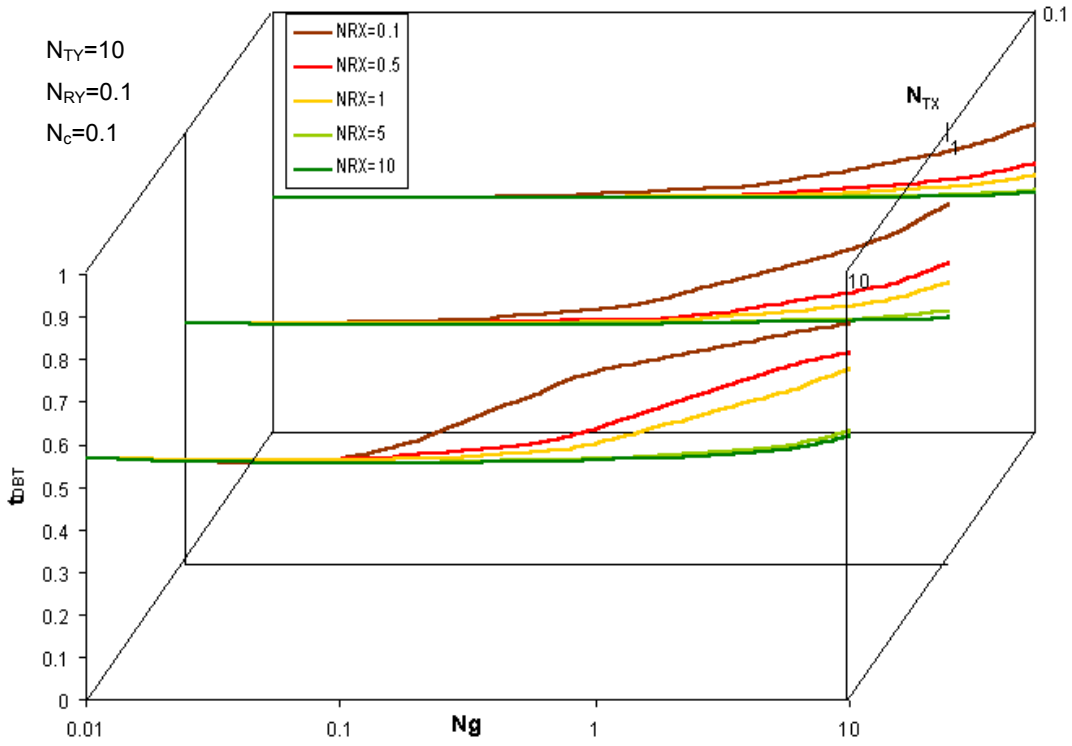

Figure 5.6. Interplay of aspect ratio and gravity number for different tilt numbers

Similar can be shown for Y-direction. Analysis of the effect of both aspect ratios revealed that after reaching the value of 5, further increase in either one of aspect ratios had almost no effect on breakthrough recovery. Hence the aspect ratio of 5 is set as a lower boundary for the vertical equilibrium. As a result if both aspect ratios are larger than five, *Z*-direction can be eliminated using VE calculations. Change in mobility did not affect VE observations– similar to 2D interpretation by Shook (1992).

All models were homogeneous and isotropic. Capillary number and spatial saturation derivative affect the details of the capillary regime. Large spatial saturation derivatives and small capillary number will yield similar behavior as small capillary number and large saturation derivative. Spatial saturation derivative depends on saturations in adjacent gridblocks. This nonlinear behavior complicates study of the effects in the capillary

dominated regime. Interplay between gravity and capillary effect needs further investigation.

Interplay of *X*- and *Y*- direction aspect ratios has shown that the behavior of the system can be strongly directional. One aspect ratio can indicate vertical equilibrium while the other can indicate no communication due to permeability assigned to the gridblock of interest. This, and the possibility of different directional physical effects (gravity, capillary) can justify directional relative pseudofunctions approach (Guzman, 1995). Gravity in each direction should be scaled using the appropriate tilt number. The resulting flow regime is also a function of tilt number.

5.4. Flow regimes and application in upscaling

Ranges for flow regimes agree with those individually reported in literature. In particular:

- Transition zones are hard to determine from coarse gridblock study
- Flow regimes depend on intermediate saturation and therefore relative permeability curvature and assigned $J(S_1)$ curve. Sensitivity to these parameters was not studied.
- The nature of boundary conditions does not allow direct testing of some directional effects (e.g., simultaneous flow in *X*-, *Y*- and *Z*-direction)

Additional observations made in this chapter can be used to re-plot the local flow regime maps on the gridblock scale. Corrected map is presented in figure 5.7. Recovery curves were created and flow behavior interpreted for particular cases. Regime cutoffs are similar in terms of gravity and capillary flow regime boundaries. Viscous flow regime boundary is set to be equal to 0.5. Vertical equilibrium (VE) occurs when aspect ratio is higher than 5 and is seemingly independent of gravity and capillary number. Gravity and capillary dominated regime limit is a function of aspect ratio, decreasing as the aspect ratio decreases.

This study utilized Berea sandstone relative permeability and capillary behavior. Comparison with 2-D work by Shook et al. 1992) shows that the VE boundary has changed. This might be a result of different relative permeability curves, however sensitivity study on changes in rock data was not performed. Flow regime map as

presented in this work provides the tool for determining the flow regime in each direction for any given gridblock. Because pseudo functions are regime dependent (Coll et al., 2000; Cao and Aziz, 1999) awareness of flow regime in each direction enables the choice of optimum upscaling method. Keeping the coarse gridblock in the same flow regime yields the same response if directional aspect groups are kept the same.

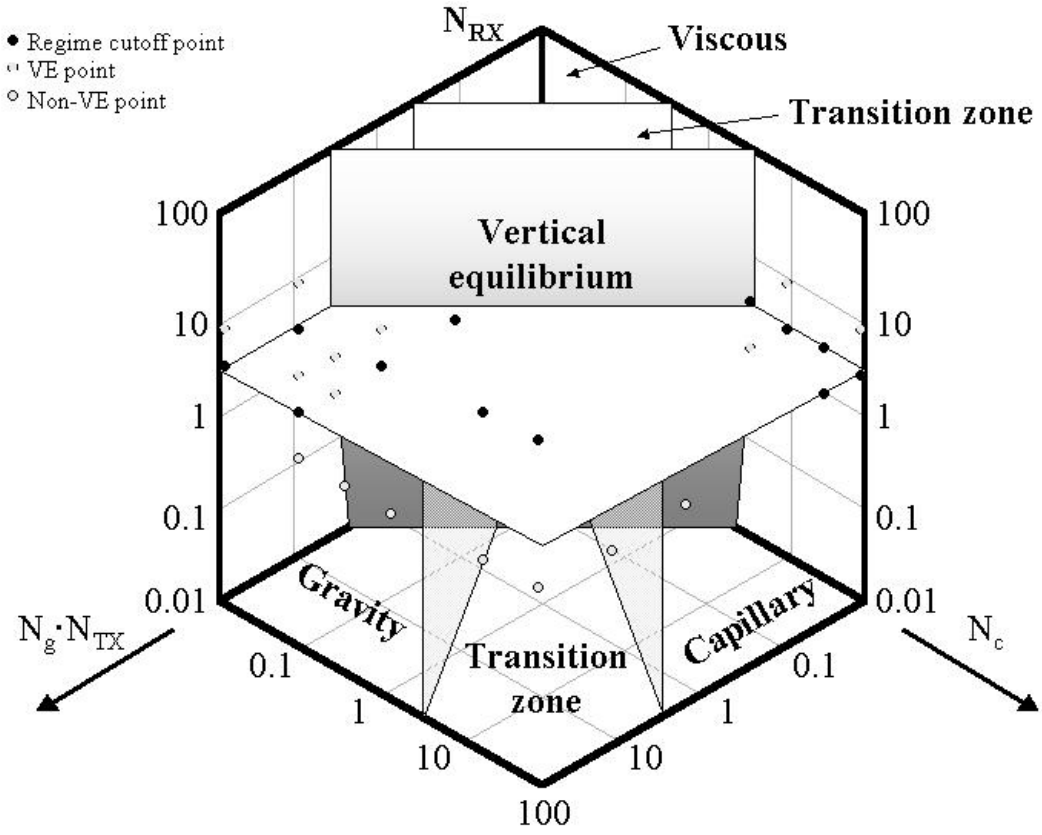

Figure 5.7. Corrected flow regime map for *X*-direction

Generality for any given set of relative permeability and $J(S_1)$ might not be possible, therefore simulation design similar to one shown here for the individual case. Ranges from sensitivity study are in agreement with those available in literature and can be used to guide the design. Rather than using a wide range of static variables as in the study, the range might be narrower. For example, the use of constant width and length of the gridblock and assuming $k_x=k_y=10k_z$ yields small change in aspect ratio and tilt number throughout the reservoir. With mobility of the system known, a simple 6 factorial dimensionless design could be used to assess the full possible range of recovery behavior.

As suggested by most recent literature and newly developed dimensionless system, proper upscaling requires two steps:

- Quantify the heterogeneity and chose the upscaling approach
- Run a set of design simulations to determine actual flow regime set based on reservoir rock relative permeability and J-function.

The effect of heterogeneity can be quantified by the approach of Li et al (1993) depicted in figure 2.7. If the dimensionless heterogeneity of a chosen coarse gridblock falls within the limits of Buckley – Leverett region, appropriate regime-dependent pseudo function can be selected for upscaling. To determine the best cutoff a set of simulations is run for given relative permeability/capillary conditions and responses monitored on a gridblock scale. Resulting cutoffs are valid for a given rock type. The variables determining cutoffs are gravity and capillary components of dimensionless fractional flow equation (section 4.4).

If recoarsening keeps heterogeneity out of Buckley-Leverett region, Li and Beckner (1999) approach presented in chapter 2 can be applied. Analysis of fractional flow equation in dimensionless space presented in chapter 4 reveals that Li and Beckner also upscale based on the flow regime.

This example illustrates benefits of dimensionless reservoir characterization. Large number of dimensional variables makes a sensitivity study too difficult to perform. Dimensionless approach reduces number of parameters to be verified and hence enables faster analysis and readily scalable results.

CHAPTER 6
CONCLUSIONS AND RECOMMENDATIONS

Dimensionless systems of equations have many benefits, especially the general applicability at all scales and the ease of extrapolating behavior. Mathematical development, experimental work and observations from most recent literature lead to following conclusions:

1. Inspectional analysis on the general flow equation provided the most succinct form of dimensionless numbers. Numbers developed in 2D systems so far have similar general form. The form of dimensionless differential equation and flux normalization in 3D changes because of the change of scaling direction.
2. Buckingham's π theorem is applicable on the dimensionless system as well. Rather than using the individual numbers for directional scaling, effects need to incorporate groups of numbers describing the physical effect in desired direction.
3. Analytical developments in dimensionless space are simpler (e.g., Dietz in 2D space). However, Buckingham's theorem states that, in general, a dimensionless group rather than individual number scales each effect.
4. If dimensionless groups are used, designed reservoir simulations can provide more general results with fewer models. Special care has to be taken when assigning dimensional variables to form a dimensionless group – unphysical dimensional variables will result in questionable results.
5. Numerical results have shown that for petroleum reservoirs with no-flow boundaries on top and bottom, scaling in *Z*-direction provides better scaling tool because with *Z*-scaling the form of equations in *X*- and *Y*-direction is the same. Any effect observed in 2D system (XZ or YZ) can be scaled to 3D (XYZ).
6. Flow regimes can be defined using dimensionless numbers. Good agreement between experimental and literature available cases has shown that the flow regimes are dependent on proposed groups.
7. Upscaling can be chosen using flow regime maps. This approach should reduce unphysical behavior of upscaled parameters and improve accuracy of responses. Flow regimes depend on the relative permeability curve shape as well as the

endpoints, complicating scaling of the results. The suggested approach is to develop a flow regime map using the relevant relative permeability and capillary pressure curve(s).

Even though the dimensionless simulation design significantly reduced the number of simulations needed to capture the system behavior, this study was confined to a homogeneous system. This is due to large number of simulations – even in dimensionless space - needed to statistically capture the effects of stochastically generated porous media.

Based on observations from this study the following can be recommended:

1. Laboratory 3D floods. This would provide physical proof of mathematically developed groups. Large number of examples exists in literature for 2D, strongly directional systems – however numerical observations on directional dependence need to be empirically verified.
2. Introduction of stochastic heterogeneity on defined flow regime intervals to separately study effects of upscaling in viscous, gravity and capillary dominated region. A single regime study on a narrower interval of physical and directional numbers rather than general study would provide numerical insight in flow regime dependence on heterogeneity.
3. Further numerical study can be done on the effect of dimensionless groups on numerical dispersion, stability and reliability. Extension could be made on effects of different flow regimes on numerical behavior of the model, and visualization and use of these dimensionless groups for reservoir studies.

BIBLIOGRAPHY

Aasum, Y., Kasap, E., Kelkar, M.: "Analytical Upscaling of Small-Scale Permeability Using a Full Tensor", Paper SPE 25913 presented at the SPE Rocky Mountain Regional/Low Permeability Reservoirs Symposium held in Denver, CO, April 12-14, 1993

Almeida, J.A., Soares, A., Pereira, M.J., Daltaban, T.S.: "Upscaling of Permeability: Implementation of a Conditional Approach to Improve the Performance in Flow Simulation", Paper SPE 35490 presented at European 3-D Reservoir Modeling Conference held in Stavanger, Norway, April 16-17, 1996

Archer, R.A., Horne, R.N.: "The Green Element Method for Numerical Well Test Analysis", Paper SPE 62916 presented at the 2000 SPE Annual Conference and Exhibition held in Dallas, TX, October 1-4, 2000

Barker, J.W., Thibeau, S.: "A Critical Review of the Use of Pseudo Relative Permeabilities for Upscaling", Paper SPE 35491 presented at European 3-D Reservoir Modeling Conference held in Stavanger, Norway, April 16-17, 1996

Bedrikovetsky, P.G., Potsch, K.T., Polyanin, A.D., Zhurov, A.I.: "Upscaling of the Waterflood Reservoir Properties on the Core Level: Laboratory Study, Macro and Micro Modeling", Paper SPE 29870 presented for SPE Middle East Oil Show held in Bahrain, March 11-14, 1995

Buckingham, E.: “On Physically Similar Systems”, Phys. Rev., Vol. IV, No. 4, 1914, p. 345-376

Cao, H., Aziz, K.: “Evaluation of Pseudo Functions”, Paper SPE 54598 presented at 1999 SPE Western Regional Meeting held in Anchorage, Alaska, May 26-28, 1999

Carpenter, C.W., Bail, P.T., Bobek, J.E.: “A Verification of Waterflood Scaling in Heterogeneous Communication Flow Models”, SPEJ, Vol. 2, 1962, p. 9

Chikhliwala, E.D.; Yortsos, Y.C.: "Investigation on Viscous Fingering by Linear and Weakly Nonlinear Stability Analysis", Paper SPE 14367 presented at the 60th Annual Technical Conference and Exhibition of the Society of Petroleum Engineers held in Las Vegas, NV, September 22-25, 1985

Christie, M.A.: "Upscaling for Reservoir Simulation", JPT, November 1996, pp. 1004-1010

Chu, L., Schatzinger, R.A., Tham, M.K.: "Application of Wavelet Analysis to Upscaling of Rock Properties", Paper SPE 36517 presented at the SPE Annual Technical Conference & Exhibition held in Denver, CO, October 6-9, 1996

Chatzis, J., Morrow, N.R.: “Magnitude and Detailed Structure of Residual Oil Saturation”, SPEJ, Vol. 23, 1986, p. 2

Ciammetti, G., Ringrose, P.S., Good, T.R., Lewis, J.M.L., Sorbie, K.S.: "Waterflood Recovery and Fluid Flow Upscaling in a Shallow Marine and Fluvial Sandstone Sequence", Paper SPE 30783 presented at the SPE Annual Technical Conference & Exhibition held in Dallas, TX, October 22-25, 1995

Coll, C., Muggeridge, A.H., Jing,, X.D.: “Regional Upscaling: A New Method to Upscale Waterflooding in Heterogeneous Reservoirs for a Range of Capillary and Gravity Effects”, Paper SPE 59337 presented at 2000 SPE/DOE Improved Oil Recovery Symposium held in Tulsa, OK, April 3-5, 2000

Craft, B.C., Hawkins, M.F.: *Applied Reservoir Engineering*, Prentice Hall, 1990

Craig, F.F., Sanderlin, J.L., Moore, D.W., Geffen, T.M.: “A Laboratory Study of Gravity Segregation in Frontal Drives”, Transactions of AIME, Vol. 210, 1957, p. 275

Dietz, D.N.: “A Theoretical Approach to a Problem of Encroaching and By-Passing Edge Water”, Akad. Van Wetenschappen, Amsterdam, Proc. V.56-B, 1953, p. 83

Dake, L.P.: *Fundamentals of Reservoir Engineering*, Elsevier Science, 1978, p. 372

Darman, N.H., Durlofsky, L.J., Sorbie, K.S., Pickup, G.E.: "Upscaling Immiscible Gas Displacements: Quantitative Use of Fine Grid Flow Data in Grid Coarsening Schemes", Paper SPE 59452 presented at 2000 SPE Asia Pacific Conference on Integrated Modeling for Asset Management held in Yokohama, Japan, April 25-26 2000

Darman, N.H., Sorbie, K.S., Pickup, G.E.: "The Development of Pseudo Functions for Gravity-Dominated Immiscible Gas Displacements", Paper SPE 51941 presented at the 1999 SPE Reservoir Simulation Symposium held in Houston, TX, February 14-17, 1999

Delhomme, J.P., Bedford, J., Colley, N.M., Kennedy, M.C.: "Permeability and Porosity Upscaling in the Near-Wellbore Domain: The Contribution of Borehole Electrical Images", paper SPE 36822 presented at the 1996 SPE European Petroleum Conference held in Milan, Italy, October 22-24 1996

Ding, Y., Urgelli, D.: “Upscaling of Transmissibility for Field Scale Flow Simulation in Heterogeneous Media”, Paper SPE 38016 presented at the 14th SPE Symposium on Reservoir Simulation held in Dallas, TX, June 8-11, 1997

Edwards, M.G.: “Symmetric Flux Continuous Positive Definite Approximation of the Elliptic Full Tensor Pressure Equation in Local Conservation Form”, Paper SPE 29417

presented at the 13th SPE Symposium on Reservoir Simulation held in San Antonio, TX, February 12-15, 1995

Earlougher, R.C.: *Advances in Well Test Analysis*, SPE Monograph, Vol. 5, 1977

Fox, R.W., McDonald, T.A.: *Introduction to Fluid Mechanics*, Wiley, 1998

Fung, L.S.K., Collins, D.A., Long, X.N: "An Adaptive-Implicit Switching Criterion Based on Numerical Stability Analysis", Paper SPE 16003, SPE Reservoir Engineering, February 1989, p. 45-51

Geertsma, J., Cross, G.A., Schwartz, N.: "Theory of Dimensionally Scaled Models of Petroleum Reservoirs", Transactions AIME, Vol. 207, 1956, p. 118

Giliberti, S., Erba, M., Rampoldi, M., Said, A.: "Optimization of the Numerical Simulation in a Giant Oil Field by Upscaling of Relative Permeability Curves", Paper SPE 29930 presented at the International Meeting on Petroleum Engineering held in Beijing, PR China, November 14-17, 1995

Goldthorpe, W.H., Chow, Y.S.: "Unconventional Modeling of Faulted Reservoirs: A Case Study", Paper SPE 13526 presented at the SPE Reservoir Simulation Symposium, Dallas, TX, February 10-13, 1985

Guzman, R.E., Giordano, D., Fayers, F.J., Godi, A., Aziz, K.: "Evaluation of Dynamic Pseudo Functions for Reservoir Simulation", Paper SPE 35157 presented at the SPE Annual Technical Conference & Exhibition held in Denver, CO, October 6-9, 1996

Hagoort, J.: "Oil Recovery by Gravity Drainage", Paper SPE 7242, SPEJ, 1980

Hales, H.B.: "Parameterization of Match-Derived Pseudo-Relative Permeabilities", Paper SPE 11494 presented at the Middle East Oil Technical Conference, held in Manama, Bahrain, March 14-17, 1983

Hirasaki, G.J., O'Dell, P.M.: "Representation of Reservoir Geometry for Numerical Simulation", Transactions AIME, 249, 1970, p. 393-404

Indelman, P.: "Upscaling of Permeability of Heterogeneous Formations: Part 1—General Approach and Applications to Isotropic Media", Paper SPE 22206, unsolicited

Indelman, P., Dagan, G.: "Upscaling of Permeability of Heterogeneous Formations: Part 2--Application to Two Dimensional Flow", Paper SPE 22532

Isaaks, H.E., Srivastava, R.M.: *Applied Geostatistics*, Oxford University Press, January 1990

Ito, Y., Settari, A., Kry, P.R., Jha, K.N.: “Development and Application of Pseudo-Functions for Reservoir Simulation To Represent Shear Failure During the Cyclic Steam Process”, paper SPE 25800 presented at the International Thermal Operations Symposium held in Bakersfield, CA, February 8-10, 1993

Jacks, H.H., Smith, O.J.E., Mattax, C.C.: “The Modeling of a Three-Dimensional Reservoir With a Two-Dimensional Reservoir Simulator, The Use of Dynamic Pseudo Functions”, Paper SPE 4071 presented at 47th SPE-AIME Annual Meeting held in San Antonio, TX, October 8-11, 1972

Johnson, R.W.: *The Handbook of Fluid Dynamics*, CRC Press, 1998

Johnson, E.F., Bossler, D.P., Naumann, V.O.: "Calculation of Relative Permeability form Displacement Experiments", Petroleum Transactions, AIME, Vol. 216, 1959, p. 370-372

Johnson, J.B., Nanney, M.M., Killogh, J.E., Lin Y.T.: “The Kuparuk River Field: A Regression Approach to Pseudo-Relative Permeabilities”, Paper SPE 10531 presented at the 6th SPE Symposium on Reservoir Simulation held in New Orleans, LA, January 31-February 3, 1982

King, M.J., Mansfield, M.: “Flow Simulation of Geologic Models”, Paper SPE 57469, SPEREE, August 1999

King, M.J., Mansfield, M.: “Flow Simulation of Geologic Models”, Paper SPE 38877 presented at the SPE Annual Technical Conference & Exhibition held in San Antonio, TX, October 5-8, 1997

Kydland, T., Haugan, P.M., Bousquet, G., Havig, S.O.: “Application of Unconventional Techniques in Constructing an Integrated Reservoir Simulation Model for Troll Field”, SPEJ, August 1988

Kyte, J.R., Berry, D.W.: “New Pseudo Functions To Control Numerical Dispersion”, Paper SPE 5105 presented at the 49th SPE-AIME Annual Fall Meeting, held in Houston, TX, October 6-9, 1974

Lake, L.W.: *Enhanced Oil Recovery*, Prentice Hall, 1989, p. 142

Lake, L.W., Hirasaki, G.J.: “Taylor’s Dispersion in Stratified Porous Media”, Paper SPE 8436 presented at 54th Annual Fall Technical Conference and Exhibition held in Las Vegas, NV, September 23-26, 1979

Lantz, R.B.: "Quantitative Evaluation of Numerical Diffusion (Truncation Error)", Paper SPE 2811 presented at the SPE Second Symposium on Numerical Simulation of Reservoir Performance held in Dallas, TX, February 5-6, 1970

Lee, J.: *Well Testing*, SPE, 1982

Lee, J., Kasap, E., Kelkar, M.G.: "Analytical Upscaling of Permeability for Three-Dimensional Grid Block", Paper SPE 27875 presented at the Western Regional Meeting held in Long Beach, CA, March 23-25, 1994

Lee, J., Kasap, E., Kelkar, M.G.: "Development and Application of a New Upscaling Technique", Paper SPE 30712 presented at the SPE Annual Technical Conference & Exhibition held in Dallas, TX, October 22-25, 1995

Lee, S.H., Durlofsky, L.J., Lough, M.F., Chen, W.H.: "Finite Difference Simulation of Geologically Complex Reservoirs With Tensor Permeabilities", Paper SPE 38002 presented at the 1997 SPE Reservoir Simulation Symposium held in Dallas, TX, June 8-11, 1997

Lee, S.T., Li, K.M.G., Culham, W.E.: "Stability Analysis of Miscible Displacement Processes", Paper SPE 12631 presented at the SPE/DOE Fourth Symposium on Enhanced Oil Recovery held in Tulsa, OK, April 15-18, 1984

Lenormand, R., Touboul, E., Zarcone, C.: "Numerical Models and Experiments on Immiscible Displacements in Porous Media", Journal of Fluid Mechanics, Vol. 189, 1988, p. 165

Li, D., Lake, L.W.: "Scaling Fluid Flow Through Heterogeneous Permeable Media", Paper SPE 26648, SPE Advanced Technology Series, Vol. 3, No. 1

Li, D., Beckner, B.: "Optimal Uplayering for Scaleup of Multimillion-Cell Geologic Models", Paper SPE 62927 presented at the 2000 SPE Annual Technical Conference and Exhibition held in Dallas, October 1-4, 2000

Li, D., Beckner, B., Kumar, A.: "A New Efficient Averaging Technique for Scaleup of Multimillion-Cell Geologic Models", Paper SPE 56554 presented at the 1999 SPE Annual Technical Conference and Exhibition held in Houston, TX, October 3-6, 1999

Lozano, J.A., Costa, L.P., Alves, F.B., Silva, A.C.: "Upscaling of Stochastic Models for Reservoir Simulation - An Integrated Approach", Paper SPE 36205 presented at the 7th Abu Dhabi International Petroleum Exhibition and Conference held in Abu Dhabi, U.A.E., October 13-16, 1996

Mattax, C.C., Dalton, R.L.: *Reservoir Simulation*, SPE Monograph Series, 1990

McCarthy, J.F.: Reservoir Characterization: "Efficient Random-Walk Methods for Upscaling and Image Selection", Paper SPE 25334 presented at the SPE Asia Pacific Oil & Gas Conference & Exhibition held in Singapore, February 8-10, 1993

Melrose, J.C., Brandner, C.F.: "Role of Capillary Forces in Determining Microscopic Displacement Efficiency for Oil Recovery by Water Flooding", JCPT, Vol. 13, 1974, p. 54

Moore, T.F., Slobod, R.L.: "The effect of Viscosity and Capillarity on the Displacement of Oil by Water", Producers Monthly, Vol. 20, 1956, p. 20

Narayanan, K., White, C.D., Lake, L.W., Willis, B.J.: "Response Surface Methods for Upscaling Heterogeneous Geologic Models", Paper SPE 51923 presented at the 1999 Reservoir Simulation Symposium held in Houston, TX, February 14-17, 1999

Oh, S.G., Slattery, J.: "Interfacial Tension Required for Significant Displacement of Residual Oil", Paper D-2 presented at Second ERDA Symposium on Enhanced Oil and Gas Recovery, Tulsa, OK, 1976

Peaceman, D.W.: "Interpretation of Well-Block Pressures in Numerical Reservoir Simulation", Paper SPE 6893 presented at the 57th SPE-AIME Annual Fall Technical Conference & Exhibition held in Denver, CO, October 9-12, 1977

Peaceman, D.W.: "Effective Transmissibilities of a Gridblock by Upscaling- Why Use Renormalization?", Paper SPE 36722 presented at the SPE Annual Technical Conference & Exhibition held in Denver, CO, October 6-9, 1996

Peaceman, D.W.: "Improved Treatment of Dispersion in Numerical Calculation of Multidimensional Miscible Displacement", Paper SPE 1362

Peaceman, D.W.: "A Nonlinear Stability Analysis for Difference Equations Using Semi-Implicit Mobility", Paper SPE 5735 presented at the SPE-AIME Fourth Symposium on Numerical Simulation of Reservoir Performance, held in Los Angeles, CA, February 19-20, 1976

Peaceman, D.W.: "Calculation of Transmissibilities of Gridblocks Defined by Arbitrary Corner Point Geometry", Paper SPE 37306, Unsolicited

Perkins, F.M. Jr., Collins, R.E., "Scaling Laws for Laboratory Flow Models of Oil Reservoirs", Transactions of AIME, Vol. 219, 1960, p. 383

Peters, B., Zhou, D., Blunt, M.J.: "Experimental Investigation of Scaling Factors that Describe Miscible Floods in Layered Systems", Paper SPE 39624 presented at the 11th SPE/DOE Symposium on Improved Oil Recovery held in Tulsa, OK, April 19-22, 1998

Pickup, G.E.: "Steady State Upscaling: From Lamina-Scale to Full-Field Model", Paper SPE 50628 presented at the 1998 SPE European Conference held in The Hague, The Netherlands, October 20-22, 1998

Pickup, G.E., Ringrose, P.S., Forrester, M.M., Jensen, J.L., Sorbia, K.S.: "The Geopseudo Atlas: Geologically Based Upscaling of Multiphase Flow", Paper SPE 27565, presented at the European Petroleum Computer Conference held in Aberdeen, UK, March 15-17, 1994

Ponting, D.K.: "Corner Point Geometry in Reservoir Simulation", Proceedings of the 1st European Conference on the Mathematics of the Oil Recovery, Cambridge, 1989

Pozzi, A.L., Blackwell, R.J.: "Design of Laboratory Models for Study of Miscible Displacement", Paper SPE 445 presented at 37th Annual Fall Meeting in Los Angeles, CA, October 7-10, 1963

Prasad, R.S., Al-Attar, B.E.H., Al-Jasmi, A.K.: "Reservoir Permeability Upscaling Indicators From Welltest Analysis", Paper SPE 36175 presented at the 7th Abu Dhabi International Petroleum Exhibition and Conference held in Abu Dhabi, U.A.E., October 13-16, 1996

Rapoport, L.A., Leas, W.J.: "Properties of Linear Waterfloods", Transactions of AIME, Vol. 198, 1953, p. 139

Rapoport, L.A.: "Scaling Laws for Use in Design and Operation of Water-Oil Flow Models", Transactions AIME, Vol. 204, 1955, p. 143

Ruark, A.E.: Inspectional Analysis: A Method Which Supplements Dimensional Analysis", Journal of Elisha Mitchell Scientific Society, Vol. 51, 1935, p. 127-133

Russel, T.F.: "Stability Analysis and Switching Criteria for Adaptive Implicit Methods Based on the CFL Condition", Paper SPE 18416 presented at the SPE Symposium on Reservoir Simulation in Houston, TX, February 6-8, 1989

Sabet, M.A.: *Well Test Analysis*, Gulf Professional Publishing Company, 1991

Shiralkar, G.S., Stephenson, R.E.: "A General Formulation for Simulating Physical Dispersion and a New Nine-Point Scheme", Paper SPE 16975 presented at 62nd Annual Technical Conference and Exhibition of the Society of Petroleum Engineers held in Dallas, TX, September 27-30, 1987

Shook, M., Li, D., Lake, L.W.: "Scaling Immiscible Flow Through Permeable Media by Inspectional Analysis", In-Situ (1992) 4, 311-349

Soeriawinata, J., Kasap, E., Kelkar, M.: "Permeability Upscaling for Near-Wellbore Heterogeneities", Paper SPE 36518 presented at SPE Annual Technical Conference & Exhibition held in Denver, CO, October 6-9, 1996

Sonier, F., Chaumet, P.: "A Fully Implicit Three-Dimensional Model In Curvilinear Coordinates", Transactions AIME 257, 1974, p. 361-370

Stone, H.L.: "Rigorous Black Oil Pseudo Functions", paper SPE 21207 presented at the 11th SPE Symposium on Reservoir Simulation held in Anaheim, CA, February 17-20, 1991

Suzuki, K., Hewett, T.A.: "Sequential Scale-Up of Relative Permeabilities", Paper SPE 59450 presented at the 2000 SPE Asia Pacific Conference on Integrated Modeling for Asset Management held in Yokohama, Japan, April 25-26, 2000

Tan, T.B.: "Estimating Two and Three Dimensional Pseudo-Relative Permeabilities With Non-Linear Regression", Paper SPE 29129 presented at the 13th SPE Symposium on Reservoir Simulation held in San Antonio, TX, February 12-15, 1995

Tang, D.H.E., Peaceman, D.W.: "New Analytical and Numerical Solutions for the Radial Convection Dispersion Problem", Paper SPE 16001 presented at the 9th Symposium on Reservoir Simulation held in San Antonio, TX, February 1-4, 1987

Testerman, J.D.: "A Statistical Reservoir-Zonation Technique", JPT, August 1962, pp. 889-893

Thibeau, S., Barker, J.W., Souilliard, P.: "Dynamical Upscaling Techniques Applied to Compositional Flows", Paper SPE 29128 presented at 13th SPE Symposium on Reservoir Simulation held in San Antonio, TX, February 12-15, 1995

Trujillo, E.M.: "A Simple Method for Calculating Pseudo-Relative Permeabilities From Laboratory Waterfloods", Paper SPE 11278, unsolicited

Van Daalen, F., Van Domselaar, H.R.: "Scaled Fluid-Flow Models With Geometry Different From That of the Prototype", SPEJ, Vol. 12, 1972, p. 220

Virnovsky, G.A., Friis, H.A., Lohne, A., Skauge, A.: "Up-scaling of Multiphase Flow Functions Using a Steady State Flow Model", Paper SPE 56413 presented at the SPE Annual Technical Conference & Exhibition held in Houston, TX, October 3-6, 1999

Wang, F.P., Lucia, F.J., Kerans, C.: "Critical Scales, Upscaling and Modeling of Shallow-Water Carbonate Reservoirs", Paper SPE 27715 presented at the SPE Permian Basin Oil and Gas Recovery Conference held in Midland, TX, March 16-18, 1994

Warren, J.E., Skiba, F.F.: "Macroscopic Dispersion", SPEJ, September 1964, p. 215

Welge, H.J.: "A Simplified Method For Computing Oil Recovery By Gas or Water Drive", Petroleum Transactions, AIME, Vol. 195, 1952, p. 91-97

White, C.D., Horne R.N.: “Computing Absolute Transmissibility in the Presence of Fine-Scale Heterogeneity“, Paper SPE 16011 presented at 9th Reservoir Simulation Symposium held in San Antonio, TX, February 1-4, 1987

White, C.D., Barton, M.D.: "Translating Outcrop Data to Flow Models, With Application to the Ferron Sandstone", Paper SPE 57482, SPEREE, August, 1999

Willis, B.J., White, C.D.: "Quantitative Outcrop Data For Flow Simulation", Journal of Sedimentary Research, Vol. 70, No. 4, July 2000, p. 788-802

Zhang, H.R., Sorbie, K.S.: "The Upscaling of Miscible and Immiscible Displacement Processes in Porous Media", paper SPE 29931 presented at the International Meeting on Petroleum Engineering held in Beijing, PR Chine, November 14-17, 1995

Zhou, D., Fayers, F.J., Orr, F.M.: “Scaling of Multiphase Flow in Simple Heterogeneous Porous Media”, paper SPE 27833 presented at ASME Winter Meeting, November 28 – December 03, 1993, New Orleans, LA

APPENDIX A

INSPECTIONAL ANALYSIS

1. Governing equations

Flow of two incompressible phases in a homogeneous anisotropic three-dimensional system accounting for the tilt in X and Y direction can be described using

$$\phi\frac{\partial S_1}{\partial t}+\frac{\partial u_{1x}}{\partial x}+\frac{\partial u_{1y}}{\partial y}+\frac{\partial u_{1z}}{\partial z}=0 \tag{A.1a}$$

$$\frac{\partial u_{1x}+\partial u_{2x}}{\partial x}+\frac{\partial u_{1y}+\partial u_{2y}}{\partial y}+\frac{\partial u_{1z}+\partial u_{2z}}{\partial z}=0 \tag{A.1b}$$

$$u_{1x}=-k_x\lambda_{r1}\left(\frac{\partial p_1}{\partial x}-\rho_1\cdot g\cdot\sin\alpha_X\cdot\cos\alpha_Y\right) \tag{A.2a}$$

$$u_{2x}=-k_x\lambda_{r2}\left(\frac{\partial p_2}{\partial x}-\rho_2\cdot g\cdot\sin\alpha_X\cdot\cos\alpha_Y\right) \tag{A.2b}$$

$$u_{1y}=-k_y\lambda_{r1}\left(\frac{\partial p_1}{\partial y}-\rho_1\cdot g\cdot\sin\alpha_Y\cdot\cos\alpha_X\right) \tag{A.2c}$$

$$u_{2y}=-k_y\lambda_{r2}\left(\frac{\partial p_2}{\partial y}-\rho_2\cdot g\cdot\sin\alpha_Y\cdot\cos\alpha_X\right) \tag{A.2d}$$

$$u_{1z}=-k_z\lambda_{r1}\left(\frac{\partial p_1}{\partial z}-\rho_1\cdot g\cdot\cos\alpha_X\cos\alpha_Y\right) \tag{A.2e}$$

$$u_{2z}=-k_z\lambda_{r2}\left(\frac{\partial p_2}{\partial z}-\rho_2\cdot g\cdot\cos\alpha_X\cos\alpha_Y\right) \tag{A.2f}$$

$$P_1=P_1^o-\int_{\frac{L}{2}}^{x}\frac{u_{1x}}{k_x\lambda_{r1}}dx-\int_{\frac{W}{2}}^{y}\frac{u_{1y}}{k_y\lambda_{r1}}dy-\int_{\frac{L}{2}}^{z}\frac{u_{1z}}{k_z\lambda_{r1}}dz$$
$$\rho_1\cdot g\cdot\left(\left(x-\frac{L}{2}\right)\cdot\sin\alpha_X\cos\alpha_Y+\left(y-\frac{W}{2}\right)\cdot\sin\alpha_Y\cos\alpha_X+\left(z-\frac{H}{2}\right)\cdot\cos\alpha_X\cos\alpha_Y\right)$$
$$\forall x\in[0,L],y\in[0,W],z\in[0,H],t \tag{A.3a}$$

$$P_2=P_2^o-\int_{\frac{L}{2}}^{x}\frac{u_{2x}}{k_x\lambda_{r2}}dx-\int_{\frac{W}{2}}^{y}\frac{u_{2y}}{k_y\lambda_{r2}}dy-\int_{\frac{H}{2}}^{z}\frac{u_{2z}}{k_z\lambda_{r2}}dz-$$
$$\rho_2\cdot g\cdot\left(\left(x-\frac{L}{2}\right)\cdot\sin\alpha_X\cos\alpha_Y+\left(y-\frac{W}{2}\right)\cdot\sin\alpha_Y\cos\alpha_X+\left(z-\frac{H}{2}\right)\cdot\cos\alpha_X\cos\alpha_Y\right)$$
$$\forall x\in[0,L],y\in[0,W],z\in[0,H],t \tag{A.3b}$$

$$\sigma\sqrt{\frac{\phi}{k_z}}j(S_1) = P_2 - P_1 \tag{A.4a}$$

$$P_2 - P_1 = H_T \Delta\rho \cdot g \cdot \cos\alpha_X \cos\alpha_Y \tag{A.4b}$$

$$\left(H_T - H_T^o\right)\Delta\rho \cdot g \cdot \cos\alpha_X \cos\alpha_Y =$$

$$\left\{\begin{array}{l} \int_{\frac{L}{2}}^{x} \frac{u_{2x}}{k_x\lambda_{r2}} - \frac{u_{1x}}{k_x\lambda_{r1}}dx + \\ \int_{\frac{W}{2}}^{y} \frac{u_{2y}}{k_y\lambda_{r2}} - \frac{u_{1y}}{k_y\lambda_{r1}}dy + \\ \int_{\frac{H}{2}}^{z} \frac{u_{2z}}{k_z\lambda_{r2}} - \frac{u_{1z}}{k_z\lambda_{r1}}dz \end{array}\right\} + \left\{\Delta\rho \cdot g \cdot \left(\begin{array}{l} \left(x - \frac{L}{2}\right) \cdot \sin\alpha_X \cos\alpha_Y + \\ \left(y - \frac{W}{2}\right) \cdot \sin\alpha_X \cos\alpha_Y + \\ \left(z - \frac{H}{2}\right) \cdot \cos\alpha_X \cos\alpha_Y \end{array}\right)\right\}$$

$$\forall x \in [0, L], y \in [0, W], z \in [0, H], t \tag{A.5}$$

2. Transformation to dimensionless space

Following are linear transformations from dimensional to dimensionless space:

$$x = x_1^* \cdot x_D + x_2^* \tag{A.6a}$$

$$y = y_1^* \cdot y_D + y_2^* \tag{A.6b}$$

$$z = z_1^* \cdot z_D + z_2^* \tag{A.6c}$$

$$t = t_1^* \cdot t_D + t_2^* \tag{A.6d}$$

$$u_{1x} = u_{1x1}^* \cdot u_{1xD} + u_{1x2}^* \tag{A.6e}$$

$$u_{2x} = u_{2x1}^* \cdot u_{2xD} + u_{2x2}^*. \tag{A.6f}$$

$$u_{1y} = u_{1y1}^* \cdot u_{1yD} + u_{1y2}^* \ . \tag{A.6g}$$

$$u_{2y} = u_{2y1}^* \cdot u_{2yD} + u_{2y2}^* \tag{A.6h}$$

$$u_{1z} = u_{1z1}^* \cdot u_{1zD} + u_{1z2}^* \tag{A.6i}$$

$$u_{2z} = u_{2z1}^* \cdot u_{2zD} + u_{2z2}^* \tag{A.6j}$$

$$P_1 = P_{11}^* \cdot P_{1D} + P_{12}^* \tag{A.6k}$$

$$P_2 = P_{21}^* \cdot P_{2D} + P_{22}^* \tag{A.6l}$$

$$S_1 = S_{11}^* \cdot S_{1D} + S_{12}^* \tag{A.6m}$$

Where

$^*_{ijk}$ or $^*_{k}$ transform k for phase i in direction j

Substituting in the equations A.1 through A.5 we obtain the following set of equations

$$\frac{\phi S_1^*}{t_1^*} \cdot \frac{\partial S_{1D}}{\partial t_D} + \frac{u_{1x1}^*}{x_1^*} \cdot \frac{\partial u_{1xD}}{\partial x_D} + \frac{u_{1y1}^*}{y_1^*} \cdot \frac{\partial u_{1yD}}{\partial y_D} + \frac{u_{1z1}^*}{z_1^*} \cdot \frac{\partial u_{1zD}}{\partial z_D} = 0 \tag{A.7a}$$

$$\begin{pmatrix} \frac{1}{x_1^*} \cdot \frac{\partial\left(u_{1x1}^* \cdot u_{1xD} + u_{2x1}^* \cdot u_{2xD}\right)}{\partial x_D} + \\ \frac{1}{y_1^*} \cdot \frac{\partial\left(u_{1y1}^* \cdot u_{1yD} + u_{2y1}^* \cdot u_{2yD}\right)}{\partial y_D} + \\ \frac{1}{z_1^*} \cdot \frac{\partial\left(u_{1z1}^* \cdot u_{1zD} + u_{2z1}^* \cdot u_{2zD}\right)}{\partial z_D} \end{pmatrix} = 0 \tag{A.7b}$$

$$u_{1x1}^* \cdot u_{1xD} + u_{1x2}^* = -k_x \lambda_{r1} \left(\frac{P_{11}^*}{x_1^*} \cdot \frac{\partial P_{1D}}{\partial x_D} - \rho_1 \cdot g \cdot \sin\alpha_d \cdot \cos\alpha_s \right) \tag{A.8a}$$

$$u_{2x1}^* \cdot u_{2xD} + u_{2x2}^* = -k_x \lambda_{r2} \left(\frac{P_{21}^*}{x_1^*} \cdot \frac{\partial P_{2D}}{\partial x_D} - \rho_2 \cdot g \cdot \sin\alpha_X \cdot \cos\alpha_Y \right) \tag{A.8b}$$

$$u_{1y1}^* \cdot u_{1yD} + u_{1y2}^* = -k_y \lambda_{r1} \left(\frac{P_{11}^*}{y_1^*} \cdot \frac{\partial P_{1D}}{\partial y_D} - \rho_1 \cdot g \cdot \sin\alpha_X \cos\alpha_Y \right) \tag{A.8c}$$

$$u_{2y1}^* \cdot u_{2yD} + u_{2y2}^* = -k_y \lambda_{r2} \left(\frac{P_{21}^*}{y_1^*} \cdot \frac{\partial P_{2D}}{\partial y_D} - \rho_2 \cdot g \cdot \sin\alpha_X \cos\alpha_Y \right) \tag{A.8d}$$

$$u_{1z1}^* \cdot u_{1zD} + u_{1z2}^* = -k_z \lambda_{r1} \left(\frac{P_{11}^*}{z_1^*} \cdot \frac{\partial P_{1D}}{\partial z_D} - \rho_1 \cdot g \cdot \cos\alpha_X \cos\alpha_Y \right) \tag{A.8e}$$

$$u_{1z1}^* \cdot u_{1xD} + u_{1z2}^* = -k_z \lambda_{r2} \left(\frac{P_{11}^*}{z_1^*} \cdot \frac{\partial P_{1D}}{\partial z_D} - \rho_2 \cdot g \cdot \cos\alpha_X \cos\alpha_Y \right) \tag{A.8f}$$

$$P_{21}^* P_{2D} + P_{22}^* = P_{11}^* P_{1D} + P_{12}^* + \sigma \sqrt{\frac{\phi}{k_z}} J\left(S_{1D}\right) \tag{A.9}$$

$$S_{11}^* S_{1D} + S_{12}^* = S_1^o \qquad \text{at } t_1^* t_D + t_2^* = 0, \quad \forall x_D, y_D, z_D \tag{A.10}$$

$$P_{11}^{*}P_{1D}+P_{12}^{*}=\left\{\begin{array}{l} P_1^o-\left(\begin{array}{l} x_1^{*}\int\limits_{\frac{L-x_2^{*}}{2x_1^{*}}}^{x_D-\frac{x_2^{*}}{x_1^{*}}}\dfrac{u_{1x1}^{*}u_{1xD}+u_{1x2}^{*}}{k_x\lambda_{r1}}dx_D+y_1^{*}\int\limits_{\frac{W-y_2^{*}}{2y_1^{*}}}^{y_D-\frac{y_2^{*}}{y_1^{*}}}\dfrac{u_{1y1}^{*}u_{1y}+u_{1y2}^{*}}{k_y\lambda_{r1}}dy_D+ \\ z_1^{*}\int\limits_{\frac{H-z_2^{*}}{2z_1^{*}}}^{x_D-\frac{x_2^{*}}{x_1^{*}}}\dfrac{u_{1z1}^{*}u_{1z}+u_{1z2}^{*}}{k_z\lambda_{r1}}dz_D \end{array}\right) \\ -\rho_1\cdot g\cdot\left(\begin{array}{l}\left(x_1^{*}x_D+x_2^{*}-\dfrac{L-x_2^{*}}{2x_1^{*}}\right)\cdot\sin\alpha_X\cos\alpha_Y+ \\ \left(y_1^{*}y_D+y_2^{*}-\dfrac{W-y_2^{*}}{2y_1^{*}}\right)\cdot\sin\alpha_X\cos\alpha_Y+ \\ \left(z_1^{*}z_D+z_2^{*}-\dfrac{H-z_2^{*}}{2z_1^{*}}\right)\cdot\cos\alpha_X\cos\alpha_Y\end{array}\right)\end{array}\right.$$

$$\forall x_D-\frac{x_2^{*}}{x_1^{*}}\in\left[0,\frac{L}{x_1^{*}}\right],y_D-\frac{y_2^{*}}{y_1^{*}}\in\left[0,\frac{W}{y_1^{*}}\right],z_D-\frac{z_2^{*}}{z_1^{*}}\in\left[0,\frac{H}{z_1^{*}}\right],t_D-\frac{t_2^{*}}{t_1^{*}} \tag{A.11a}$$

$$P_{21}^{*}P_{2D}+P_{22}^{*}=\left\{\begin{array}{l} P_2^o-\left(\begin{array}{l} x_1^{*}\int\limits_{\frac{L-x_2^{*}}{2x_1^{*}}}^{x_D-\frac{x_2^{*}}{x_1^{*}}}\dfrac{u_{2x1}^{*}u_{2xD}+u_{2x2}^{*}}{k_x\lambda_{r2}}dx_D+y_1^{*}\int\limits_{\frac{W-y_2^{*}}{2y_1^{*}}}^{y_D-\frac{y_2^{*}}{y_1^{*}}}\dfrac{u_{2y2}^{*}u_{1y}+u_{2y2}^{*}}{k_y\lambda_{r2}}dy_D+ \\ z_1^{*}\int\limits_{\frac{H-z_2^{*}}{2z_1^{*}}}^{z_D-\frac{z_2^{*}}{z_1^{*}}}\dfrac{u_{2z1}^{*}u_{2z}+u_{2z2}^{*}}{k_z\lambda_{r2}}dz_D \end{array}\right) \\ -\rho_2\cdot g\cdot\left(\begin{array}{l}\left(x_1^{*}x_D+x_2^{*}-\dfrac{L-x_2^{*}}{2x_1^{*}}\right)\cdot\sin\alpha_X\cos\alpha_Y+ \\ \left(y_1^{*}y_D+y_2^{*}-\dfrac{W-y_2^{*}}{2y_1^{*}}\right)\cdot\sin\alpha_Y\cos\alpha_X+ \\ \left(z_1^{*}z_D+z_2^{*}-\dfrac{H-z_2^{*}}{2z_1^{*}}\right)\cdot\cos\alpha_X\cos\alpha_Y\end{array}\right)\end{array}\right.$$

$$\forall x_D-\frac{x_2^{*}}{x_1^{*}}\in\left[0,\frac{L}{x_1^{*}}\right],y_D-\frac{y_2^{*}}{y_1^{*}}\in\left[0,\frac{W}{y_1^{*}}\right],z_D-\frac{z_2^{*}}{z_1^{*}}\in\left[0,\frac{H}{z_1^{*}}\right],t_D-\frac{t_2^{*}}{t_1^{*}} \tag{A.11b}$$

$$\left(H_T - H_T^o\right)\Delta\rho \cdot g \cdot \cos\alpha_X \cos\alpha_Y =$$

$$\left\{ \begin{array}{l} \int\limits_{\frac{L-x_2^*}{2x_1^*}}^{x_D-\frac{x_2^*}{x_1^*}} \dfrac{u_{2x1}^* u_{2xD} + u_{2x2}^*}{k_x \lambda_{r2}} - \dfrac{u_{1x1}^* u_{1xD} + u_{1x2}^*}{k_x \lambda_{r1}} dx + \\ \int\limits_{\frac{W-y_2^*}{2y_1^*}}^{y_D-\frac{y_2^*}{y_1^*}} \dfrac{u_{2y1}^* u_{2yD} + u_{2y2}^*}{k_y \lambda_{r2}} - \dfrac{u_{1y1}^* u_{1yD} + u_{1y1}^*}{k_y \lambda_{r1}} dy + \\ \int\limits_{\frac{H-z_2^*}{2z_1^*}}^{z_D-\frac{z_2^*}{z_1^*}} \dfrac{u_{2z1}^* u_{2zD} + u_{2z2}^*}{k_z \lambda_{r2}} - \dfrac{u_{1z1}^* u_{1zD} + u_{1z2}^*}{k_z \lambda_{r1}} dz \end{array} \right\} + \left\{ \Delta\rho \cdot g \cdot \left(\begin{array}{l} \left(x_1^* x_D + x_2^* - \dfrac{L - x_2^*}{2x_1^*} \right) \cdot \sin\alpha_X \cos\alpha_Y + \\ \left(y_1^* y_D + y_2^* - \dfrac{W - y_2^*}{2y_1^*} \right) \cdot \sin\alpha_X \cos\alpha_Y + \\ \left(z_1^* z_D + z_2^* - \dfrac{H - z_2^*}{2z_1^*} \right) \cdot \cos\alpha_X \cos\alpha_Y \end{array} \right) \right\}$$

$$\forall x_D - \frac{x_2^*}{x_1^*}, y_D - \frac{y_2^*}{y_1^*}, z_D - \frac{z_2^*}{z_1^*}, t_D - \frac{t_2^*}{t_1^*} \qquad \text{(A.12)}$$

3. Inspectional analysis

After the presented initial substitution we need to multiply equations with scale factors of choice to obtain the final form of the dimensionless system. At this stage scale factors are arbitrary, however the form of the equation should be preserved. Even though the usual approach is scaling in x-direction, the form of gravitational vector in velocity equations indicates that the best way to scale velocities is using a z-direction. Therefore

$$\frac{\partial S_{1D}}{\partial t_D} + \boxed{1}\ \frac{t_1^* u_{1x1}^*}{\phi S_1^* x_1^*} \cdot \frac{\partial u_{1xD}}{\partial x_D} + \boxed{2}\ \frac{t_1^* u_{1y1}^*}{\phi S_1^* y_1^*} \cdot \frac{\partial u_{1yD}}{\partial y_D} + \boxed{3}\ \frac{t_1^* u_{1z1}^*}{\phi S_1^* z_1^*} \cdot \frac{\partial u_{1zD}}{\partial z_D} = 0$$

$$\boxed{4}\ \frac{u_{1x1}^* z_1^*}{u_{1z1}^* x_1^*} \frac{\partial\left(u_{1xD} + \boxed{5}\ \frac{u_{2x1}^*}{u_{1x1}^*} \cdot u_{2xD}\right)}{\partial x_D} + \boxed{6}\ \frac{u_{1y1}^* z_1^*}{u_{1z1}^* y_1^*} \frac{\partial\left(u_{1yD} + \boxed{7}\ \frac{u_{2y1}^*}{u_{1y1}^*} \cdot u_{2yD}\right)}{\partial y_D} + \frac{\partial\left(u_{1zD} + \boxed{8}\ \frac{u_{2z1}^*}{u_{1z1}^*} \cdot u_{2zD}\right)}{\partial z_D} = 0$$

$$u_{1xD} = -\left(\boxed{9}\ \frac{k_x \lambda_{r1} P_{11}^*}{u_{1x1}^* x_1^*} \frac{\partial P_{1D}}{\partial x_D} - \boxed{10}\ \frac{x_1^* \cdot \rho_1 \cdot g \cdot \sin\alpha_X \cdot \cos\alpha_Y}{P_{11}^*} \right) - \boxed{11}\ \frac{u_{1x2}^*}{u_{1x1}^*}$$

$$u_{2xD} = -\boxed{12\ \frac{k_x \lambda_{r2} P_{21}^*}{u_{2x1}^* x_1^*}}\left(\frac{\partial P_{2D}}{\partial x_D} - \boxed{13\ \frac{x_1^* \cdot \rho_2 \cdot g \cdot \sin\alpha_X \cdot \cos\alpha_Y}{P_{21}^*}}\right) - \boxed{14\ \frac{u_{2x2}^*}{u_{2x1}^*}}$$

$$u_{1yD} = -\boxed{15\ \frac{k_y \lambda_{r1} P_{11}^*}{u_{1y1}^* y_1^*}}\left(\frac{\partial P_{1D}}{\partial y_D} - \boxed{16\ \frac{y_1^* \cdot \rho_1 \cdot g \cdot \sin\alpha_X \cdot \cos\alpha_Y}{P_{11}^*}}\right) - \boxed{17\ \frac{u_{1y2}^*}{u_{1y1}^*}}$$

$$u_{2yD} = -\boxed{18\ \frac{k_y \lambda_{r2} P_{21}^*}{u_{2y1}^* y_1^*}}\left(\frac{\partial P_{2D}}{\partial y_D} - \boxed{19\ \frac{y_1^* \rho_2 \cdot g \cdot \sin\alpha_Y \cdot \cos\alpha_X}{P_{21}^*}}\right) - \boxed{20\ \frac{u_{2y2}^*}{u_{2y1}^*}}$$

$$u_{1zD} = -\boxed{21\ \frac{k_z \lambda_{r1} P_{11}^*}{u_{1z1}^* z_1^*}}\left(\frac{\partial P_{1D}}{\partial z_D} - \boxed{22\ \frac{z_1^* \rho_1 \cdot g \cdot \cos\alpha_X \cos\alpha_Y}{P_{11}^*}}\right) - \boxed{23\ \frac{u_{1z2}^*}{u_{1z1}^*}}$$

$$u_{2zD} = -\boxed{24\ \frac{k_z \lambda_{r2} P_{21}^*}{u_{2z1}^* z_1^*}}\left(\cdot\frac{\partial P_{2D}}{\partial z_D} - \boxed{25\ \frac{z_1^* \rho_2 \cdot g \cdot \cos\alpha_X \cos\alpha_Y}{P_{21}^*}}\right) - \boxed{26\ \frac{u_{2z2}^*}{u_{2z1}^*}}$$

$$P_{2D} = \boxed{27\ \frac{P_{11}^*}{P_{21}^*}} P_{1D} + \boxed{28\ \frac{P_{12}^* - P_{22}^*}{P_{21}^*}} + \boxed{29\ \frac{\sigma}{P_{21}^*}\sqrt{\frac{\phi}{k_z}}} J(S_D)$$

$$S_{1D} = \boxed{30\ \frac{S_1^o - S_{12}^*}{S_{11}^*}} \qquad \text{at } t_D = \boxed{31\ \frac{t_2^*}{t_1^*}}, \quad \forall x_D, y_D, z_D$$

$$P_{1D} = \left\{ \frac{P_1^o - P_{12}^*}{P_{11}^*} - \frac{u_{1z1}^* z_1^*}{k_z \lambda_{r1} P_{11}^*} \left[\frac{k_z u_{1x1}^* x_1^*}{k_x u_{1z1}^* z_1^*} \int_{\frac{2x_2^* - L}{2x_1^*}}^{x_D} \left(u_{1xD} + \frac{u_{1x2}^*}{u_{1x1}^*} \right) dx_D + \frac{k_z u_{1y1}^* y_1^*}{k_y u_{1z1}^* z_1^*} \int_{\frac{2y_2^* - W}{2y_1^*}}^{y_D} \left(u_{1yD} + \frac{u_{1y2}^*}{u_{1y1}^*} \right) dy_D + \int_{\frac{2z_2^* - H}{2z_1^*}}^{z_D} \left(u_{1zD} + \frac{u_{1z2}^*}{u_{1z1}^*} \right) dz_D \right] \right\}$$

$$- \frac{z_1^* \rho_1 \cdot g \cdot \cos\alpha_X \cos\alpha_Y}{P_{11}^*} \cdot \left\{ \frac{x_1^* \sin\alpha_X \cos\alpha_Y}{z_1^* \cos\alpha_X \cos\alpha_Y} \left(x_D + \frac{2x_2^* - H}{2x_1^*} \right) + \frac{y_1^* \sin\alpha_Y \cos\alpha_X}{z_1^* \cos\alpha_Y \cos\alpha_X} \left(y_D + \frac{2z_2^* - H}{2z_1^*} \right) + \left(z_D + \frac{2z_2^* - H}{2z_1^*} \right) \right\}$$

$$P_{2D} = \left\{ \frac{P_2^o - P_{22}^*}{P_{21}^*} - \frac{u_{2z1}^* z_1^*}{k_z \lambda_{r2} P_{21}^*} \left[\frac{k_z u_{2x1}^* x_1^*}{k_x u_{2z1}^* z_1^*} \int_{\frac{2x_2^* - L}{2x_1^*}}^{x_D} \left(u_{2xD} + \frac{u_{2x2}^*}{u_{2x1}^*} \right) dx_D + \frac{k_z u_{2y1}^* y_1^*}{k_y u_{2z1}^* z_1^*} \int_{\frac{2y_2^* - W}{2y_1^*}}^{y_D} \left(u_{2yD} + \frac{u_{2y2}^*}{u_{2y1}^*} \right) dy_D + \int_{\frac{2z_2^* - H}{2z_1^*}}^{z_D} \left(u_{2zD} + \frac{u_{2z2}^*}{u_{2z1}^*} \right) dz_D \right] \right\}$$

$$- \frac{z_1^* \rho_2 \cdot g \cdot \cos\alpha_X \cos\alpha_Y}{P_{21}^*} \cdot \left\{ \frac{x_1^* \sin\alpha_X \cos\alpha_Y}{z_1^* \cos\alpha_X \cos\alpha_Y} \left(x_D + \frac{2x_2^* - H}{2x_1^*} \right) + \frac{y_1^* \sin\alpha_Y \cos\alpha_X}{z_1^* \cos\alpha_X \cos\alpha_Y} \left(y_D + \frac{2y_2^* - H}{2y_1^*} \right) + \left(z_D + \frac{2z_2^* - H}{2z_1^*} \right) \right\}$$

$$\frac{(H_T - H_T^o)}{z_1^*} \quad \frac{k_z \lambda_{r1} \Delta\rho \cdot g \cdot \cos\alpha_X \cos\alpha_Y}{u_{2z1}^*} =$$

$$\left\{ \frac{u_{2x1}^* k_z x_1^*}{u_{2z1}^* z_1^* k_x} \int_{\frac{L-x_2^*}{2x_1^*}}^{x_D} \left(\frac{\lambda_{r1}}{\lambda_{r2}} u_{2xD} + \frac{\lambda_{r2} u_{2x2}^* - \lambda_{r1} u_{1x2}^*}{\lambda_{r2}} - u_{1xD} \right) dx_D + \right.$$

$$\frac{u_{2y1}^* k_z y_1^*}{u_{2z1}^* z_1^* k_y} \int_{\frac{W-y_2^*}{2y_1^*}}^{y_D} \left(\frac{\lambda_{r1}}{\lambda_{r2}} u_{2yD} + \frac{\lambda_{r2} u_{2y1}^* - \lambda_{r1} u_{1y2}^*}{\lambda_{r2}} - u_{1yD} \right) dy_D + \Bigg\} +$$

$$\int_{\frac{H-z_2^*}{2z_1^*}}^{z_D} \left(\frac{\lambda_{r1}}{\lambda_{r2}} u_{2zD} + \frac{\lambda_{r2} u_{2z2}^* - \lambda_{r1} u_{1z2}^*}{\lambda_{r2}} - u_{1zD} \right) dz_D$$

$$\frac{k_z \lambda_{r1} \Delta\rho \cdot g \cdot \cos\alpha_X \cos\alpha_Y}{u_{2z1}^*} \left(\begin{array}{l} \frac{x_1^* \sin\alpha_X \cos\alpha_Y}{z_1^* \cos\alpha_X \cos\alpha_Y} \left(x_D + \frac{2x_2^* - H}{2x_1^*} \right) + \\ \frac{y_1^* \sin\alpha_X \cos\alpha_Y}{z_1^* \cos\alpha_X \cos\alpha_Y} \left(y_D + \frac{2y_2^* - W}{2y_1^*} \right) + \\ \left(z_D + \frac{2z_2^* - H}{2z_1^*} \right) \end{array} \right)$$

The total of 82 dimensionless groups will result from the transformation to dimensionless space. These groups are marked using a red box with the group number assigned (e.g. 15). The next step is to assign the values for the groups. Two separate steps will follow. The first step is *primary elimination* of groups that violate the form of

original equation by assigning them to be equal to 0 or 1 for additive or multiplicative groups, respectively. The second step is *secondary substitution*. The resulting remaining groups cease to be arbitrary, and should be assigned using parameters of equations, following the process of primary elimination. The process of secondary substitution is still based on arbitrary transformation factors chosen to translate dimensional to dimensionless space. Careful choice and inspection of transformation factors will be needed to achieve physically meaningful set of dimensionless numbers. Overview of arbitrary (0,1) and non-arbitrary (NA) parameters is given in table A.1.

Table A.1 Overview of arbitrary and non-arbitrary dimensionless groups

π		π		π		π		π		π	
1	1	15	NA	29	NA	43	-½	57	0	71	-½
2	1	16	NA	30	NA	44	NA	58	NA	72	0
3	1	17	0	31	NA	45	NA	59	-½	73	NA
4	1	18	NA	32	NA	46	-½	60	NA	74	-½
5	1	19	NA	33	-½	47	-½	61	NA	75	0
6	1	20	0	34	0	48	NA	62	-½	76	NA
7	1	21	1	35	NA	49	-½	63	-½	77	NA
8	1	22	NA	36	1	50	0	64	NA	78	-½
9	NA	23	0	37	NA	51	NA	65	NA	79	NA
10	NA	24	1	38	-½	52	1	66	NA	80	NA
11	0	25	NA	39	0	53	NA	67	-½	81	-½
12	NA	26	0	40	-½	54	-½	68	0	82	-½
13	NA	27	NA	41	0	55	0	69	NA		
14	0	28	NA	42	NA	56	-½	70	NA		

The process of primary elimination begins with arbitrary assignment of spatial transformation factors. It is convenient to have the spatial transformation yield numbers between 0 and 1; we therefore choose following transformation factors: $x_1^* = L$, $y_1^* = W$, $z_1^* = H$. This transformation implies that parameters x_2^*, y_2^* and z_2^* are equal to 0. As a result groups 33, 38, 40, 43, 46, 47, 49, 54, 56, 59, 62, 63, 67, 71, 74, 78, 81, 82 become -½.

To maintain the form of equations we assign groups 1 through 8, 21, 24, 36 and 52 equal to 1. Further analysis shows that groups 11, 14, 17, 20, 23, 26, 28, 34, 39, 41, 50, 55,

57, 68, 72 and 75 violate the form of equations. Since these groups are additive their value is set to zero. This makes u_{1x2}^*, u_{1x2}^*, u_{1x2}^*, u_{1x2}^*, u_{1x2}^* and u_{1x2}^* equal to 0.

Groups 31 and 51 will determine the scaling of the pressure. The value for these factors is arbitrary, so the value of pressure at the center for displacing phase (group 35) will be set to 0. This provides us with $P_{12}^* = P_1^o$. Since the group 28 is equal to 0, we can determine $P_{22}^* = P_{12}^* = P_1^o$.

Capillary, viscous and gravity forces direct the flow. Because of the relevance for vertical equilibrium calculations (in which capillary and gravity forces balance in the vertical direction), the Z direction is chosen for scaling purposes. Also, more complete analysis shows that easiest to scale for the combinations of trigonometric functions arising from the rotation. Hence,

$$u_{1z1}^* = u_T \tag{A.13a}$$

$$u_{1x1}^* = \frac{L}{H} u_T \tag{A.13b}$$

$$u_{1y1}^* = \frac{W}{H} u_T \tag{A.13c}$$

$$P_{11}^* = P_{21}^* = \frac{u_T \cdot H}{k_x \cdot \lambda_{r1}} \tag{A.13d}$$

Groups 30 and 31 are saturation related groups. By assigning the S_{11}^* to $1\text{-}S_{1r}\text{-}S_{2r}$ and S_{12}^* to S_{1r} we get the Corey-Brooks' representation of relative permeability. S_1 is current saturation in the system. Term S_{11}^* is a movable displaced phase saturation, later in the text marked as ΔS_M. The usual representation of dimensionless time is pore volumes injected. Our representation is movable pore volumes injected; hence the time can be defined as

$$t = \frac{\phi \cdot \Delta S_M \cdot H}{u_T} = \frac{\phi \cdot \Delta S_M \cdot L \cdot W \cdot H}{q_T} \tag{A.14}$$

Group 35 will be assigned to 0 yielding $P_{12}^* = P_1^o$. Since the capillary pressure is determined as a difference in phase pressures, initial values contained in the group 52 have to be scaled similar way. Hence we assign $P_{22}^* = P_{12}^* = P_1^*$ where P_1^* is the minimum pressure that the whole system of blocks is scaled on.

This concludes the primary arbitrary elimination. The remaining groups are not arbitrary any more so they need to be determined through the process of secondary elimination. The following is the set of remaining dimensionless groups, together with the group from which they originate.

$$\pi_1 = \frac{k_x}{k_z}\frac{H^2}{L^2}$$ **9**

$$\pi_2 = \frac{L}{H}\frac{k_z \lambda_{r1}{}^{o} \rho_1 g \cdot \sin\alpha_X \cos\alpha_Y}{u_T}$$ **10**

$$\pi_3 = \frac{k_x}{k_z}\frac{H^2}{L^2}\frac{\lambda_{r2}{}^{o}}{\lambda_{r1}{}^{o}}$$ **12**

$$\pi_4 = \frac{L}{H}\frac{k_z \lambda_{r2}{}^{o} \rho_2 g \cdot \sin\alpha_X \cos\alpha_Y}{u_T}$$ **13**

$$\pi_5 = \frac{k_y}{k_z}\frac{H^2}{W^2}$$ **15**

$$\pi_6 = \frac{W}{H}\frac{k_z \lambda_{r1}{}^{o} \rho_1 g \cdot \sin\alpha_Y \cos\alpha_X}{u_T}$$ **16**

$$\pi_7 = \frac{k_y}{k_z}\frac{H^2}{W^2}\frac{\lambda_{r2}{}^{o}}{\lambda_{r1}{}^{o}}$$ **18**

$$\pi_8 = \frac{W}{H}\frac{k_z \lambda_{r2}{}^{o} \rho_2 g \cdot \sin\alpha_Y \cos\alpha_X}{u_T}$$ **19**

$$\pi_9 = \frac{k_z \lambda_{r1}{}^{o} \rho_1 g \cdot \cos\alpha_X \cos\alpha_Y}{u_T}$$ **22**

$$\pi_{10} = \frac{k_z \lambda_{r2}{}^{o} \rho_2 g \cdot \cos\alpha_X \cos\alpha_Y}{u_T}$$ **25**

$$\pi_{11} = \frac{\sigma k_z \lambda_{r1}{}^{o}}{u_T H}\sqrt{\frac{\phi}{k_z}}$$ **29**

$$\pi_{12} = \frac{k_z}{k_x}\frac{L^2}{H^2}$$ **32**

$$\pi_{13} = \frac{k_z}{k_x}\frac{L^2}{H^2}$$ **37**

$$\pi_{14} = \frac{L}{H}\tan\alpha_X$$ **42**

$$\pi_{15} = \frac{k_z \lambda_{r1}^{\ o} \rho_1 g \cdot \cos\alpha_X \cos\alpha_Y}{u_T}$$ **44**

$$\pi_{16} = \frac{W}{H}\tan\alpha_X$$ **45**

$$\pi_{17} = \frac{k_z}{k_x}\frac{L^2}{H^2}$$ **48**

$$\pi_{18} = \frac{k_z \lambda_{r1}^{\ o}}{u_T}\frac{P_2^0 - P_1^o}{H}$$ **51**

$$\pi_{19} = \frac{k_z}{k_x}\frac{L^2}{H^2}$$ **53**

$$\pi_{20} = \frac{L}{H}\tan\alpha_Y$$ **58**

$$\pi_{21} = \frac{k_z \lambda_{r1}^{\ o} \rho_1 g \cdot \cos\alpha_X \cos\alpha_Y}{u_T}$$ **60**

$$\pi_{22} = \frac{W}{H}\tan\alpha_X$$ **61**

$$\pi_{23} = \frac{\Delta H_T}{H}$$ **64**

$$\pi_{24} = \frac{k_z \lambda_{r1}^{\ o} \Delta\rho g \cdot \cos\alpha_X \cos\alpha_Y}{u_T}$$ **65**

$$\pi_{25} = \frac{k_z}{k_x}\frac{L^2}{H^2}$$ **66**

$$\pi_{26} = \frac{\lambda_{r2}^{\ o}}{\lambda_{r11}^{\ o}}$$ **69**

$$\pi_{27} = \frac{k_z}{k_y}\frac{W^2}{H^2}$$ **70**

$$\pi_{28} = \frac{\lambda_{r1}^{\ o}}{\lambda_{r2}^{\ o}} \qquad 73$$

$$\pi_{29} = \frac{\lambda_{r1}^{\ o}}{\lambda_{r2}^{\ o}} \qquad 76$$

$$\pi_{30} = \frac{L}{H}\tan\alpha_X \qquad 77$$

$$\pi_{31} = \frac{k_z \lambda_{r1} \Delta\rho g \cdot \cos\alpha_X \cos\alpha_Y}{u_T} \qquad 79$$

$$\pi_{32} = \frac{W}{H}\tan\alpha_X \qquad 80$$

These 32 groups once introduced make the previous set of flow equations completely dimensionless. Flow equations can be written in dimensionless form as

$$\frac{\partial S_{1D}}{\partial t_D} + \frac{\partial u_{1xD}}{\partial x_D} + \frac{\partial u_{1yD}}{\partial y_D} + \frac{\partial u_{1zD}}{\partial z_D} = 0 \qquad \text{(A.15a)}$$

$$\frac{\partial u_{1xD} + \partial u_{2xD}}{\partial x_D} + \frac{\partial u_{1yD} + \partial u_{2yD}}{\partial y_D} + \frac{\partial u_{1zD} + \partial u_{2zD}}{\partial z_D} = 0 \qquad \text{(A.15b)}$$

$$u_{1xD} = -\pi_1 (S_{1D})^{n_1} \left(\frac{\partial p_{1D}}{\partial x_D} - \pi_2 \right) \qquad \text{(A.16a)}$$

$$u_{2xD} = -\pi_3 (S_{2D})^{n_2} \left(\frac{\partial p_{2D}}{\partial x_D} - \pi_4 \right) \qquad \text{(A.16b)}$$

$$u_{1yD} = -\pi_5 (S_{1D})^{n_1} \left(\frac{\partial p_{1D}}{\partial y_D} - \pi_6 \right) \qquad \text{(A.16c)}$$

$$u_{2yD} = -\pi_7 (S_{2D})^{n_2} \left(\frac{\partial p_{2D}}{\partial y_D} - \pi_8 \right) \qquad \text{(A.16d)}$$

$$u_{1zD} = -(S_{1D})^{n_1} \left(\frac{\partial p_1}{\partial z} - \pi_9 \right) \qquad \text{(A.16e)}$$

$$u_{2zD} = -\pi_{27} (S_{2D})^{n_2} \left(\frac{\partial p_{2D}}{\partial z_D} - \pi_{10} \right) \qquad \text{(A.16f)}$$

$$P_{2D} = P_{1D} + \pi_{11} J(S_{1D}) \qquad \text{(A.17)}$$

$$P_{1D}=\left\{\begin{array}{l} P_{1D}^{*}-\left(\pi_{12}\int_{\frac{1}{2}}^{x_D}\left(\frac{u_{1xD}}{(S_{1D})^{n_1}}\right)dx_D+\pi_{13}\int_{\frac{1}{2}}^{y_D}\left(\frac{u_{1yD}}{(S_{1D})^{n_1}}\right)dy_D+\int_{\frac{1}{2}}^{z_D}\left(\frac{u_{1zD}}{(S_{1D})^{n_1}}\right)dz_D\right) \\ -\pi_{15}\left(\pi_{16}\left(x_D-\frac{1}{2}\right)+\pi_{17}\left(y_D-\frac{1}{2}\right)+\left(z_D-\frac{1}{2}\right)\right) \end{array}\right\}$$

$$\forall x_D\in[0,1],y_D\in[0,1],z_D\in[0,1],t_D \qquad \text{(A.18a)}$$

$$P_{2D}=\left\{\begin{array}{l} P_{2D}^{*}-\frac{1}{\pi_{26}}\left(\pi_{17}\int_{\frac{1}{2}}^{x_D}\left(\frac{u_{2xD}}{(S_{2D})^{n_2}}\right)dx_D+\pi_{19}\int_{\frac{1}{2}}^{y_D}\left(\frac{u_{2yD}}{(S_{2D})^{n_2}}\right)dy_D+\int_{\frac{1}{2}}^{z_D}\left(\frac{u_{2zD}}{(S_{2D})^{n_2}}\right)dz_D\right) \\ -\pi_{21}\left(\pi_{20}\left(x_D-\frac{1}{2}\right)+\pi_{22}\left(y_D-\frac{1}{2}\right)+\left(z_D-\frac{1}{2}\right)\right) \end{array}\right\}$$

$$\forall x_D\in[0,1],y_D\in[0,1],z_D\in[0,1],t_D \qquad \text{(A.18b)}$$

$$\Delta z_{TD}\quad \pi_{24}=\left\{\begin{array}{l} \pi_{25}\int_{0}^{x_D-\frac{1}{2}}\left(\frac{u_{2xD}}{(S_{2D})^{n_2}}-\pi_{26}\frac{u_{1xD}}{(S_{2D})^{n_1}}\right)dx_D+\pi_{27}\int_{0}^{y_D-\frac{1}{2}}\left(\frac{u_{2yD}}{(S_{2D})^{n_2}}-\pi_{28}\frac{u_{1yD}}{(S_{1D})^{n_1}}\right)dy_D+ \\ \int_{0}^{z_D-\frac{1}{2}}\left(\frac{u_{2zD}}{(S_{2D})^{n_2}}-\pi_{29}\frac{u_{1zD}}{(S_{1D})^{n_1}}\right)dz_D+\pi_{30}\left(\pi_{31}\left(x_D-\frac{1}{2}\right)+\pi_{32}\left(y_D-\frac{1}{2}\right)+\left(z_D-\frac{1}{2}\right)\right) \end{array}\right\}$$

$$\forall x_D\in[0,1],y_D\in[0,1],z_D\in[0,1],t_D \qquad \text{(A.19)}$$

4. Redundancy elimination

Some of the groups obtained through inspectional analysis recur and the rest are not independent making it possible and desirable to perform further reduction of the dimensionless groups. Groups 18 and 23 are omitted at this point since they do not affect the general form and are only included for the ease of later analysis.

All the dimensionless groups are multiplicative hence if logarithms are taken it is possible to translate this system to a system of linear equations. After setting up the coefficient matrix, linear algebra further reduces the number of dimensionless groups. We need to determine the rank of the following matrix:

$$
\begin{bmatrix}
\log \pi_1 \\ \log \pi_2 \\ \log \pi_3 \\ \log \pi_4 \\ \log \pi_5 \\ \log \pi_6 \\ \log \pi_7 \\ \log \pi_8 \\ \log \pi_9 \\ \log \pi_{10} \\ \log \pi_{11} \\ \log \pi_{15} \\ \log \pi_{17} \\ \log \pi_{25} \\ \log \pi_{27}
\end{bmatrix}
=
\begin{bmatrix}
-2 & 2 & 0 & 1 & 0 & -1 & 0 & 0 & 0 & 0 & 0 & 0 & 0 & 0 & 0 & 0 & 0 & 0 & 0 & 0 & 0 \\
1 & -1 & 0 & 0 & 0 & 1 & 1 & 0 & 1 & 1 & 0 & 0 & 1 & 0 & 0 & 1 & -1 & 0 & 0 & 0 & 0 \\
-2 & 2 & -2 & 1 & 0 & -1 & -1 & 1 & 0 & 0 & 0 & 0 & 0 & 0 & 0 & 0 & 0 & 0 & 0 & 0 & 0 \\
1 & -1 & 0 & 0 & 0 & 1 & 0 & 1 & 1 & 0 & 1 & 0 & 1 & 0 & 0 & 1 & -1 & 0 & 0 & 0 & 0 \\
0 & 2 & -2 & 0 & 1 & -1 & 0 & 0 & 0 & 0 & 0 & 0 & 0 & 0 & 0 & 0 & 0 & 0 & 0 & 0 & 0 \\
0 & -1 & 1 & 0 & 0 & 1 & 1 & 0 & 1 & 1 & 0 & 0 & 0 & 1 & 0 & 0 & -1 & 0 & 0 & 0 & 0 \\
0 & 2 & -2 & 0 & 1 & -1 & 0 & 0 & 0 & 0 & 0 & 0 & 0 & 0 & 0 & 0 & 0 & 0 & 0 & 0 & 0 \\
0 & -1 & 1 & 1 & 0 & 1 & 0 & 1 & 1 & 0 & 1 & 0 & 0 & 1 & 0 & 0 & -1 & 0 & 0 & 0 & 0 \\
0 & 0 & 0 & 0 & 0 & 1 & 1 & 0 & 1 & 1 & 0 & 0 & 0 & 0 & 1 & 1 & -1 & 0 & 0 & 0 & 0 \\
0 & 0 & 0 & 0 & 0 & 1 & 0 & 1 & 1 & 0 & 1 & 0 & 0 & 0 & 1 & 1 & -1 & 0 & 0 & 0 & 0 \\
0 & -1 & 0 & 0 & 0 & 0.5 & 1 & 0 & 1 & 0 & 0 & 1 & 0 & 0 & 1 & 1 & -1 & 0 & 0 & -0.5 & 1 \\
1 & -1 & 1 & 0 & 0 & 0 & 0 & 0 & 0 & 0 & 0 & 0 & 1 & 0 & -1 & 0 & 0 & 0 & 0 & 0 & 0 \\
0 & -1 & 1 & 0 & 0 & 0 & 0 & 0 & 0 & 0 & 0 & 0 & 0 & 1 & -1 & -1 & 0 & 0 & 0 & 0 & 0 \\
0 & 0 & 0 & 0 & 0 & 1 & 0 & 1 & 1 & 0 & 0 & 1 & 0 & 0 & 1 & 1 & -1 & 0 & 0 & 0 & 0 \\
0 & 0 & 0 & 0 & 0 & 0 & -1 & 1 & 0 & 0 & 0 & 0 & 0 & 0 & 0 & 0 & 0 & 0 & 0 & 0 & 0
\end{bmatrix}
\begin{bmatrix}
\log L \\ \log H \\ \log W \\ \log k_x \\ \log k_y \\ \log k_z \\ \log \lambda_{r1} \\ \log \lambda_{r2} \\ \log g \\ \log \rho_1 \\ \log \rho_2 \\ \log \Delta\rho \\ \log \sin\alpha_d \\ \log \sin\alpha_s \\ \log \cos\alpha_d \\ \log \cos\alpha_s \\ \log u_T \\ \log U_{1y} \\ \log U_{1z} \\ \log \phi \\ \log \sigma
\end{bmatrix}
$$

To simplify the estimate, similar groups have already been taken out. After elementary matrix operations and additional inspection, the minimum set of nonredundant dimensionless groups is determined to be

$$\frac{1}{\pi_1} = D_1 = \frac{L^2}{H^2}\frac{k_z}{k_x} \tag{A.20a}$$

$$\frac{1}{\pi_5} = D_2 = \frac{W^2}{H^2}\frac{k_z}{k_y} \tag{A.20b}$$

$$\frac{\pi_6}{\pi_9} = \frac{\pi_8}{\pi_{10}} = D_3 = \frac{W}{H}\tan\alpha_X \tag{A.20c}$$

$$\frac{\pi_2}{\pi_9} = \frac{\pi_4}{\pi_{10}} = D_4 = \frac{L}{H}\tan\alpha_Y \tag{A.20d}$$

$$\frac{\pi_{25}}{\pi_{10}} = D_5 = \frac{\Delta\rho}{\rho_1} \tag{A.20e}$$

$$\pi_{24} = D_6 = \frac{k_z\lambda_{r1}\Delta\rho g \cdot \cos\alpha_X \cos\alpha_Y}{u_T} \tag{A.20f}$$

$$\frac{\pi_1}{\pi_3} = \frac{\pi_5}{\pi_7} = \pi_{27} = D_7 = \frac{\lambda_{r1}}{\lambda_{r2}} \tag{A.20g}$$

$$\pi_{11} = D_8 = \frac{\sigma k_z \lambda_{r1}}{u_T L}\sqrt{\frac{\phi}{k_z}} \tag{A.20h}$$

The description of final dimensionless numbers, accepted symbol and equations are listed in table A.2.

Table A.2. Dimensionless groups and description

Group	**Symbol**	**Equation**
X-direction aspect ratio	N_{RX}	$\frac{L^2}{H^2}\frac{k_z}{k_x}$
Y-direction aspect ratio	N_{RY}	$\frac{W^2}{H^2}\frac{k_z}{k_y}$
X-direction tilt number	N_{TX}	$\frac{W}{H}\tan\alpha_X$
Y-direction tilt number	N_{TY}	$\frac{L}{H}\tan\alpha_Y$
Density number	N_ρ	$\frac{\Delta\rho}{\rho_1}$
Gravity number	N_g	$\frac{k_z\lambda_{r1}^{\ o}\Delta\rho g\cdot\cos\alpha_X\cos\alpha_Y}{u_T}$
Mobility ratio	M	$\frac{\lambda_{r1}^{\ o}}{\lambda_{r2}^{\ o}}$
Capillary number	N_c	$\frac{\sigma k_z\lambda_{r1}^{\ o}}{u_T H}\sqrt{\frac{\phi}{k_z}}$

Process of elimination provided us with group $\frac{\Delta\rho}{\rho_2}$. This group was eliminated, since this group can be written as $\frac{N_\rho}{1-N_\rho}$. Dependent dimensionless groups appearing in equations A.1a through A.5 can therefore be estimated using the following set of equations

$$\pi_1 = \frac{1}{N_{RX}} \qquad \textbf{9}$$

$$\pi_2 = \frac{N_g N_{TX}}{N_\rho} \qquad \textbf{10}$$

$$\pi_3 = \frac{1}{N_{RX} M} \qquad \textbf{12}$$

$$\pi_4 = \frac{N_g\left(1 - N_\rho\right)N_{TX}}{N_\rho}$$ 13

$$\pi_5 = \frac{1}{N_{RY}}$$ 15

$$\pi_6 = \frac{N_g N_{TY}}{N_\rho}$$ 16

$$\pi_7 = \frac{1}{N_{RY} M}$$ 18

$$\pi_8 = \frac{N_g N_{TY}\left(1 - N_\rho\right)}{N_\rho}$$ 19

$$\pi_9 = \frac{N_g}{N_\rho}$$ 22

$$\pi_{10} = \frac{N_g\left(1 - N_\rho\right)}{N_\rho}$$ 25

$$\pi_{11} = N_c$$ 29

$$\pi_{12} = N_{RX}$$ 32

$$\pi_{13} = N_{RY}$$ 37

$$\pi_{14} = N_{TX}$$ 42

$$\pi_{15} = \frac{N_g}{N_\rho}$$ 44

$$\pi_{16} = N_{TY}$$ 45

$$\pi_{17} = N_{RX}$$ 48

$$\pi_{19} = N_{RY}$$ 53

$$\pi_{20} = N_{TX}$$ 58

$$\pi_{21} = \frac{N_g\left(1 - N_\rho\right)}{N_\rho}$$ 60

$$\pi_{22} = N_{TY}$$ 61

$\pi_{24} = N_g$ **65**

$\pi_{25} = N_{RX}$ **66**

$\pi_{26} = M$ **69**

$\pi_{27} = N_{RY}$ **70**

$\pi_{28} = M$ **73**

$\pi_{29} = M$ **76**

$\pi_{30} = N_{TX}$ **77**

$\pi_{31} = N_g$ **79**

$\pi_{32} = N_{TY}$ **81**

Development of dimensionless groups using an inspectional analysis needs only the elementary set of equations. Two-phase incompressible system is completely defined with equations A.7a through A.10. Minimum set of groups needed for complete dimensionless description are those numbered **1** through **31**. Equations A.11a through A.12 are developed from the set of base equations. They are included in the analysis for the purpose of verification of scaling process and to ease the elimination of redundancy.

Redundancy is a result of consistent scaling. Consistent scaling means that all the variables are scaled to dimension and phase of choice rendering redundancy to be *directional* or *physical*. Directionally redundant group is the one used to scale the behavior of both phase fluxes for the same direction. Examples for directional redundancy are groups N_{RX} and N_{TX} for X- and N_{RY} and N_{TY} for Y-direction flow. Lack of directionally redundant groups in Z-direction shows that Z-direction was used for scaling. Physical redundancy occurs due to scaling of both phase fluxes to a common physical denominator (e.g. end point mobility of displacing phase or density difference). Examples of physical redundancy are N_ρ and M.

Scaling through inspectional analysis introduces both redundancies at the same time. As a result dimensionless groups are not independent. For example group $\boldsymbol{\pi_3}$ is a combination of $\boldsymbol{\pi_2}$ and $\boldsymbol{\pi}_{28}$. Purpose of inspectional analysis is to provide minimum number

of dimensionless groups. As a result mixed dependencies have to be recognized and separated. Separation provides the final set of independent dimensionless groups.

APPENDIX B

DIFFERENCE EQUATION ANALYSIS

Saturation can be expressed in dimensionless form using the following form of normalization

$$S_{iD} = \frac{S_i - S_{i_{Min}}}{S_{i_{Max}} - S_{i_{Min}}} \tag{B.1}$$

Once the saturation is dimensionless, velocities from equations 3.2a through 3.2f can be substituted in equations 3.1a and 3.1b providing with common form of flow equation used for differentiation. For displacing and displaced phases these are respectively

$$\phi \frac{\partial S_{1D}}{\partial t} = \begin{pmatrix} \frac{\partial}{\partial x}\left(k_x \lambda_{r1} \frac{\partial}{\partial x}\left(p_1 - \rho_1 \cdot g \cdot z\right)\right) + \\ \frac{\partial}{\partial y}\left(k_y \lambda_{r1} \frac{\partial}{\partial y}\left(p_1 - \rho_1 \cdot g \cdot z\right)\right) + \\ \frac{\partial}{\partial z}\left(k_z \lambda_{r1} \frac{\partial}{\partial z}\left(p_1 - \rho_1 \cdot g \cdot z\right)\right) \end{pmatrix} \tag{B.2a}$$

$$\phi \frac{\partial S_{2D}}{\partial t} = \begin{pmatrix} \frac{\partial}{\partial x}\left(k_x \lambda_{r1} \frac{\partial}{\partial x}\left(p_2 - \rho_2 \cdot g \cdot z\right)\right) + \\ \frac{\partial}{\partial y}\left(k_y \lambda_{r1} \frac{\partial}{\partial y}\left(p_2 - \rho_2 \cdot g \cdot z\right)\right) + \\ \frac{\partial}{\partial z}\left(k_z \lambda_{r1} \frac{\partial}{\partial z}\left(p_2 - \rho_2 \cdot g \cdot z\right)\right) \end{pmatrix} \tag{B.2b}$$

Since the system has no mass transfer between phases, material balance dictates

$$S_{2D} = 1 - S_{1D} \tag{B.3}$$

Mobility for phase 'i' can be expressed through end-point mobilities using Corey-Brooks' model as

$$\lambda_i = \lambda_{ri}^{o}\left(S_{iD}\right)^{n_i} \tag{B.4}$$

Displacing phase is the wetting phase, hence the pressures can be related through capillary pressure as

$$p_1 = p_2 - P_c = p_2 - \sigma\sqrt{\frac{\phi}{k}} J(S_{1D}) \tag{B.5}$$

To simplify notation observation on general form of differential and hence difference equation is utilized. The form is

$$C_{Si} = C_{Pix} + C_{Piy} + C_{Piz} \tag{B.6}$$

Where coefficient C_S is change in saturation and C_P are changes in pressure in corresponding directions for phase 'i'. Difference equation coefficients for displacing phase become

$$C_{S1} = \frac{\phi}{\Delta t}\left(S_{1D\ i,j,k}^{\ n+1} - S_{1D\ i,j,k}^{\ n}\right) \tag{B.7}$$

$$C_{P1x} = \begin{Bmatrix} \frac{1}{\Delta x_D}\left[k_{x\ i+1,j,k} \cdot \lambda_{r1}^{\ o}\left(S_{1D\ i+1,j,k}^{\ n}\right)^{n_1} \frac{1}{\Delta x}\left(\begin{pmatrix} p_{2\ i+1,j,k}^{\ n+1} - \sigma\sqrt{\frac{\phi}{k}} J(S_{1D\ i+1,j,k}^{\ n+1}) - \rho_1 \cdot g \cdot z_{i+1,j,k} \end{pmatrix} - \begin{pmatrix} p_{2\ i,j,k}^{\ n+1} - \sigma\sqrt{\frac{\phi}{k}} J(S_{1D\ i,j,k}^{\ n+1}) - \rho_1 \cdot g \cdot z_{i,j,k} \end{pmatrix} \right) \right] \\ \frac{1}{\Delta x}\left[-k_{x\ i,j,k} \cdot \lambda_{r1}^{\ o}\left(S_{1D\ i,j,k}^{\ n}\right)^{n_1} \frac{1}{\Delta x}\left(\begin{pmatrix} p_{2\ i,j,k}^{\ n+1} - \sigma\sqrt{\frac{\phi}{k}} J(S_{1D\ i,j,k}^{\ n+1}) - \rho_1 \cdot g \cdot z_{i,j,k} \end{pmatrix} - \begin{pmatrix} p_{2\ i-1,j,k}^{\ n+1} - \sigma\sqrt{\frac{\phi}{k}} J(S_{1D\ i-1,j,k}^{\ n+1}) - \rho_1 \cdot g \cdot z_{i-1,j,k} \end{pmatrix} \right) \right] \end{Bmatrix}$$

$$\forall i, j, k \tag{B.8}$$

$$C_{P1y} = \begin{Bmatrix} \frac{1}{\Delta y}\left[k_{y\ i,j+1,k} \cdot \lambda_{r1}^{\ o}\left(S_{1D\ i,j+1,k}^{\ n}\right)^{n_1} \frac{1}{\Delta y}\left(\begin{pmatrix} p_{2\ i,j+1,k}^{\ n+1} - \sigma\sqrt{\frac{\phi}{k}} J(S_{1D\ i,j+1,k}^{\ n+1}) - \rho_1 \cdot g \cdot z_{i,j+1,k} \end{pmatrix} - \begin{pmatrix} p_{2\ i,j,k}^{\ n+1} - \sigma\sqrt{\frac{\phi}{k}} J(S_{1D\ i,j,k}^{\ n+1}) - \rho_1 \cdot g \cdot z_{i,j,k} \end{pmatrix} \right) \right] \\ -\frac{1}{\Delta y}\left[k_{y\ i,j,k} \cdot \lambda_{r1}^{\ o}\left(S_{1D\ i,j,k}^{\ n}\right)^{n_1} \frac{1}{\Delta y}\left(\begin{pmatrix} p_{2\ i,j,k}^{\ n+1} - \sigma\sqrt{\frac{\phi}{k}} J(S_{1D\ i,j,k}^{\ n+1}) - \rho_1 \cdot g \cdot z_{i,j,k} \end{pmatrix} - \begin{pmatrix} p_{2\ i,j-1,k}^{\ n+1} - \sigma\sqrt{\frac{\phi}{k}} J(S_{1D\ i,j-1,k}^{\ n+1}) - \rho_1 \cdot g \cdot z_{i,j-1,k} \end{pmatrix} \right) \right] \end{Bmatrix}$$

$$\forall i, j, k \tag{B.9}$$

$$C_{P1z}=\left\{\begin{array}{l}\dfrac{1}{\Delta z}\left[k_{z\ i,j,k+1}\cdot\lambda_{r1}{}^{o}\left(S_{1D\ i,j,k+1}^{\ n}\right)^{n_1}\dfrac{1}{\Delta z}\left(\begin{array}{l}\left(p_{2\ i,j,k+1}^{\ n+1}-\sigma\sqrt{\dfrac{\phi}{k}}J(S_{1D\ i,j,k+1}^{\ n+1})-\rho_1\cdot g\cdot z_{i,j,k+1}\right)\\ -\left(p_{2\ i,j,k}^{\ n+1}-\sigma\sqrt{\dfrac{\phi}{k}}J(S_{1D\ i,j,k}^{\ n+1})-\rho_1\cdot g\cdot z_{i,j,k}\right)\end{array}\right)\right]\\ -\dfrac{1}{\Delta z}\left[k_{z\ i,j,k}\cdot\lambda_{r1}{}^{o}\left(S_{1D\ i,j,k}^{\ n}\right)^{n_1}\dfrac{1}{\Delta z}\left(\begin{array}{l}\left(p_{2\ i,j,k}^{\ n+1}-\sigma\sqrt{\dfrac{\phi}{k}}J(S_{1D\ i,j,k}^{\ n+1})-\rho_1\cdot g\cdot z_{i,j,k}\right)-\\ \left(p_{2\ i,j,k-1}^{\ n+1}-\sigma\sqrt{\dfrac{\phi}{k}}J(S_{1D\ i,j,k-1}^{\ n+1})-\rho_1\cdot g\cdot z_{i,j,k-1}\right)\end{array}\right)\right]\end{array}\right\}$$

$\forall i,j,k$ (B.10)

Similar, displaced phase coefficients are

$$C_{S2}=-\frac{\phi}{\Delta t}\left(S_{1D\ i,j,k}^{\ n+1}-S_{1D\ i,j,k}^{\ n}\right)$$ (B.11)

$$C_{P2x}=\left\{\begin{array}{l}\dfrac{1}{\Delta x}\left[k_{x\ i+1,j,k}\cdot\lambda_{r2}{}^{o}\left(1-S_{1D\ i+1,j,k}^{\ n}\right)^{n_1}\dfrac{1}{\Delta x}\left(\begin{array}{l}\left(p_{2\ i+1,j,k}^{\ n+1}-\rho_1\cdot g\cdot z_{i+1,j,k}\right)-\\ \left(p_{2\ i,j,k}^{\ n+1}-\rho_1\cdot g\cdot z_{i,j,k}\right)\end{array}\right)\right]-\\ \dfrac{1}{\Delta x}\left[k_{x\ i,j,k}\cdot\lambda_{r2}{}^{o}\left(1-S_{1D\ i,j,k}^{\ n}\right)^{n_1}\dfrac{1}{\Delta x}\left(\begin{array}{l}\left(p_{2\ i,j,k}^{\ n+1}-\rho_1\cdot g\cdot z_{i,j,k}\right)-\\ \left(p_{2\ i,j,k-1}^{\ n+1}-\rho_1\cdot g\cdot z_{i,j,k-1}\right)\end{array}\right)\right]\end{array}\right\}$$

$\forall i,j,k$ (B.12)

$$C_{P2y}=\left\{\begin{array}{l}\dfrac{1}{\Delta y}\left[k_{y\ i,j+1,k}\cdot\lambda_{r2}{}^{o}\left(1-S_{1D\ i,j+1,k}^{\ n}\right)^{n_1}\dfrac{1}{\Delta y}\left(\begin{array}{l}\left(p_{2\ i,j+1,k}^{\ n+1}-\rho_1\cdot g\cdot z_{i,j+1,k}\right)-\\ \left(p_{2\ i,j,k}^{\ n+1}-\rho_1\cdot g\cdot z_{i,j,k}\right)\end{array}\right)\right]-\\ \dfrac{1}{\Delta y}\left[k_{y\ i,j,k}\cdot\lambda_{r2}{}^{o}\left(1-S_{1D\ i,j,k}^{\ n}\right)^{n_1}\dfrac{1}{\Delta y}\left(\begin{array}{l}\left(p_{2\ i,j,k}^{\ n+1}-\rho_1\cdot g\cdot z_{i,j,k}\right)-\\ \left(p_{2\ i,j-1,k}^{\ n+1}-\rho_1\cdot g\cdot z_{i,j-1,k}\right)\end{array}\right)\right]\end{array}\right\}$$

$\forall i,j,k$ (B.13)

$$C_{P2z} = \begin{Bmatrix} \frac{1}{\Delta z}\left[k_{z\ i,j,k+1} \cdot \lambda_{r2}{}^{o} \left(1 - S_{1D\ i,j,k+1}^{\ n}\right)^{n_1} \frac{1}{\Delta z}\left(\begin{pmatrix} p_{2\ i,j,k+1}^{\ n+1} - \rho_1 \cdot g \cdot z_{i,j,k+1} \end{pmatrix} - \right) \right] - \\ \frac{1}{\Delta z}\left[k_{z\ i,j,k} \cdot \lambda_{r2}{}^{o} \left(1 - S_{1D\ i,j,k}^{\ n}\right)^{n_1} \frac{1}{\Delta z}\left(\begin{pmatrix} p_{2\ i,j,k}^{\ n+1} - \rho_1 \cdot g \cdot z_{i,j,k} \end{pmatrix} - \right) \right] \end{Bmatrix}$$

$$\forall i, j, k \tag{B.14}$$

To set the difference variables in dimensionless form we need to chose the normalization variable. Let *L*, *W* and *H* become scaling parameters for space. Each spatial coefficient can be multiplied by corresponding directional scaling parameter in the form of L^2/L^2, W^2/W^2 and H^2/H^2 for respective *X*-, *Y*- and *Z*-direction. Complete equation is afterwards multiplied by H^2 to scale in Z direction.

Velocity is defined the same way as in Appendix A. If the whole equation is multiplied by $u_T \cdot H$ saturation coefficient for displacing phase becomes

$$C_{S1} = \frac{\phi}{\frac{\Delta t \cdot u_T}{H}} \left(S_{1D\ i,j,k}^{\ n+1} - S_{1D\ i,j,k}^{\ n} \right) \tag{B.15}$$

Coefficient for pressure in *X*-direction is initially multiplied with L^2/L^2. This operation introduces dimensionless $1/\Delta x_D{}^2$ in a form of $1/(\Delta x/L)^2$. Remaining portion $(1/L^2)$ becomes a directional part of aspect number. Existing permeability in X-direction is multiplied with (k_z/k_z) estimated at the same point (*i, j, k*) as the pressure in the C_{Pz}. In order to obtain the remaining portion of aspect number the whole equation is multiplied with H^2. As a result, unused parameter $(1/H^2)$ in C_{Pz} coefficient disappears. Aspect ratio in C_{Py} is obtained in the similar manner.

Multiplication with $u_T \cdot H$ results in the final form of the difference equation coefficients. Similar procedure is repeated for the displaced phase. To obtain the correct difference notation for displacing phase subscripts in equations B.17, B.16, B.17 and B.18 should be changed from 1 to 2 for pressure and saturation terms.

Following are the difference equation coefficients for the displacing phase

$$C_{P1x} = \left\{ \begin{array}{l} \frac{1}{\Delta x_D}\left[\boxed{1}\ \frac{k_{x\ i+1,j,k}}{k_{z\ i+1,j,k}}\left(\frac{H}{L}\right)^2 \cdot \left(S_{1D\ i+1,j,k}^{\ n}\right)^{n_1} \frac{1}{\Delta x_D} \left(\begin{array}{l} \boxed{2}\ \frac{\lambda_{r1}{}^{o}k_{z\ i+1,j,k}\, p_{2\ i+1,j,k}^{\ n+1}}{Hu_T} - \\ \boxed{3}\ \frac{\lambda_{r1}{}^{o}k_{z\ i+1,j,k}\,\sigma}{Hu_T}\sqrt{\frac{\phi}{k}}\, J(S_{1D\ i+1,j,k}^{\ n+1}) - \\ \boxed{4}\ \frac{\lambda_{r1}{}^{o}k_{z\ i+1,j,k}\,\rho_1 \cdot g \cdot z_{i+1,j,k}}{Hu_T} \end{array} \right) - \right. \\ \left. \left(\begin{array}{l} \boxed{5}\ \frac{\lambda_{r1}{}^{o}k_{z\ i+1,j,k}\, p_{2\ i,j,k}^{\ n+1}}{Hu_T} - \\ \boxed{6}\ \frac{\lambda_{r1}{}^{o}k_{z\ i+1,j,k}\,\sigma}{Hu_T}\sqrt{\frac{\phi}{k}}\, J(S_{1D\ i,j,k}^{\ n+1}) - \\ \boxed{7}\ \frac{\lambda_{r1}{}^{o}k_{z\ i+1,j,k}\,\rho_1 \cdot g \cdot z_{i,j,k}}{Hu_T} \end{array} \right) \right] \\ \frac{1}{\Delta x_D}\left[-\boxed{8}\ \frac{k_{x\ i,j,k}}{k_{z\ i,j,k}}\left(\frac{H}{L}\right)^2 \cdot \left(S_{1D\ i,j,k}^{\ n}\right)^{n_1} \frac{1}{\Delta x_D} \left(\begin{array}{l} \boxed{9}\ \frac{\lambda_{r1}{}^{o}k_{z\ i,j,k}\, p_{2\ i,j,k}^{\ n+1}}{Hu_T} - \\ \boxed{10}\ \frac{\lambda_{r1}{}^{o}k_{z\ i,j,k}\,\sigma}{Hu_T}\sqrt{\frac{\phi}{k}}\, J(S_{1D\ i,j,k}^{\ n+1}) - \\ \boxed{11}\ \frac{\lambda_{r1}{}^{o}k_{z\ i,j,k}\,\rho_1 \cdot g \cdot z_{i,j,k}}{Hu_T} \end{array} \right) - \right. \\ \left. \left(\begin{array}{l} \boxed{12}\ \frac{\lambda_{r1}{}^{o}k_{z\ i,j,k}\, p_{2\ i-1,j,k}^{\ n+1}}{Hu_T} - \\ \boxed{13}\ \frac{\lambda_{r1}{}^{o}k_{z\ i,j,k}\,\sigma}{Hu_T}\sqrt{\frac{\phi}{k}}\, J(S_{1D\ i-1,j,k}^{\ n+1}) - \\ \boxed{14}\ \frac{\lambda_{r1}{}^{o}k_{z\ i,j,k}\,\rho_1 \cdot g \cdot z_{i-1,j,k}}{Hu_T} \end{array} \right) \right] \end{array} \right\}$$

$\forall i, j, k$ (B.16)

$$C_{P1y} = \left\{ \begin{array}{l} \dfrac{1}{\Delta y_D}\left[\boxed{15}\dfrac{k_{x\ i+1,j,k}}{k_{z\ i+1,j,k}}\left(\dfrac{H}{W}\right)^2 \cdot \left(S_{1D\ i,j+1,k}^{\ n}\right)^{n_1} \dfrac{1}{\Delta y_D}\left[\left(\boxed{16}\dfrac{\lambda_{r1}{}^{o}k_{z\ i,j+1,k}\, p_{2\ i,j+1,k}^{\ n+1}}{Hu_T} - \right.\right.\right. \right. \\ \left. \left. \left. \boxed{17}\dfrac{\lambda_{r1}{}^{o}k_{z\ i,j+1,k}\,\sigma}{Hu_T}\sqrt{\dfrac{\phi}{k}}\, J(S_{1D\ i,j+1,k}^{\ n+1}) - \boxed{18}\dfrac{\lambda_{r1}{}^{o}k_{z\ i,j+1,k}\,\rho_1 \cdot g \cdot z_{i,j+1,k}}{Hu_T} \right) \right. \\ \left. - \left(\boxed{19}\dfrac{\lambda_{r1}{}^{o}k_{z\ i,j+1,k}\, p_{2\ i,j,k}^{\ n+1}}{Hu_T} - \boxed{20}\dfrac{\lambda_{r1}{}^{o}k_{z\ i,j+1,k}\,\sigma}{Hu_T}\sqrt{\dfrac{\phi}{k}}\, J(S_{1D\ i,j,k}^{\ n+1}) - \boxed{21}\dfrac{\lambda_{r1}{}^{o}k_{z\ i,j+1,k}\,\rho_1 \cdot g \cdot z_{i,j,k}}{Hu_T} \right) \right] \\ \dfrac{1}{\Delta x_D}\left[-\boxed{22}\dfrac{k_{y\ i,j,k}}{k_{z\ i,j,k}}\left(\dfrac{H}{W}\right)^2 \cdot \left(S_{1D\ i,j,k}^{\ n}\right)^{n_1} \dfrac{1}{\Delta y_D}\left[\left(\boxed{23}\dfrac{\lambda_{r1}{}^{o}k_{z\ i,j,k}\, p_{2\ i,j,k}^{\ n+1}}{Hu_T} - \right.\right.\right. \right. \\ \left. \left. \left. \boxed{24}\dfrac{\lambda_{r1}{}^{o}k_{z\ i,j,k}\,\sigma}{Hu_T}\sqrt{\dfrac{\phi}{k}}\, J(S_{1D\ i,j,k}^{\ n+1}) - \boxed{25}\dfrac{\lambda_{r1}{}^{o}k_{z\ i,j,k}\,\rho_1 \cdot g \cdot z_{i,j,k}}{Hu_T} \right) \right. \\ \left. - \left(\boxed{26}\dfrac{\lambda_{r1}{}^{o}k_{z\ i,j,k}\, p_{2\ i,j-1,k}^{\ n+1}}{Hu_T} - \boxed{27}\dfrac{\lambda_{r1}{}^{o}k_{z\ i,j,k}\,\sigma}{Hu_T}\sqrt{\dfrac{\phi}{k}}\, J(S_{1D\ i,j-1,k}^{\ n+1}) - \boxed{28}\dfrac{\lambda_{r1}{}^{o}k_{z\ i,j,k}\,\rho_1 \cdot g \cdot z_{i,j-1,k}}{Hu_T} \right) \right] \end{array} \right\}$$

$\forall i, j, k$ (B.17)

$$C_{P1z} = \left\{ \begin{array}{l} \frac{1}{\Delta z_D} \left[\cdot \left(S_{1D\ i,j,k+1}^{\ n} \right)^{n_1} \frac{1}{\Delta z_D} \left[\left(\begin{array}{l} 29 \frac{\lambda_{r1}{}^{o}k_{z\ i,j+1,k}\, p_{2\ i,j,k+1}^{\ n+1}}{Hu_T} - \\ 30 \frac{\lambda_{r1}{}^{o}k_{z\ i,j+1,k}\,\sigma}{Hu_T}\sqrt{\frac{\phi}{k}} J(S_{1D\ i,j,k+1}^{\ n+1}) - \\ 31 \frac{\lambda_{r1}{}^{o}k_{z\ i,j+1,k}\,\rho_1 \cdot g \cdot z_{i,j+1,k}}{Hu_T} \end{array} \right) - \right. \right. \right. \\ \left. \left. \left. \left(\begin{array}{l} 32 \frac{\lambda_{r1}{}^{o}k_{z\ i,j+1,k}\, p_{2\ i,j,k}^{\ n+1}}{Hu_T} - \\ 33 \frac{\lambda_{r1}{}^{o}k_{z\ i,j+1,k}\,\sigma}{Hu_T}\sqrt{\frac{\phi}{k}} J(S_{1D\ i,j,k}^{\ n+1}) - \\ 34 \frac{\lambda_{r1}{}^{o}k_{z\ i,j+1,k}\,\rho_1 \cdot g \cdot z_{i,j,k}}{Hu_T} \end{array} \right) \right] \right] \\ \frac{1}{\Delta z_D} \left[-\left(S_{1D\ i,j,k}^{\ n} \right)^{n_1} \frac{1}{\Delta z_D} \left[\left(\begin{array}{l} 35 \frac{\lambda_{r1}{}^{o}k_{z\ i,j,k}\, p_{2\ i,j,k}^{\ n+1}}{Hu_T} - \\ 36 \frac{\lambda_{r1}{}^{o}k_{z\ i,j,k}\,\sigma}{Hu_T}\sqrt{\frac{\phi}{k}} J(S_{1D\ i,j,k}^{\ n+1}) - \\ 37 \frac{\lambda_{r1}{}^{o}k_{z\ i,j,k}\,\rho_1 \cdot g \cdot z_{i,j,k}}{Hu_T} \end{array} \right) - \right. \right. \right. \\ \left. \left. \left. \left(\begin{array}{l} 38 \frac{\lambda_{r1}{}^{o}k_{z\ i,j,k}\, p_{2\ i,j,k-1}^{\ n+1}}{Hu_T} - \\ 39 \frac{\lambda_{r1}{}^{o}k_{z\ i,j,k}\,\sigma}{Hu_T}\sqrt{\frac{\phi}{k}} J(S_{1D\ i,j,k-1}^{\ n+1}) - \\ 40 \frac{\lambda_{r1}{}^{o}k_{z\ i,j,k}\,\rho_1 \cdot g \cdot z_{i,j-1,k}}{Hu_T} \end{array} \right) \right] \right] \end{array} \right\}$$

$\forall i, j, k$ (B.18)

Difference groups corresponding to dimensionless groups from Appendix A are enumerated and marked with separate boxes. Groups 1, 8, 15 and 22 are spatially differentiated aspect ratios. Groups 2, 5, 9 and 12 are dimensionless pressure differentiated in *X*-direction. Similarly groups 16, 19, 23, 26 and 29, 32, 35, 38 are dimensionless pressure differentiated in *Y*- and *Z*- direction respectively.

Same principle applies to dimensionless capillary pressure. Dimensionless pressure consists of capillary number and Leverett's J(S) function. Differentiation of Leverett's J(S) function is simple. Groups 3, 6, 10, 13 are capillary number differentiated in *X*-, groups 17, 20, 24, 27 in Y- and groups 30, 33, 36, 40 in Z-direction.

Tilt and gravity number corrected for density form a single gravity group in each direction. Groups 4, 8, 11, 14 represent gravity effect in *X*-, groups 18, 21, 25, 27 in *Y*- and groups 31, 34, 37 and 41 in *Z*-direction. Some similarity with dimensionless gravity numbers can be observed however transform of variables and assignment of H, W and L needs to be discussed further in order to explain the trigonometric functions from Chapter 3. To simplify the similarity discussion, focus is kept on the 2D geometrical problem. Schematic of 2D differentiation is presented in figure B.1.

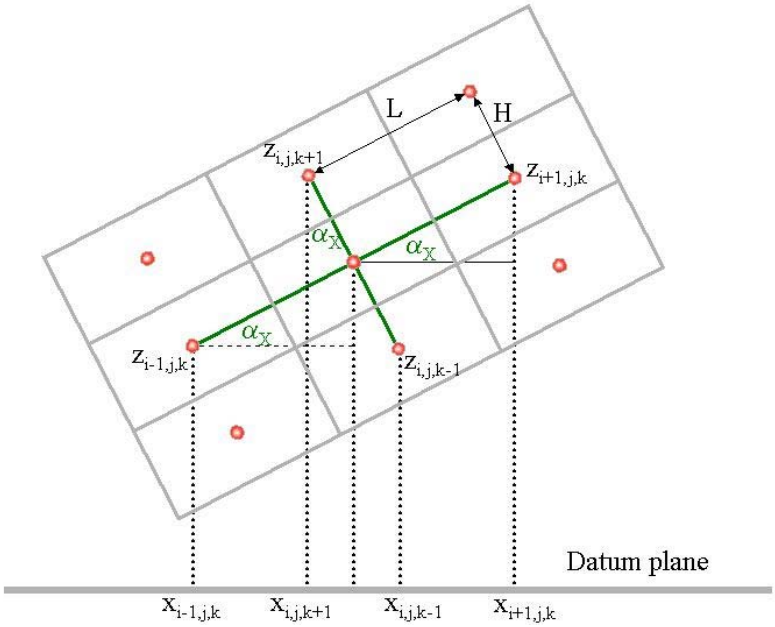

Figure B.1. 3D Difference scheme slice at a given 'j' slice

One of the gravity terms is difference of groups 4 and 7. This difference is

$$\Delta_{gX} = \frac{\lambda_{r1}{}^{o}k_{z\ \ i+1,j,k}\rho_1 \cdot g \cdot z_{i+1,j,k}}{Hu_T} - \frac{\lambda_{r1}{}^{o}k_{z\ \ i+1,j,k}\rho_1 \cdot g \cdot z_{i,j,k}}{Hu_T} \tag{B.19}$$

Rearranged, this difference becomes

$$\Delta_{gX} = \frac{\lambda_{r1}{}^{o}k_{z\ \ i+1,j,k}\rho_1 \cdot g \cdot \left(z_{i+1,j,k} - z_{i,j,k}\right)}{Hu_T} \tag{B.20}$$

Difference can be multiplied by unity ($\Delta x_D/\Delta x_D$) and rearranged as

$$\Delta_{gX} = \Delta x_D \frac{\lambda_{r1}{}^{o}k_{z\ \ i+1,j,k}\rho_1 \cdot g \cdot \left(z_{i+1,j,k} - z_{i,j,k}\right)}{u_T \Delta x}\frac{L}{H} \tag{B.21}$$

Figure B.1 shows that $(z_{i+1,j,k}\text{-}z_{i,j,k})/\Delta x$ can be replaced by $\sin \alpha_X$. Gravity number is defined using group in *Z*-direction. Hence the difference of groups 11 and 14 can be written as

$$\Delta_{gZ} = \Delta z_D \frac{\lambda_{r1}{}^{o}k_{z\ \ i,j,k+1}\rho_1 \cdot g \cdot \left(z_{i,j,k+1} - z_{i,j,k}\right)}{u_T \Delta z} \tag{B.22}$$

Term Δz is the distance between two centers of blocks used to estimate the distance change in *Z*-direction. Again, figure B.2 shows that term $(z_{i,j,k+1}\text{-}z_{i,j,k})/\Delta z$ can be replaced by $\cos(\alpha x)$. Hence the gravity difference term in Z-direction becomes

$$\Delta_{gZ} = \frac{\Delta z_D}{N_\rho}\left(N_g\right)_{k+} \tag{B.23}$$

Accounting for the difference in trigonometric function using the tilt number, gravity difference term in X direction becomes

$$\Delta_{gX} = \frac{\Delta x_D}{N_\rho}\left(N_g N_{TX}\right)_{i+} \tag{B.24}$$

An interesting case is when gridblocks are vertically aligned. In that case term $(z_{i,j,k+1}\text{-}z_{i,j,k})/\Delta z$ becomes equal to 1. Term $(z_{i+1,j,k}\text{-}z_{i,j,k})/\Delta x$ becomes $\tan(\alpha_X)$, so the equation B.24 remains accurate. However, gravity number doesn't contain the trigonometric term. It becomes

$$N_g = \frac{\lambda_{r1}{}^{o}k_z \Delta\rho \cdot g}{u_T} \tag{B.25}$$

Similar analysis can be done for both phases and in three dimensions. Geometrically, term $(z_{i,j,k+1}-z_{i,j,k})/\Delta z$ in equation B.22 becomes $cos(\alpha x)cos(\alpha_Y)$ and term $(z_{i+1,j,k}-z_{i,j,k})/\Delta x$ in equation B.21 becomes $sin(\alpha x)cos(\alpha_Y)$. To analyze the results in dimensionless form on a gridblock basis it is not necessary to explicitly determine each angle. Explicit estimate could be done applying basic geometric transforms, however much easier way is the direct determination of dimensionless groups from difference equations. To determine gravity number we can use equation B.23. Hence gravity number is

$$\left(N_g\right)_{k+} = \frac{\Delta_{gZ} N_\rho}{\Delta z_D} \tag{B.26}$$

Tilt in X-direction is therefore

$$\left(N_{TX}\right)_{i+} = \frac{\Delta_{gX} N_\rho}{\Delta x_D \left(N_g\right)_{k+}} \tag{B.27}$$

Similarly, tilt in *Y*-direction is

$$\left(N_{TY}\right)_{j+} = \frac{\Delta_{gY} N_\rho}{\Delta y_D \left(N_g\right)_{k+}} \tag{B.28}$$

Scaling variables L, W and H can theoretically be any number. However, the ranges should be between Δx and $L_{reservoir}$ for L, Δy and $W_{reservoir}$ for W and between Δz and $H_{reservoir}$ for H. Three separate behavioral cases can be studied in dimensionless space:

- *Local behavior* can be observed if $L=\Delta x$, $W=\Delta y$ and $H=\Delta z$. This sets the aspect ratio to aspect ratio of a gridblock. Resulting gravity number and tilt number will also be at the gridblock scale. Elements Δx_D, Δy_D and Δz_D become equal to 1. This is useful for observations on time-step length and error estimates for the particular gridblock.
- *Global behavior* can be observed if L, W and H are set to respective reservoir values. In this case observations on stability and behavior of numerical method are replaced by observations on gridblock contribution on general behavior of the reservoir. One of the examples of use of global numbers is designed simulation with purpose of determining best recovery regime and corresponding rates or scaling outcrop to reservoir behavior.

- *Regional behavior* can be observed if intermediate values are used for *L*, *W* and *H*. Regional behavior is useful in characterizing local flow regimes and upscaling (Coll and Muggeridge, 2001). Local flow regimes occur as a result of local heterogeneity and its distribution.

Let the scaling be local with $L=\Delta x$, $W=\Delta y$ and $H=\Delta z$. Transmissibility in dimensional system for rectangular isotropic system is

$$T_x = \frac{\Delta y \Delta z}{k_x} \tag{B.29a}$$

$$T_y = \frac{\Delta x \Delta z}{k_x} \tag{B.29b}$$

$$T_x = \frac{\Delta x \Delta y}{k_x} \tag{B.29c}$$

If *X*- and *Y*-direction transmissibility is normalized with respect to Z-direction, the following is gained

$$T_x' = \frac{k_x \Delta z}{k_z \Delta x} \tag{B.30a}$$

$$T_y' = \frac{k_y \Delta z}{k_z \Delta y} \tag{B.30b}$$

$$T_z' = 1 \tag{B.30c}$$

Normalized transmissibility in dimensional is equivalent to reciprocal aspect ratio in dimensionless space. The difference between the two indicated in equations B.30 through B.30c are scaling terms ($\Delta z/\Delta x$) and ($\Delta z/\Delta y$). Scaling terms missing in normalized transmissibility terms are introduced when spatial variables *x*, *y* and *z* were transformed to dimensionless space.

To conclude the discussion remaining variables need to be examined. Velocity (volume throughput per area in *Z*-direction) should always follow the volume indicated by *L*, *W* and *H* for equations B.15 through B.16 to remain consistent. Unlike development for differential equation, pressure in difference equation doesn't need to be rescaled to a fixed pressure since pressure difference rather than pressure itself becomes a variable of interest.

Any consistent addition in normalization process is taken out when differences are calculated.

VITA

Djuro Novakovic is born March 29, 1971, in Zagreb, Croatia. He was graduated from Math and Computer High School in 1989 and pursued a degree in petroleum engineering at the University of Zagreb, Croatia. Djuro received his bachelor of science degree in Petroleum Engineering in 1996, and continued his education at Louisiana State University, Craft and Hawkins Department of Petroleum Engineering where he received his master's degree in 1999. In August, 2002, he will receive the degree of Doctor of Philosophy.